Catalytic Conversion of Undesired Organic Compounds to Syngas in Biomass Gasification and Pyrolysis Applications

Pouya H. Moud

Doctoral Thesis, 2017
KTH Royal Institute of Technology
Department of Chemical Engineering
School of Chemical Science and Engineering
SE-100 44 Stockholm, Sweden

Catalytic Conversion of Undesired Organic Compounds to Syngas in Biomass Gasification and Pyrolysis Applications
POUYA H. MOUD

TRITA-CHE Report 2017:36
ISSN 1654-1081
ISBN 978-91-7729-509-9

Akademisk avhandling Som med tillstånd av Kungliga Tekniska Högskolan framläggs till offentlig granskning för avläggande av teknisk doktorsexamen i kemiteknik fredagen den 29 September 2017, kl 10:00 i Kollegiesalen, Kungl Tekniska högskolan, Brinellvägen 8, Stockholm.
Fakultetsopponent: Professor Anker D. Jensen, DTU Technical University of Denmark, Copenhagen, Denmark

Tryck: US-AB, Stockholm 2017

Abstract

Reliable energy supply is a major concern and crucial for development of the global society. To address the dependency on fossil fuel and the negative effects of this reliance on climate, there is a need for a transition to cleaner sources. An attractive solution for replacing fossil-based products is renewable substitutes produced from biomass. Gasification and pyrolysis are two promising thermochemical conversion technologies, facing challenges before large-scale commercialization becomes viable. In case of biomass gasification, undesired by-product of hydrocarbons, known as tar, must be handled prior to syngas utilization. An attractive option, among hot gas conditioning methods, is nickel-based catalytic steam reforming. In case of biomass pyrolysis, catalytic steam reforming is in early stages of investigation as a feasible option for conversion of bio-crude to syngas.

The focus of the thesis is partly dedicated to describe research aimed at increasing the knowledge around tar reforming mechanisms and effect of biomass-derived impurities on Ni-based tar reforming catalyst downstream of gasifiers. The work contributes to a better understanding of gas-phase alkali uptake, equilibration, and interaction with Ni-based catalyst surface under realistic conditions. A methodology was successfully developed to enable controlled investigation of the combined sulfur (S) and potassium (K) interaction with the catalyst. The methodology includes an implementation of precise alkali dosing, elimination of transient effects in activity, and catalyst characterization. The most striking result was that K appears to lower the sulfur coverage and increases methane and tar reforming activity. Additionally, for a clearer elucidation of elementary steps involved in tar reforming, a combined experimental and theoretical surface science approach using a Ni(111) model system was performed. The results obtained are discussed in terms of naphthalene adsorption, dehydrogenation and carbon passivation of nickel.

Additionally, the thesis describes research performed on pyrolysis gas pre-conditioning at a small-industrial scale, using an Fe-based catalyst for

mild deoxygenation of bio-crude and H_2-rich gas production. Findings showed that Fe-based materials are potential candidates for application in a pyrolysis gas pre-conditioning step before further treatment or use, and a way for generating a hydrogen-enriched gas without the need for bio-crude condensation.

Keywords: tar reforming, biomass gasification, Ni-based catalyst, potassium, sulfur, pyrolysis gas, bio-crude conditioning, gas conditioning, Fe-based catalyst

Sammanfattning

Tillförlitlig energiförsörjning är en stor utmaning och avgörande för utvecklingen av det globala samhället. För att ta möta beroendet av fossil råvara och de negativa effekter som detta beroende medför för klimatet finns ett stort behov av en övergång till renare energiråvaror. En attraktiv lösning är att ersätta nuvarande fossil råvara med produkter från biomassa. Förgasning och pyrolys är två lovande teknologier för termokemisk omvandling av biomassa. Kommersialisering av dessa teknologier är inte helt problemfritt. I fallet förgasning så behöver, bl.a. oönskade tyngre kolväten (tjära) hanteras innan den producerade orenade produktgasen kan användas i syntesgastillämpningar. Ett effektivt alternativ för detta är gaskonditionering vid höga temperaturer, baserade på katalytisk ångreformering med en nickelkatalysator. Katalytisk ångreformering är en möjlig teknik för omvandling av bioråvara, producerad från pyrolys av biomassa, till syntesgas.

Avhandlingen fokuserar delvis på att beskriva den forskning som utförts för att öka kunskapen kring mekanismer för tjärreformering och effekterna av föroreningar från biomassan på en nickelkatalysator nedströms förgasare. Arbetet bidrar till en bättre förståelse av hur alkali i form av kalium (K) i gasfasen upptas, jämviktas och växelverkar med ytan hos nickelkatalysatorn under fullt realistiska förhållanden. Inledningsvis utvecklades en metod för att möjliggöra kontrollerade studier av den kombinerade effekten av S och K, vilken inkluderar exakt dosering av alkali till en produktgas, eliminering av transienter i katalysatoraktiviteten samt katalysatorkarakterisering. Det mest lovande resultatet är att K både sänker ytans svavelinnehåll och ökar aktiviteten för omvandlingen av metan och tjära. För att ytterligare fördjupa kunskaperna i mekanismerna för tjärnedbrytning utfördes experimentella och teoretiska ytstudier på en enkristallnickelyta med naftalen som modellförening. Resultat avseende naftalenadsorption, dehydrogenering av naftalen och kolpassivering av nickelytan diskuteras.

Därutöver så beskriver avhandlingen den forskning som utförts inom förkonditionering av pyrolysgas med en järnkatalysator för varsam deoxygenering av biooljan och vätgasproduktion. Detta utfördes vid en småskalig industriell anläggning. De experimentella studierna visar att den undersökta järnkatalysatorn resulterar i en vätgasberikad gas och att den är en potentiell kandidat för tillämpning i ett förkonditioneringssteg.

Nyckelord: tjärreformering, biomassaförgasning, Ni-baserad katalysator, kalium, svavel, pyrolysgas, konditionering bio-råolja, gaskonditionering, Fe-baserad katalysator

List of Publications

This thesis is a summary of the following publications and manuscripts, which are cited in the text by their Roman numerals. The articles and manuscripts can be found in the appendix. All papers are reproduced with permission from copyright holders.

Paper [I]
Moud PH, Andersson KJ, Lanza R, Pettersson JBC, Engvall K.
Effect of gas phase alkali species on tar reforming catalyst performance: initial characterization and method development.
Fuel 154 (2015) 95–106.

Paper [II]
Moud PH, Andersson KJ, Lanza R, Engvall K.
Equilibrium potassium coverage and its effect on a Ni tar reforming catalyst in alkali- and sulfur-laden biomass gasification gases.
Applied Catalysis B: Environmental 190 (2016) 137–146.

Paper [III]
Yazdi MG,[1] **Moud PH**,[1] Marks K, Piskorz W, Öström H, Hansson T, Kotarba A, Engvall K, Götelid M.
Naphthalene on Ni(111): experimental and theoretical insights into adsorption, dehydrogenation and carbon passivation.
Submitted to Journal of Physical Chemistry (2017).

Paper [IV]
Moud PH, Kantarelis E, Andersson KJ, Engvall K.
Biomass pyrolysis gas conditioning over an iron-based catalyst for mild deoxygenation and hydrogen production.
Submitted to Fuel (2017).

[1] These authors contributed equally to the paper.

Contributions to the Papers

The author of this thesis was the main person responsible for these publications. All co-authors contributed to planning the research, and to the acquisition and analysis of the data and results, as well as reviewing the text.

Paper [I] I am the main author of this paper and was responsible for analyzing the experimental data and for the writing. I performed all the activity and catalyst characterization tests at *KTH Royal Institute of Technology*, except for the sulfur/carbon content measurements, which were made at *Haldor Topsoe*. I performed all the thermodynamics and theoretical calculations. The catalyst was provided by *Haldor Topsoe*, Denmark.

Paper [II] I am the main author of this paper and was responsible for analyzing the experimental data and for the writing. I performed the major part of the experimental work at *KTH Royal Institute of Technology*. I performed all the catalyst characterization tests, except for the sulfur/carbon content measurement, which were made at *Haldor Topsoe*. I performed all the thermodynamics calculations. The catalyst was provided by *Haldor Topsoe*, Denmark.

Paper [III] I am the main author together with Milad G. Yazdi, of the *Dept.* of *Material Physics* at *KTH Royal Institute of Technology*. All experiments reported in this paper (i.e. sample preparation, STM, and TPD measurements) were executed jointly. The data evaluation and the writing were shared equally between Milad G. Yazdi and me. The results were interpreted in collaboration with Klas J. Andersson, of *Haldor Topsoe, Denmark*. The TPD experiments were performed at the *Dept. of physics, Stockholm University*, and the STM experiments were performed at the *Dept. of Material Physics, KTH Royal Institute of Technology*. The density functional theory (DFT) modeling was performed at the *Faculty of Chemistry, Jagiellonian University*, Kraków, Poland.

Paper [IV] I am the main author of this paper and was responsible for analysing the experimental data and for the writing. I performed all the experimental activity tests at the *Cortus Energy* test facility. The experimental setup was developed at the *Dept. of Chemical Engineering,*

KTH Royal Institute of Technology. The sulfur/carbon content measurement, XRD analysis, and WGS activity were performed at *Haldor Topsoe*, Denmark. The GC-MS analysis of bio-crude was performed by Efthymios Kantarelis at *KTH Royal Institute of Technology*. The C/H/O/S and ash analysis of bio-crude was performed by *Karlshamnsverkets Laboratory, UNIPER, Sweden*. I performed all the theoretical calculations. The catalyst was provided by *Haldor Topsoe*, Denmark.

Related Contributions

Technical Report (Peer Review)

Moud PH, Holm DF, Halvarsson A, Andersson KJ, Kantarelis E, Amovic M, Ljunggren R, Engvall K.
Catalytic conversion of pyrolysis gas in the WoodRoll process for enhancing process reliability.
Energiforsk report, 2016: 340.

Presentations at conferences

The presenting author is indicated in bold font.

Oral presentations

Moud PH, Andersson KJ, Engvall K.
Catalytic hot-gas cleaning of biomass gasification gas: tar reforming surface chemistry.
Presented at the Swedish Gasification Center (SFC) Annual Conference, Stockholm, Sweden, 21–22 March 2017.

Moud PH, Andersson KJ, Götelid M, Engvall K.
Equilibrium potassium coverage and its effect on a Ni tar reforming catalyst in alkali- and sulfur-laden biomass gasification gases.
Presented at the 251st American Chemical Society National Meeting, San Diego, USA, 13–17 March 2016.

Moud PH, Andersson KJ, Engvall K.
Equilibrium potassium coverage and its effect on a Ni tar reforming catalyst: method development and results.
Presented at the Swedish Gasification Center (SFC) Annual Conference, Gothenburg, Sweden, 1–3 February 2017.

Moud PH, Granestrand J, Dahlin S, Nilsson M, **Andersson KJ**, Pettersson LJ, Engvall K.
The role of alkali in heterogeneous catalysis for gas cleaning in stationary and mobile applications.
Presented at American Chemical Society National Meeting (ACS), Denver (CO), USA, April 2–6 2015.

Moud PH, Andersson KJ, Engvall K.
Effect of gas phase alkali on tar reforming catalyst.
Presented at 6th International Freiberg Conference on IGCC & XtL, Freiberg, Germany, May 19–22 2014.

Poster presentations

Moud PH, Andersson KJ, Götelid M, Kotarba A, Engvall K.
The role of gas-phase alkali in heterogeneous catalysis for gas cleaning.
Presented at 13th Nordic Symposium on Catalysis, Lund, Sweden, June 14–16 2016.

Moud PH, Andersson KJ, Engvall K.
Alkali uptake studies under realistic conditions on a sulfur equilibrated Nickel based tar reforming catalyst.
Presented at 24th North American Catalysis Society Meeting (NAM), Pittsburgh (PA), USA, 14–19 June 2015.

Moud PH, Andersson KJ, Lanza R, Engvall K.
Effect of gas phase alkali species on tar reforming catalyst performance: initial characterization and method development.
Presented at the Swedish Gasification Center (SFC) Annual Conference, Luleå, Sweden, 2–4 February 2015.

Moud PH, Andersson KJ, Lanza R, Engvall K.
Impurities interaction with tar reforming catalyst in biomass gasification.
Presented at 3rd International Conference on Thermochemical Conversion of Biomass (tcbiomass 2013), Chicago, USA, 3–6 September 2013.

Contents

PART A: INTRODUCTION

1 Setting the scene

Synthesis gas (also known as syngas), a mixture of CO, H_2, and CO_2, is a key intermediate product in the chemical industry. It is used for the production of chemicals and fuels and as a source of pure hydrogen and CO. This energy source/intermediate will continue to play an important role in energy conversion in the 21st century [1]. Syngas can be produced from plentiful carbon or hydrocarbon sources, including natural gas, coal, naphtha, and biomass [2, 3], traditionally via steam reforming, autothermal reforming, and partial oxidation. Natural gas and naphtha, to a lesser extent, are the dominant feedstock for production of syngas [3]. Demands for greater energy supply and new processes with improved efficiency has never been higher worldwide due to an increasing population and standard of living [4-6]. Today, roughly 81 % of the world energy supply is from fossil fuel (i.e. oil, natural gas, and coal) sources [7]. Environmental concerns, such as the threat posed by greenhouse gas emissions, possible future shortages, such as depletion of fossil fuel sources, and energy security issues facing oil- and gas-importing countries are some of the main energy and environmental challenges posed by non-renewable sources. These concerns have boosted research into alternatives to fossil fuel-derived products [8]. Biomass has environmental advantages over fossil fuels, such as lower CO_2 and other greenhouse gas emissions [9]. Biomass is widespread, abundant, and can be sustainably developed as well as being considered renewable [10-13].

Potential routes for the production of syngas and pure H_2 from biomass are thermochemical conversion processes; gasification and pyrolysis. Biomass gasification has attracted the most attention due to its high conversion efficiency and its versatility in accepting a wide range of biomass feedstocks to produce an intermediate product suitable for upgrading to syngas and various high-value end products [2, 10, 14, 15]. There are few examples of demonstration or commercial plants for biomass gasification to syngas around the world [16-18]. Biomass pyrolysis is also an attractive route, overcoming some of the disadvantages of large-scale biomass

utilization, such as low energy density and low annual yields of biomass [16]. It converts biomass into gas, liquid, and char. The ultimate goal of this technology is generally to produce a pyrolysis oil that can be used as a fuel, fuel additive, and/or intermediate to be further utilized for different purposes.

Biomass gasification and pyrolysis, produces certain problematic organic compounds that need to be treated. In the case of biomass gasification, one of the main challenges before additional conditioning and conversion to chemicals and fuels is to remove heavy hydrocarbons (referred to as tar) or to convert them to syngas molecules [19]. An attractive way to mitigate tars and decompose lighter hydrocarbons is secondary catalytic tar reforming, converting tar to useful permanent gases [20]. In the case of biomass pyrolysis, pyrolysis bio-crude (i.e., the liquid condensate) is problematic to handle and exploit, so upgrading routes are needed for their use. In the case of hydrogen or syngas production, catalytic steam reforming of bio-crude is considered a CO_2-neutral and therefore sustainable route [21].

In conclusion, a key stage in the examined biomass utilization pathways is the reforming and conditioning of biomass gasification and pyrolysis gas by means of heterogeneous catalysis, which has a fundamental role in the development of gas cleaning and conditioning technologies for the production of synthesis gas.

1.1 Scope of the thesis

The scope of this thesis is separated into two parts, as illustrated in figure 1.1, which shows the scientific relevance, as well as type of catalyst and characterization methods used:

1. Catalyst stability and resistance to different contaminants in biomass affect the lifetime of the catalyst, which ultimately influences the feasibility and profitability of the process. Likewise, understanding the detailed mechanisms of complex reaction networks in tar reforming units can significantly facilitate the design of new processes and catalysts. These two considerations are the basis for the study performed in papers I–III and can be sub-categorized as follows:

    a. Combined effects of biomass-derived impurities in the gas phase under fully realistic steady-state conditions on a typical tar (steam) reforming catalyst downstream of the gasifier: this fills a gap in the fundamental understanding of the interactions of gas-phase impurities with the catalyst. The impact of gas-phase alkali on the catalyst is less well understood than that of sulfur. Although the effect of alkali may be masked by the more dominant sulfur effect, the minor effect could limit the lifetime of the catalyst over longer time scales and lead to more complex phenomena. This area is becoming increasingly important given the expanding interest in the conversion of biomass in which impurities such as alkali metals are natural trace elements. For this study, activity tests were performed in a catalytic reactor downstream of a bench scale gasification reactor and a hot-gas filter at KTH Royal Institute of Technology. A system for precise dosing of the impurities into raw producer gas was developed and integrated into the gasification system. The tar (steam) reforming catalyst used was a $Ni/MgAl_2O_4$, HT-25934,

Haldor Topsoe A/S, catalyst. During this study, several techniques were used to characterize the spent catalyst.

b. An atomistic investigation of the surface chemistry of naphthalene on nickel: this system for tar reforming has not been examined in detail from the surface science point of view. A broad combined experimental and theoretical approach was implemented to understand the chemical reaction pathway from naphthalene to possibly graphene. This study was performed in cooperation with the Dept. of Material Physics, KTH Royal Institute of Technology, Dept. of physics, Stockholm University, and Jagiellonian University. In this study, a single nickel crystal was used as the model system.

2. The steam reforming of bio-crude is in its early stages of development. Many challenges remain to be investigated before industrial application of this process, challenges such as the kinetics and mechanisms of bio-crude reforming and carbon formation, the influence of sulfur, and different process designs such as concept of using pre-reformer-reformer technology. These challenges are the basis for the study performed in paper IV. The small industrial-scale catalytic conditioning and mild treatment of pyrolysis gas was performed without having to condense out bio-crude, using an inexpensive catalyst and no addition of extra hydrogen and/or steam under fully realistic conditions. The technology was evaluated through an in-depth investigation of the chemistry taking place at the catalyst surface in real biomass pyrolysis gas. The activity tests were primarily conducted at bench-scale (KTH Royal Institute of Technology) and small industrial-scale (Cortus Energy AB) test facility. The reactor setup and bio-crude sampling system were developed during this project at KTH Royal Institute of Technology. The catalyst used for the

experiments was an Fe-based catalyst, HT-25409, Haldor Topsoe A/S. Characterization techniques were deployed to evaluate the spent catalyst as well as raw and treated bio-crude.

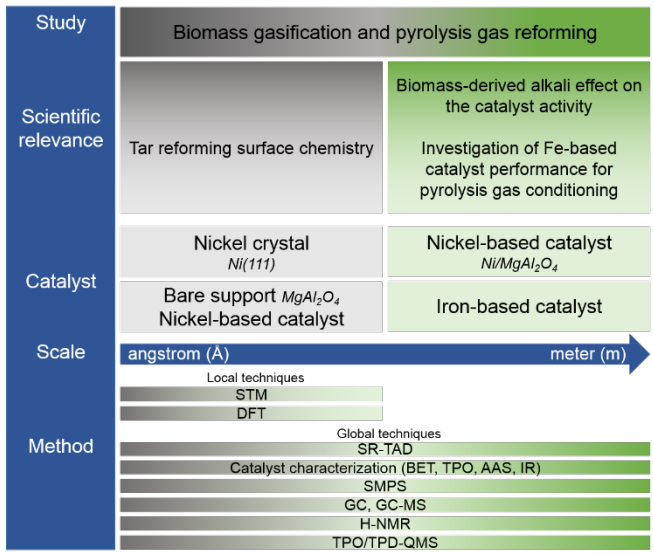

Fig. 1.1. Scope of the thesis: the scale, catalysts, and methods used. DFT and STM are local techniques at the angstrom scale. All other techniques are average (global) techniques measuring the response of many atoms/molecules.

1.2 Thesis outline

The thesis is, to a major part, based on the four appended papers and manuscripts, including unpublished results that support the findings. Following this chapter, chapter 2 gives background on the thermochemical conversion pathway to produce syngas from biomass as well as on tar reforming and bio-crude steam reforming. Chapter 3 summarizes the experimental setups, materials, and methods used in this thesis. Chapters 4 and 5 focus on the study of catalytic tar reforming and presents the most important results and discussions (papers I–III). Chapter 6 is focused on catalytic pyrolysis gas conditioning studies, performed in a small

industrial-scale test facility. It describes and discusses the most important results (paper IV). Finally, Chapter 7 summarizes the conclusions and makes recommendations for future work.

2 Thermochemical conversion of biomass to syngas

Figure 2.1 presents the overall schematic of the thermochemical pathway from biomass to syngas and further processing to secondary products. The pathway from gasification and pyrolysis to syngas is highlighted in red. The gasification route, has two main steps: the production of raw producer gas (here referred to as producer gas) and the subsequent conditioning. The two main steps of pyrolysis are the production of gas, liquid, and char and the subsequent conditioning. Sections 2.1 and 2.2 provide an overview of the biomass gasification and pyrolysis route to synthesis gas, with a special focus on catalytic tar and bio-crude steam reforming.

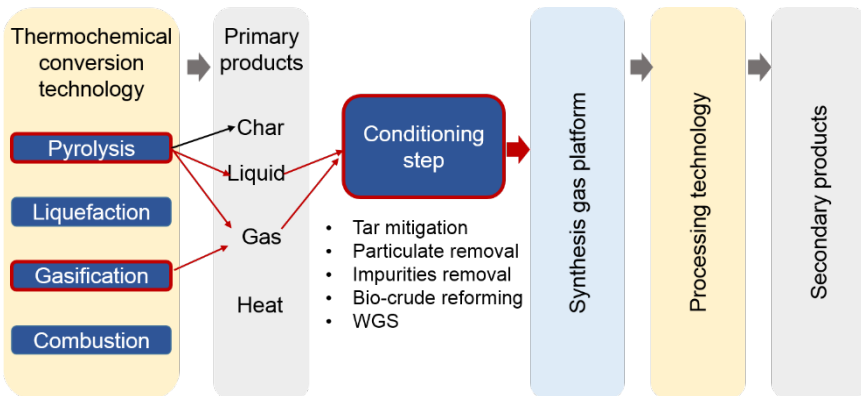

Fig. 2.1. Overall schematic: from biomass conversion to syngas.

2.1 Biomass gasification to syngas route

Gasification is the partial oxidation of the solid biomass, which ideally yields a low to medium heating-value energy gas. This gas is for direct use or further upgrading to high-value end products in industry and society. Gasification technology dates back to the end of the 18th century, and all major commercial gasification technologies made their debut from 1850 to 1940, such as Winkler's fluidized-bed gasifier in 1926, Lurgi's pressurized gasifier in 1931, and Koppers-Totzek's entrained-flow gasifier. From 1940 to 1975, many cars and trucks in Europe operated on gas from coal or biomass gasified onboard. At the same time, syngas production from natural gas and naphtha by steam reforming increased in this period. From 1975 to 2000, gasification found commercial use in chemical feedstock production besides providing gas for heating. Despite the drop in oil prices, some governments recognized the need for cleaner environments and supported biomass-fueled integrated gasification combined cycle (IGCC) power plants. [22]

Coal gasification is a well-established process in industry [23]. However, biomass gasification, due to differences in properties between feedstock, is not directly comparable to coal gasification. Producer gas obtained from biomass gasification includes larger amounts of secondary products such as light and heavy organic compounds [24], and different levels of particulates and inorganic impurities [25-27], depending on the type of gasifier and biomass feedstock. Table 2.1 shows some selected biomass and coal characteristics.

Table 2.1. Characteristics of biomass and coal [28].

	Softwood, %	**Hardwood, %**	**Bituminous coal, %**
C (daf[1])	54.9	50.8	82.3
H (daf)	6.7	5.9	5.1
N (daf)	0.2	0.18	1.5
S (daf)	0.1	0.01	0.8
O (daf)	38	43.0	10.2
Ash (ar[2])	2	1.6	7.9
Moisture (ar)	37.3	20.2	4

1) Dry ash-free 2) As received

These impurities need to be dealt with before further synthesis and upgrading. Figure 2.2 summarizes two overall pathways from the biomass gasification process to syngas: a low- and a high-temperature route in terms of gas cleaning and conditioning requirement. The low-temperature route consists of gasification technologies with relatively low gasification temperatures (800–950°C), and therefore relatively high tar contents; the reverse is true of the high-temperature route, in which high gasification temperatures (1200–1500°C) result in low or no tar contents in the gas [20, 29]. The low-temperature route generally includes a tar mitigation step outside the gasifier in addition to gas cleaning and conditioning [19, 20]. These two routes, together with gas cleaning and conditioning and tar removal, are described in more detail in the following subsections.

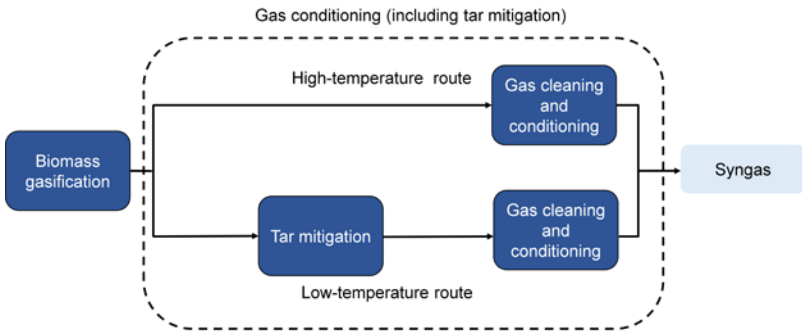

Fig. 2.2. High-temperature and low-temperature routes from biomass gasification to syngas.

2.1.1 Biomass gasification

Gasification takes place via heterogeneous and homogenous reactions by partial oxidation at high temperatures using a gasifying agent such as air, oxygen, steam, or a combination of those. This process converts the carbonaceous feedstock to a mixture of CO, H_2, CO_2, CH_4, H_2O, in some cases N_2 (if air is used), and small amounts higher hydrocarbons. The main chemical reactions taking place during the thermochemical conversion in a gasifier can be summarized as follows [20]:

$$Feedstocks \rightarrow char + tars + CO_2 + H_2O + CO + H_2 + (C_2 - C_5) \quad \text{(Eq. 2.1)}$$

(Endothermic)

$$C + \frac{1}{2}O_2 \rightarrow CO \qquad \Delta H_r^0 = -109 \text{ kJ/mol} \quad \text{(Eq. 2.2)}$$

(Partial oxidation)

$$C + CO_2 \leftrightarrow 2CO \qquad \Delta H_r^0 = +172 \text{ kJ/mol} \quad \text{(Eq. 2.3)}$$

(Reverse Boudouard)

$C + H_2O \leftrightarrow CO + H_2$ (Water gas reaction) $\Delta H_r^0 = +131$ kJ/mol (Eq. 2.4)

$CH_4 + H_2O \leftrightarrow CO + 3H_2$ (Steam reforming) $\Delta H_r^0 = +159$ kJ/mol (Eq. 2.5)

$CO + H_2O \leftrightarrow CO_2 + H_2$ (Water-gas shift) $\Delta H_r^0 = -42$ kJ/mol (Eq. 2.6)

$CO + 3H_2 \leftrightarrow CH_4 + H_2O$ (Methanation) $\Delta H_r^0 = -206$ kJ/mol (Eq. 2.7)

In case of complete carbon conversion, the composition of the raw producer gas is determined by the water-gas shift (equation 2.6) and steam methane reforming (equation 2.5) reactions [16]. The composition of the raw producer gas for a certain type of biomass depends on the gasifying agent, type of gasifier, and its operating conditions. The choice of the preferred gasifying agent depends on the desired gas composition and energy consumption. For example, steam or steam/oxygen as gasifying agent produces higher heating value product gas and higher yields of hydrogen than does air [30]. Gasification using air produces a gas low in calorific value, mainly suitable as a fuel for gas turbines or combustion in conventional boilers, not for hydrogen production or fuel and chemical synthesis [31]. Table 2.2 presents the composition range of major products in typical producer gas for an atmospheric fluidized-bed gasifier using different gasifying agents. For economical, compact and overall efficient conversion system for large scale production of transportation fuels and chemicals, pressurized gasification systems, using steam or steam/oxygen, are inevitable [20].

Table 2.2. Composition of major products in biomass gasification gas produced in an atmospheric fluidized bed gasifier for three gasifying agent [25]

Gas composition (vol-%, dry basis)	Air	Steam	Steam + oxygen
H_2	5.0–16	38–56	14–32
CO	10–22	17–32	43–52
CO_2	9–19	13–17	14–36
CH_4	2–6	7–12	6–8
C_2H_n	0.2–3	2	3–4
N_2	42–62	0	0
H_2O (wet basis)	11–34	52–60	38–61

The main challenge in biomass gasification is the formation of organic compounds referred to as tar. The term “tar” does not have a generally accepted definition [24, 32], but it often refers to the condensable fractions of organic compounds from gasification products with molecular weights greater than 78 g/mol (benzene) [24, 32]. Tar derives from the organic part of biomass through series of complex thermochemical reactions. The schematic of tar maturation as a function of temperature is shown in Figure 2.3. At low temperatures, primary tars are formed. With increasing temperature, tar transforms into secondary and tertiary tars. According to Milne et al [24], primary tars thermally crack into CO, H_2, and other light gases before tertiary products appear. The tertiary products are usually more refractory and more difficult to decompose than primary and secondary tars. The tar composition produced based on the gasification temperature was reported by Huber et al. [33]. Tars can also be classified based on their appearance or molecular weight [34]. Tar sampling and analysis is preformed off-line and on-line. Traditional offline methods are the tar protocol [35] and solid phase adsorption (SPA) [36]. There are a number of recent online methods for tar analysis in biomass gasification [37, 38], some of which are still under development [39].

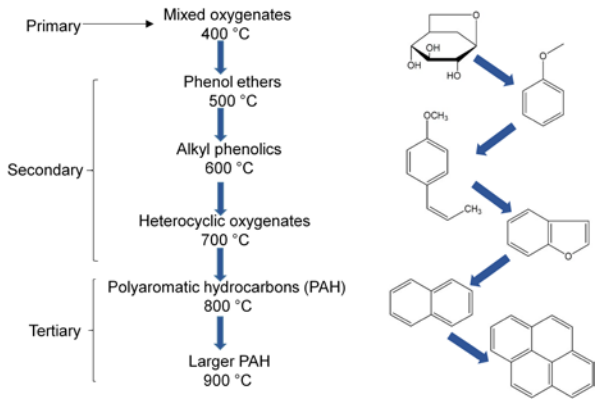

Fig. 2.3. The tar maturation scheme; adapted from Ref. [40].

According to Milne et al. [24], a very crude generalization of tar level produced by different gasifiers is in the range of 1–100 g/Nm^3, where in general terms, fluidized bed gasifiers are in the low to intermediate range (5–75 g/Nm^3), consisting a mixture of secondary and tertiary tars [24, 33, 41]. Fixed-bed updraft gasifiers yield high tar content, mainly consisting of primary tars, while fixed-downdraft gasifiers are the cleanest technology and the tars produced are almost exclusively tertiary tars [19, 33].

The concentrations of gas impurities vary, depending on the type of gasifier as well as the feedstock characteristic. The ranges of impurities for particulates is 5–30 g/Nm^3 [29]. Particulates consist of unconverted biomass material in the form of ash (i.e. the mineral components of the biomass), char, and bed material in the case of fluidized-bed gasification. Torres et al. [25] noted a range of 1000-14000 ppmv (db) for NH_3, while NH_3 values of 500–3000 ppmv (db) are more representative when woody biomass is used [42]. The sulfur, chlorine, and nitrogen compound contents in the gas phase appear well correlated with the composition of the biomass and gasification conditions [25, 27]. For both S (mainly H_2S and some COS) and Cl (mainly HCl) compounds, the impurity levels in the biomass producer gas are generally 20–200 ppm volumetric (ppmv) on a dry gas basis (db) [25]. Typical gas-phase K-species levels are around 0.01–5 ppmv (db), with one case reported as high as 25–30 ppmv [26, 27, 43-45].

The high-temperature gasification route, shown in figure 2.2, includes, for instance, fixed-downdraft gasifiers, with concurrent flows of gases and solids through a descending packed bed, and entrained-flow gasifiers, with the co-feeding of powder feedstock and oxidant in down-flow “spray”, yielding relatively small amounts of tar due to a high gasifier temperatures. However, the higher gas temperature in entrained-flow gasifiers (1200–1500°C) promote ash melt conditions (slagging), problems with construction materials selection, and also soot formation [30]. Feeding powdered biomass is problematic in entrained-flow gasification and biomass milling and preparation can be cumbersome. Biomass is not suitable to be directly fed to this type of reactor. Due to short residence times of the entrained-flow reactors require a small particle size to ensure full gasification of the char. In the case of downdraft gasifiers, although the product gas has lower tar and particulate contents, physical limitations and particle size relation makes it difficult to scale-up the technology [29, 30], rendering it unsuitable, for example, for large-scale syngas production and further upgrading to fuels and chemicals.

The low-temperature gasification route, shown in figure 2.2, includes, for example, fluidized-bed and fixed-updraft gasifiers. In a fluidized bed, all the reactions take place in a fluid bed, in which solid bed particles behave as a fluid through contact with a gas with a sufficient high gas velocity [20], whereas in an updraft gasifier, the gasifying agent is added at the bottom and the downward-moving feedstock is first dried by producer gas, then pyrolyzed, and the remaining char is finally gasified. Tar is either condensed out on the cool descending fuel particles or be carried out of the reactor with producer gas, thus contributing to its high tar content [30]. The tar content in the product gas is very high and the condensed-out tar is generally recycled back [30]. Fluidized-bed gasifier exit temperatures are typically 800–900°C. Therefore tar is not condensed out in the exit gas but still needs to be handled prior to syngas utilization. In co-firing applications, the problem with tar can be avoided by maintaining the gas at a temperature above the dew point of the tar. On the other hand, the content of tar in fluidized bed gasification gas is well above the maximum content allowed for gas turbines and diesel engines that prohibits the direct

utilization of the gas stream and thus also for syngas applications [24, 29]. Fluidized bed biomass gasification is well-known for being flexible regarding feedstock requirement compared to entrained flow gasification [17] and for larger-scale biomass gasification, with long operation hours, delivering raw synthesis gas that has been converted to pure synthesis gas, the choice of technology has been fluidized bed gasifier [17]. Besides handling of tar, particulates and impurities must be handled as well. The level of particulates are higher in fluidized-bed gasifier than fixed-bed gasifiers [29]. The greater part of fuel alkali is retained in the gasifier ash and bed solids in the case of fluidized bed gasifiers. However, the gas containing alkali metal compounds in their vapor state may cause problems in downstream processing units. The technology for fluidized bed gasification is already demonstrated with biomass for production of heat and/or electricity [20]. Some of the examples for biomass fluidized bed gasification are Lurgi circulating fluid-bed (CFB), Foster Wheeler CFB, TPS process of TPS Termiska Processor AB for ARBRE IGCC project, Repotec gasifier in Güssing, Carbona process, fast internally circulating fluid-bed (FICFB)-Austria, and GoBiGas in Gothenburg, Sweden [17, 46, 47].

2.1.2 Gas conditioning

Gas conditioning refers to removing undesired impurities from biomass gasification gas that usually involves multi-step, integrated approach and it may also include WGS process for hydrogen production. Gas cleaning and conditioning, including tar abatement, have been among the challenges of biomass gasification processes, and one promising pathway is based on hot-gas cleaning and conditioning, the basic idea of which is to process the raw gas at high temperatures (above 500°C) to destroy the tar and also remove particulates. Hot gas conditioning for tar mitigation downstream of gasifiers may be used in combination with primary tar mitigation techniques, such as using catalytic bed materials, in case of fluidized bed gasification, and additives as well as optimizing operational conditions [48]. In this section, the focus will be on tar mitigation and particulate removal techniques.

2.1.2.1 Tar mitigation and gas clean-up

High content of tar can lead to many operational difficulties, such as condensation at temperatures below 350–400°C, plugging of pipes and equipment, as well as the formation of carbon deposits on catalysts in downstream processing, even at very low concentrations [19, 49]. The accepted levels of tar in the conditioned gas should also be compatible with user-end applications [25].

There are several tar mitigation techniques such as scrubbing, catalytic cracking, thermal cracking (e.g. via partial oxidation), and plasma treatment [19, 24, 25, 50]. If the end use of the product gas requires near ambient temperatures, removal techniques such as wet scrubbing and filtration is feasible. No severe heat penalty (i.e., from cooling and re-heating) is incurred, so overall efficiency is unaffected. Wet scrubbing technology is available and can be optimized for tar removal.

Cracking involves breaking molecules into small ones and in the case of tar, conversion into permanent gases [22]. Secondary hot gas cleaning via the catalytic steam reforming of tar was early on recognized to be one of the most efficient mitigation methods [19], improving carbon efficiency by converting tar to syngas components. This catalytic conversion technique considerably reduces wastewater treatment requirements compared with wet scrubbing. A more recent wet scrubbing technique (OLGA) uses oil to scrub tars and the oil and tar can get re-circulated to the gasifier, recovering the energy in the tar [51]. The disadvantage of this method is the need for cooling the gas prior to cleaning, decreasing the efficiency of the process. Catalytic steam reforming can also be thermally integrated with the gasifier exit gas temperature, for example catalytic steam reforming of hydrocarbons is well-suited for the 800–900°C temperature range [52-57], typical of fluidized-bed gasifier exit temperatures [32]. This allows for the tar mitigation process at temperatures close to those of the gasifier exit. Catalytic tar reforming is usually carried out in a separate fixed bed reactor downstream of gasifiers, operating under different process conditions than gasification unit [24, 32]. Additionally, steam can be added to ensure complete tar reforming [19] . A thermal cracking is also a hot gas

conditioning process, but it is energy intensive due to the high temperatures (>1100°C) required to achieve high conversion efficiencies. Thermal cracking also produces soot which is an unwanted impurity [58]. The difficulties of achieving complete thermal cracking together with operational and economic considerations, often makes this route an unattractive option [30]. Plasma treatment also suffers from high energy requirement throughout the whole process and high operating and investment costs for large-scale biomass gasifiers [25].

In terms of particulate removal, the fine carbon-containing ash particles are difficult to remove in cyclones. Filters are applied for separating the particulates from the gas which may cause erosion and plugging in downstream process equipment [32]. A barrier filtration method either using a baghouse (woven ceramic, polymeric or natural fibers) at low temperatures below 350°C or metallic or ceramic candle filters, suitable for moderate to high temperatures up to 700°C are therefore employed [15]. Alkali and heavy metals can also be removed using barrier filters after cooling the gas below alkali condensation temperature (i.e. 650°C) [15]. Some issues related to filtration can be addressed by cooling the gas and lowering the gas velocities through filter [30]. However, temperatures should not be allowed to fall below the condensation temperature of tar (350-400°C) , which may lead to condensation of tar in dust cake and stickiness of dust [59]. Therefore, tar must be either removed before gas filtration (via dusty tar reforming), or hot gas filters with high temperatures must be used to remove particulates. In the latter case, at temperatures higher than 600°C, filter blinding may occur, resulting in pressure drop across the filter [60]. Furthermore, if a hot gas filter is used to remove particulates, the impurity levels will also depend on the filtration conditions including the temperature, as well as on the chemical and physical properties of the dust particles collected in the filter cake [26, 61, 62]. Phenomena such as gradual buildup of the cake on the filter can have complex sorption effects that influence the levels of impurities reaching downstream units [26, 61-64].

Figure 2.4a shows a schematic view of the biomass gasification to syngas via two routes, dusty and clean tar reforming. Tar reforming in a dusty gas

(gas with particulates) is referred to as “dusty” and tar reforming carried out in a gas nearly free of particulates is referred to as “clean” tar reforming. A monolith catalyst is used in dusty tar reforming, whereas monolith or pelletized catalysts can be used in clean tar reforming.

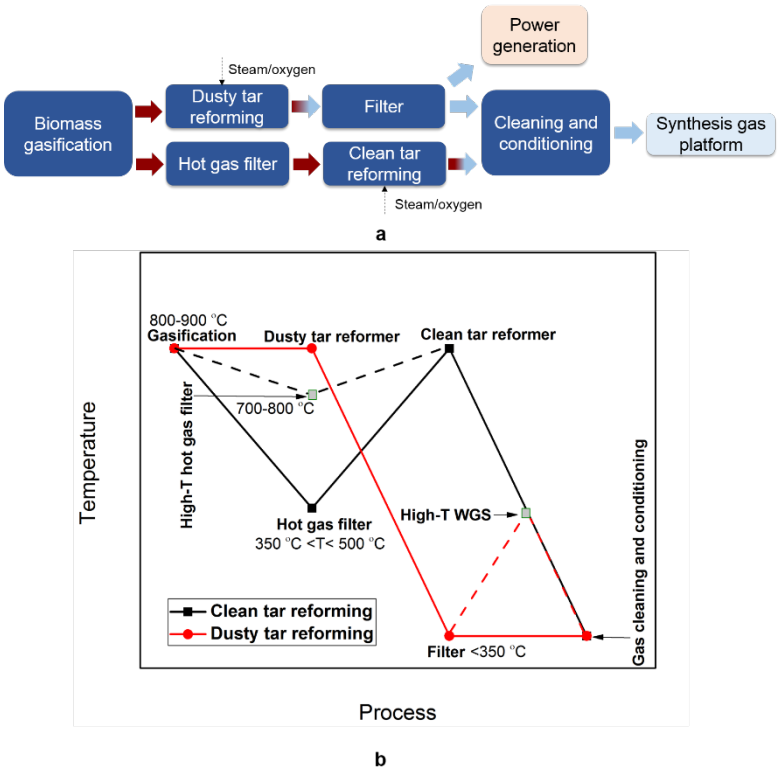

Fig. 2.4. a) Biomass gasification to syngas via “dusty” and “clean” tar reforming. b) Temperature changes in the dusty and clean tar reforming routes.

Dusty tar reforming was fully commercially developed for synthetic natural gas (SNG) and power/heat production[17], and the catalyst is dust robust, preventing fouling issues since the monolith catalyst allows dust to pass through the channels [17]. The disadvantages of dusty tar reforming are a lower density of active materials and the exposure of the catalyst to impurities (e.g. silica and volatile alkali) that affect catalyst performance.

Clean tar reforming, on the other hand, was developed for chemical and fuel production applications [17]. In case of using monolith, there is lower density of active materials, whereas the disadvantage of clean tar reforming over a pelletized catalyst is sensitivity to dust and subsequent fouling and pressure drop issues. As shown in figure 2.4b, since the hot gas filter temperature ranges from well below to near the tar reformer temperature, there is a heat penalty lowering the efficiency of this route. In this case, it may be necessary to feed oxygen together with steam to the reformer to increase and achieve target operation temperature. An autothermal (steam) reforming (ATR), in which oxygen is added to a combustion zone before the catalytic reactor, may be a better choice of technology, taking into consideration the scale of operation and diameter of the reformer reactor. Another option for reformer in clean tar reforming is the staged reformer concept, developed by Simell et al. [59], in which the first stage (pre-reformer) operates at partial oxidation (POX) mode to decompose soot-forming light hydrocarbons, followed by a final reformer stage operating at ATR mode.

The trade-off in using the clean tar reforming route is between efficiency and impurity removal: if a well-below tar reforming temperature path is chosen, as indicated in figure 2.4b by black lines, most of the alkali and other impurities is condensed out in the filter but this pathway imposes a heat penalty, lowering the process efficiency. On the other hand, a near reformer temperature choice for hot gas filter, decreases the heat penalty at the expense of exposing the catalyst to for example higher levels of alkali compounds. Particulate removal in near tar reformer (gasifier exit) temperature, as indicated in figure 2.4b by dashed black line , is also a challenge considering the corrosion and material fatigue problems occurring at high temperatures for hot gas filters with the gas containing different impurities [20]. This area, calls for introduction of novel technologies such as higher degree of process integration (i.e. integration of catalytic tar cracking in a barrier filter), as well as better understanding of filter blinding mechanism [14, 59, 62, 65].

There are demo- and industrial-scale example of both dusty and clean tar reforming, as shown in table 2.3 together with the composition of the tar

reformer exit gas [17, 66]. Dusty tar reforming concept is also used in Kokemäki biomass gasification-based CHP plant [67]. No hot gas filtration technology in the range of 400–800°C was available for Skive and Kokemäki at the time of basic engineering of these plants. For this reason, the reformers were built on a massive scale so it can handle the high particle load [68].

There are other instances in which other tar mitigation techniques have been used downstream of fluidized-bed gasifiers. For example in the Göteborg Energi 20MW bio-methane GoBiGas plant in Gothenburg, Sweden, rapeseed methyl ester (RME) scrubber is used to remove the bulk of the tar, followed by regenerative carbon filters to remove the remaining light tars [18, 47].

Table 2.3. Dusty and clean tar reforming at the demo- and industrial-scales [17, 66].

	Skive-Denmark	**GTI-Chicago**
Gasifier	Bubbling fluidized-bed, air-blown, 1–3 barg	Bubbling fluidized-bed, oxygen-steam (+CO_2) blown, 6–9 barg
Application	Combined heat and power, gas engines	Gasoline synthesis
Tar reformer	Dusty	Clean
Operation	since 2009, tar reformer revamp in 2014	1200 h
Inlet gas temperature, °C	850–930	750–950
Inlet H_2S level, ppmv	40	30–160
Tar reformer exit gas composition Major components, vol %		
N_2	40	<0.5
CO	20	16
CO_2	12	30
H_2	14	18
CH_4	4	1
H_2O	10	36

2.1.2.2 Water-gas shift (WGS)

Raw synthesis gas needs to be adjusted depending on its user-end application. Biomass gasification gas typically has an H_2/CO ratio lower than 2, which needs to be adjusted to the stoichiometry of synthesis reactions. H_2/CO ratio can be increased by means of a water-gas shift (WGS) reaction. After steam reforming step, the conditioned gas

undergoes high-temperature (HT) (350–500°C) or/and low temperature-(LT) (around 200 °C) WGS reactions. An Fe-based catalyst is typically used as the HT WGS catalyst. Thermodynamically, it is preferable to operate at low temperatures but the Fe-based catalyst is not sufficiently active at temperatures of approximately 200°C. However, this choice of catalyst is inexpensive, resistant to sintering, and has a certain sulfur-tolerance [3]. High-activity Cu-based catalysts are the choice for LT WGS and are used after HT WGS to further convert CO. Cu is highly sensitive to sulfur poisoning [3]. If the desulfurization step is installed after WGS step, due to sulfur content in syngas, Cu-based catalysts are not an option. Due to low sulfur content of biomass gasification gas, high-temperature iron-based WGS catalysts may be used for WGS. Due to the low sulfur content in product gas, sulfur-resistant catalysts such as Mo-sulfide and Co-sulfide, are limited to low temperature since they otherwise participate in hydrolysis or hydrogenation reactions and loose activity [3, 17]. Therefore, if several shift reactors are required, a combination of low and high temperature WGS catalyst may be needed downstream of dusty/clean tar reforming to achieve the desired H_2/CO ratio.

2.1.2.3 Removal of other impurities and trace components

Besides the tar abatement, particulate removal, and WGS, the producer gas must be further cleaned and suitable for downstream devices [26, 69]. The accepted levels of these impurities depend on the syngas application. For example, the accepted sulfur level for energy production in gas turbines is less than 20 ppmv, whereas for chemical processes (e.g. Fischer-Tropsch synthesis) the sulfur level is limited to less than 0.01 ppmv. Compounds such as COS and HCN are converted via hydrolysis to H_2S and NH_3. H_2S, NH_3, HCl, alkali, and alkaline metals are removed by means of sorbents at low temperatures [70-72]. An alternative for abatement of H_2S is mixed metal oxides [25].

After the steps mentioned, the syngas only contains trace amounts of poison. There are few industrial instances of final gas purification downstream of biomass gasification process and the summary of some examples can be found in Andersson et al. study [17].

2.1.3 Catalytic (steam) tar reforming

Catalytic tar reforming has been recognized as an attractive hot gas conditioning method that mitigates tar with lower heat penalty than the low-temperature scrubbing, high-temperature cracking, or plasma technologies previously described. As described in previous sections, there are two types of tar reforming, dusty and clean, referring to raw producer gas with and without particulates. This section briefly describes the kinetics and mechanisms of catalytic (steam) tar reforming, as well as the choice of catalyst and the effects of sulfur and potassium on the performance of nickel-based catalysts.

2.1.3.1 Kinetics and mechanism

Catalytic tar reforming can be divided into dry or wet reforming as shown in reaction 2.8 and 2.9. For syngas applications intended for hydrogen-rich gas production, wet reforming using steam is preferred. Tar (steam) reforming involves the oxidation of tar compounds, using steam to produce hydrogen and carbon oxides, and the reaction pathway can be described as follows [34, 73]:

$$C_xH_y + xH_2O \rightarrow xCO + (x + \frac{y}{2})H_2 \quad \text{Steam reforming} \qquad \text{(Eq. 2.8)}$$

$$C_xH_y + xCO_2 \rightarrow 2xCO + \frac{y}{2}H_2 \quad \text{Dry reforming} \qquad \text{(Eq. 2.9)}$$

Equations (2.5), (2.6), and (2.7) are also important to consider.

The extents of these reactions are dependent on the operating conditions. All tars are converted into CO and H_2 in an irreversible steam reforming reaction, whereas steam, carbon monoxide, and carbon dioxide reach thermodynamic equilibrium. If the final desired product is synthetic natural gas (SNG), one might want to limit methane steam reforming. The competing heterogeneous reaction for the steam reforming of tar is carbon formation [73], as will be described further below.

In general, the mechanism for the steam reforming of hydrocarbons is that the hydrocarbons dissociatively adsorbs on the metal, forming C_XH_Y species, while the steam dissociatively adsorbs on the support or on the metal, forming OH-species, that then react at the interface of metal and support with the C_XH_Y species, and finally forming CO, CO_2, and H_2 [74, 75]. In methane steam reforming, it has been shown that the mechanism proceeds as described above for hydrocarbons [75]. In catalytic steam tar reforming, one of the proposed mechanisms by Kaewpanha et al. [76] is that tar molecules are broken down to lighter molecules and reformed to syngas on the active sites as shown in figure 2.5, step 1 and 2, and at the same time, tar molecules are decomposed and formed radicals on the surface, generating coking on the catalyst (figure 2.5, step 3).

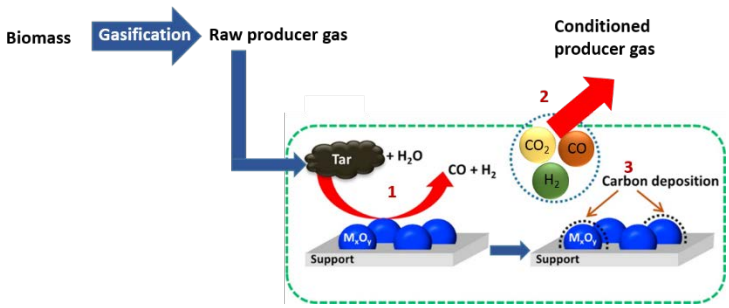

Fig. 2.5. Proposed mechanism for catalytic steam tar reforming over a metal oxide catalyst, adapted from Ref. [76].

Kinetic models of tar reforming are mostly simplified by selecting model compounds such as toluene and naphthalene, or by considering the catalytic tar removal as a single reaction, in which all tar components are treated as one group, removed by several simultaneous reforming and cracking reactions [77-79].

Recent surface science related experimental and theoretical studies have described the mechanism and structural detail of hydrocarbon and aromatic compounds dehydrogenation [80-82], which can be associated with mechanisms involved in catalytic tar reforming on active metals. For instance figure 2.6 shows a proposed mechanism for five elementary steps

of the naphthalene catalytic chemical reaction pathway into graphene, based on molecular dynamics modeling [82]. Altogether, the mechanism for the steam reforming of heavy tars is still unclear and the proposed mechanisms are not generally close to realistic conditions.

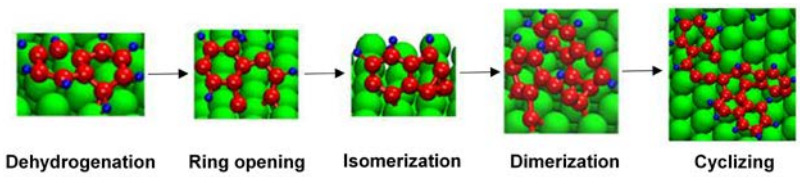

Fig. 2.6. Five elementry steps from naphthalene to graphene formation on nickel catalyst; adapted from Ref. [82].

2.1.3.2 Catalysts

The fundamental features of an effective catalyst for tar removal are tar removal activity, methane steam reforming for production of syngas molecules, resistance to coking and sintering, easy regeneration, robustness and low cost [33, 58]. Several different catalysts, synthetic as well as mineral-based, exist for catalytic tar conversion. Transition metals are considered good catalysts for the steam and dry reforming of methane and hydrocarbons. Although Rh-, Ru-, Pd-, and Pt-based reforming catalysts outperform Ni in terms of activity, due to its favorable cost-to-activity ratio, Ni-based catalysts continue to be the most frequently studied materials for steam reforming downstream of biomass gasifiers [19, 25, 32, 50, 58, 83]. Some recent studies have also investigated the synergetic effect of the combination of active nickel and other metals, such as cobalt, and all the results indicated that with the optimum compositions of active metals, the performance of bi-metallic catalysts was higher than that of monometallic Ni catalysts in terms of activity in the steam reforming of biomass tar [84-86]. These studies are recent and the application of such catalysts are still under development.

2.1.3.3 Nickel-based (steam) tar reforming

Ni-based catalysts for tar reforming downstream of gasifiers are exposed to particulates and a number of inorganic trace components, such as alkali, sulfur, phosphor and chloride species, as well as other trace elements [25-27, 87]. As mentioned earlier, the level of inorganic impurities in the biomass gasification gas depends on several parameters, such as the gasification technology employed, the process conditions of the given gasifier, the type of biomass, and the choice of technology for gas cleaning upstream of the catalytic reactor. Important issues concerning nickel catalyst performance and life time in steam reforming are briefly described in the next section.

2.1.3.3.1 Main challenges

The main challenges of nickel catalysts in steam reforming that affect the activity of catalyst have been recognized to be sulfur poisoning, carbon formation, and sintering, all of which are interconnected [53].

Sintering: In the process of sintering, fewer and larger metal particles are formed either by Ostwald ripening or cluster migration coalescence. Sintering affects catalyst activity, sulfur poisoning and carbon formation. The coking limits are affected by the nickel particle size, the nickel surface area determines the sulfur capacity, and the activity is related to nickel particle size. Sintering is primarily caused by the elevated temperature, high metal loadings or high H_2O partial pressures [53]. For the steam reforming of $Ni/MgAl_2O_4$, catalyst thermal sintering is typically significant for the first 200 run hours of operation, and generally levels off to fairly low sintering rates after approximately 500–600 hours [53, 88].

Carbon formation: Carbon formation may increase the pressure drop, crush the catalyst, and block active sites. Therefore, the limit for carbon-free operation is important [2] . Three types of carbon formation have been observed in reformers: pyrolytic, gum, and whisker carbon. Pyrolytic and whisker carbon formation are problematic at high temperatures and gum carbon formation at low temperatures [2]. The temperature window in which carbon-free operation occurs increases with an increasing

steam-to-carbon ratio [2]. Whisker carbon is the most destructive type of carbon and a major problem for steam reforming; its formation is thermodynamically limited in the case of equilibrated gas but it can also be kinetically formed from higher hydrocarbons [2]. In summary, using the principle of equilibrated gas (thermodynamics), one can predict whether there is an affinity for carbon formation in methane steam reforming, while using principle of actual gas (kinetics), one can say if the operation is in the no-carbon formation zone. For hydrocarbons higher than methane, it is shown that the rate of carbon formation depend strongly on the type of hydrocarbon (figure 2.7) [89] and for aromatic compounds, it is known that the tendency toward coke formation grows as the molecular weight of the aromatic compounds increases [73] .

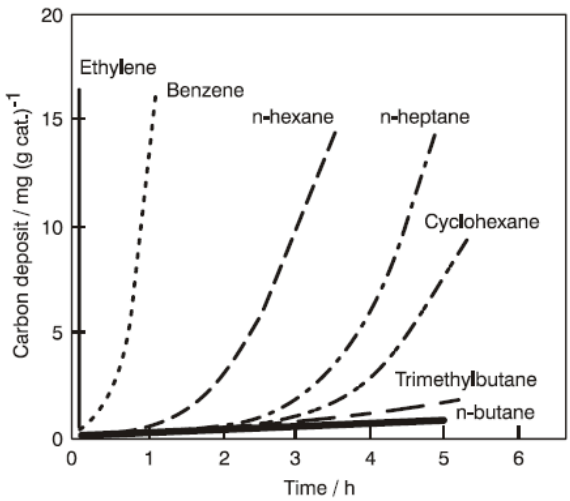

Fig. 2.7 Rate of carbon formation for different hydrocarbons (H_2O/C= 2 mol/atom, 1 bar, 500 °C) [89]. Reproduced with the kind permission of Dr. Jens Rostrup-Nielsen.

Impurities: Whereas Cl and NH_3 do not seem to affect the reforming performance of the Ni catalyst [90, 91], other impurities such as sulfur and alkali compounds play an important role in the activity of tar reforming nickel-based catalysts. Based on chemisorption of H_2S on different catalytic metals at the, nickel is the most sensitive metal to sulfur compared

to other metals with the following order in terms of Gibbs free energy of formation, ΔG^{o} ($kJ/\frac{1}{2}$ mol S_2): Ni > Ir > Co > Ru > Cu > Fe> Pt [92]. Therefore, the sulfur adsorption capacity of nickel under reforming conditions is an important parameter. Adsorption isobar data were published by Alstrup et al. [93] for determining the sulfur coverage at different temperatures, and sulfur chemical potentials in gas and are shown in figure 2.8.

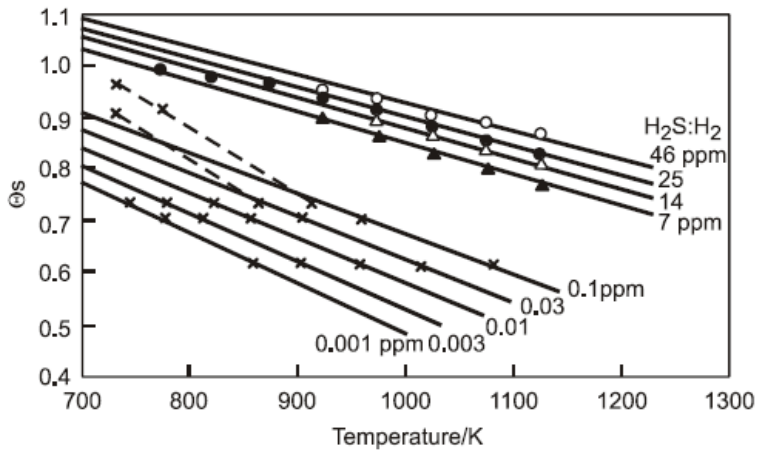

Fig. 2.8. Sulfur adsorption isobars [93].

Figure 2.9 shows the specific activity of Ni-based catalyst and the impact of sulfur on the catalyst activity. The rates are compared by referring to free nickel surface using a Maxted model for poisoning [94]. The intrinsic rate of poisoned catalyst (R_{sp}) is around two order of magnitudes less than of the rates for non-poisoned catalyst (R^{0}_{sp}) [2].

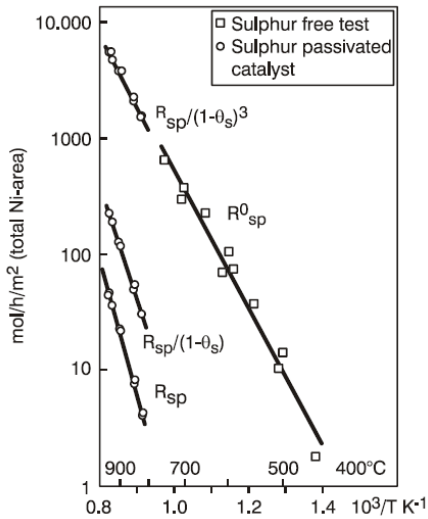

Fig. 2.9. Impact of sulfur on reforming reactions [94].

The sulfur coverage distribution in a reformer is complex due to axial and radial changes in temperature and hydrogen partial pressure. Although, the chemisorption of sulfur on nickel is very rapid, diffusion restrictions are present in industrial reactors, so a sulfur gradient exists in catalyst pellets and the diffusion limitations have complex effects on the transient sulfur profiles. The sulfidation of the catalyst particles progresses in a profile from the outer shell toward the center of the particle, as well as in a front moving through the catalytic bed [95].

Nevertheless, sulfur tends to retard the formation of whisker carbon above certain coverages [2, 53, 94, 96]. Table 2.4 shows the result of a study in which a series of experiments was performed with different sulfur contents in gas at conditions in which carbon formation was predicted [95]. The results indicate the existence of a threshold content of sulfur below which carbon formation occurs. Sulfur-passivated reforming (SPARG) process was developed from relevant fundamental and pilot-scale studies [97].

Table 2.4. Series of bench-scale tests for sulfur passivated reforming: optimum sulfur content below which carbon formation occurs, T_{in}= 793 K, feed flows for H_2O, H_2, CO, CO_2, and CH_4 were fixed; adapted from Ref. [95].

Experiments	No.1	No.2	No.3	No.4
H_2S, ppmv	1	5	14	28
CH_4 (dry exit), %	-	0.36	0.7	0.71
Carbon formation	yes	no	no	no

Sulfur-passivated reforming studies by Jens Rostrup Nielsen [94] revealed that the stronger dependence of the coking rate on sulfur coverage than on the reforming rate is the result of the larger number of sites needed for carbon formation than methane steam reforming [94]. As sulfur coverage increases, the potential for carbon formation decreases on sulfur-passivated catalysts than on sulfur-free catalysts [94]. Sulfur-passivated methane steam reforming is shown in a simple schematic in figure 2.10 for three different cases. Case 1 is for low sulfur coverage, in which both steam reforming and carbon formation occur. Case 2 describes a scenario in which sulfur coverage is a monolayer (θ_s=1), leading to full catalyst deactivation. The optimal case is number 3, where steam reforming prevails with no whisker carbon formation due to the partial sulfidation of nickel. In a study by Koningen et al. [98] , sulfur-passivated methane steam reforming in the biomass producer gas was possible without carbon formation. The point here is that at temperatures above 800°C and typical H_2S levels in biomass gasification gas, the nickel surface is not completely covered with sulfur and still has significant steam reforming activity.

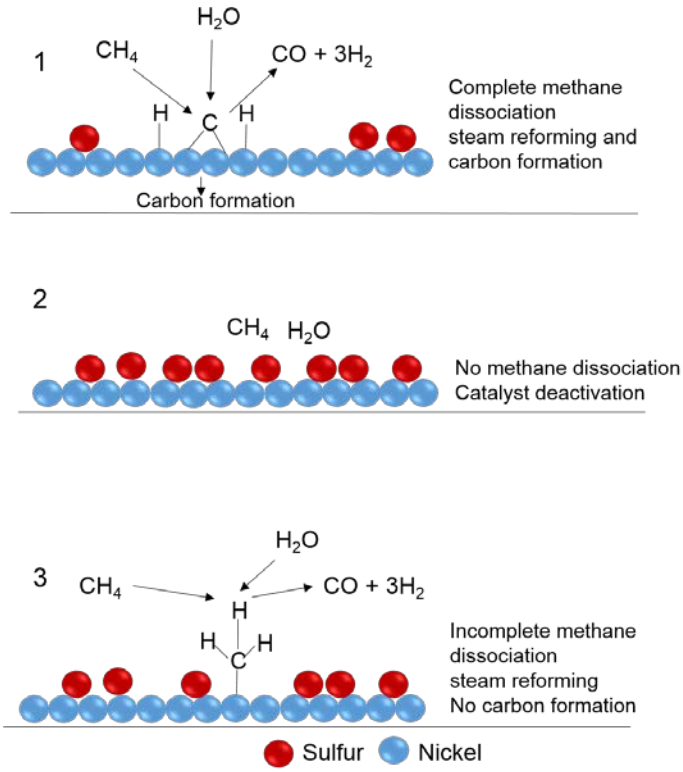

Fig. 2.10. Schematic of sulfur-passivated methane steam reforming on a Ni catalyst, based on the work published by Jens Rostrup-Nielsen [94, 99]. Reproduced with the kind permission of Dr. Jens Rostrup-Nielsen.

An alternative explanation for why sulfur passivation retards whisker carbon formation was presented by Bengaard et al. [100] DFT calculations, indicating that the lowest energy barriers for methane reforming are on the step sites rather than the terraces, suggesting the step sites to be more active toward methane reforming. It was demonstrated that the stronger binding of sulfur to step sites and the fact that carbon nucleates only at step sites explain the decrease in carbon formation rates with increasing sulfur coverage. However, the authors also mentioned that rate of methane reforming may be controlled by terrace sites rather than step sites at the high temperatures of steam reforming [100].

Potassium in K-promoted nickel catalysts increases the resistance to carbon formation [2, 101]. Bengaard et al. [100] demonstrated that the step site blocking effect of potassium promotes the catalysts in terms of higher tolerance toward carbon formation. However, it was also demonstrated that potassium, above a certain threshold concentration, decreases the steam reforming activity [2, 53]. Potassium may also constrain hydrocarbon C–H bond dissociation [102]. Optimally, catalysts promoted with sulfur and potassium will have just enough additives to block coke formation and still proceed at sufficient reaction rates [100]. Very few studies examine the effect of gas-phase alkali on tar reforming catalysts [56, 57, 91, 103]; in summary, these studies observe a general deactivation of reforming reaction and loss in the surface area of nickel. Nevertheless, a limitation in all these studies is the method used to investigate the influence of K on catalyst, which is different from actual mechanisms of potassium transport, deposition and equilibration on the catalyst [91]. In addition, few of these studies were performed under exposure to real producer gas from biomass [103], as well as none were investigated under realistic steady-state conditions [56, 57, 91, 103].

2.2 Biomass pyrolysis to syngas route

Another interesting possibility, as shown earlier in section 2.1, is to convert biomass via a pyrolysis process. Pyrolysis is the thermochemical decomposition of organic matter in the absence of oxygen, which converts biomass into char, gas, and liquid known as bio-oil or bio-crude [104] [105-108]. There are several examples of pyrolysis reactors in demonstration- and industrial- scale around the world [109]. Char, gas, and bio-crude from biomass pyrolysis can be utilized for different applications as shown in figure 2.12. Gases can be used to be combusted and provide energy for the pyrolysis process [33]. The char can be combusted to provide energy, or be used as for example soil amendment and activated carbon [110]. Bio-crude is considered a platform feedstock that can be converted via hydrodeoxygenation (HDO) into liquid hydrocarbon products or to synthesis gas by steam reforming.

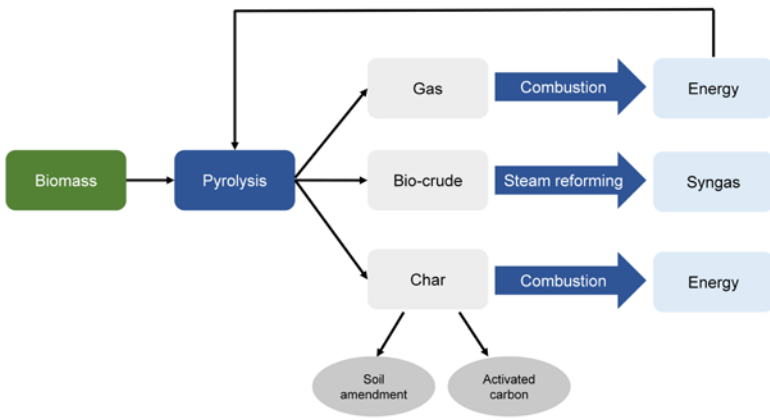

Fig. 2.11. Biomass pyrolysis route to syngas; adapted from Ref. [21].

The pyrolysis bio-crude, i.e., the liquid condensate consisting predominantly of oxygenated organic compounds (oxygenates), is problematic to handle and exploit, so oxygenates must be removed/converted. HDO and steam reforming of bio-crude industrial implementation is limited due to severe coking and deactivation of the

catalytic processes as well as carbon laydown and catalyst deactivation due to troublesome oxygenate compounds (e.g. heterocycles, phenols, and methoxy phenols) [21]. Section 2.2.1 and 2.2.2 present a brief overview of biomass pyrolysis and bio-crude steam reforming and describe, from a process perspective, a possible process technology to overcome the mentioned disadvantages of the steam reforming of bio-crude.

2.2.1 Biomass pyrolysis

Biomass pyrolysis can be divided into conventional or slow pyrolysis, intermediate pyrolysis, and fast/flash pyrolysis (table 2.5). This somewhat arbitrary classification, is mainly related to the strong effect of the heating rate on product distribution. Generally, lower process temperature and long vapor residence time increase the char yield, whereas high temperature and long residence time increase the gas yield. Moderate temperature and short vapor residence time favors production of liquids. Fast pyrolysis is of particular interest due to its high yields of liquid (bio-crude), which can be used in various applications [110].

Table 2.5. Temperature ranges and heating rates for slow, intermediate, and fast pyrolysis [111].

Type of pyroysis	**Slow**	**Intermediate**	**Fast**
Temperature, K	550–950	500–650	850–1250
Heating rate, K/s	0.1–1.0	1.0–10	10–200

The biomass pyrolysis mechanism is not well understood. Nevertheless, details of reaction involved in biomass pyrolysis pathways for cellulose, hemicellulose, and lignin are available in several reviews and studies [112, 113]. Bio-crude can be produced in different types of reactors ranging from entrained-flow to ablative and fluidized bed systems. It consists of many different oxygenate compounds, with distribution among them varying

depending on type of feedstock and the pyrolysis operating conditions [110].

The complex nature of bio-crude requires several analytical techniques for complete characterization such as GC-MS HPLC, GPC and FTIR [110]. The average composition of bio-crude from softwood together with typical properties of bio-crude can be found in table 2.6. The bio-crude has higher energy density than biomass and is therefore more fit for transport as the transportation cost will be much lower compared with biomass [114]. It is important to know the chemical composition of bio-crude since it gives insight into the type of downstream processing is needed. A high content of oxygen in bio-crude results in low heating value, high acidity, and instability [21]. The sulfur content of bio-crude is much lower that of fossil crude oil, but as it is non-negligible, it may still be problematic for downstream catalytic processes and thus needs to be handled.

Table 2.6. Typical properties of bio-crude and average composition of bio-crude from softwood mixture [21, 115].

Composition	Softwood mixture	Property	Typical values
Water, wt%	30–35	Moisture, %	20–30
Acids, wt%	3–27	pH	2–3
Others, wt%	2–27	C, wt% db	56.00
Sugars, wt%	4–7	H, wt% db	7.00
Phenols, wt%	1–3	O, wt% db	37.00
Lignins, wt%	13–32	N, wt% db	0.10
PAH, wt%	3	Ash, wt% db	0–0.2
		Viscosity, cP	40–100
		Particulates, wt%	< 0.3–1

db: dry basis cP: centipoise

2.2.2 Bio-crude steam reforming

Bio-crude steam reforming produces syngas which can then be converted into a range of fuels. One of the applications for this technology would be to have number of small plants that produces bio-crude, which then is transported to a large central bio-refinery where bio-crude is converted into syngas and the desired final product [116]. Steam reforming of bio-crude is an extension of a well-established technology for steam reforming of fossil fuels. For full conversion of bio-crude, temperature range between 600–800°C is needed, depending on the other operating conditions [21]. This technology for bio-crude has been tested over different catalysts and reactor setups and a summary of the catalysts and operating conditions used for bio-crude steam reforming can be found in Trane et al. [21] study. Catalysts used are from base to noble metals, although nickel catalysts are favored. The reactors used in steam reforming of bio-crude range from fixed bed with trickle flow or liquid spray injection to fluidized beds. It has been shown that steam reforming of bio-crude in fixed bed reactors required a catalyst regeneration step after short period of time-on-stream [117]. Catalysts are more stable in the fluidized bed reactor compared to a fixed-bed reactor due to better contacting of the catalyst particle with steam [33]. However, problems exists for this choice of technology, such as catalyst attrition and the time of stable operation being far from what would be required for an industrial process [33].

The reaction which occurs in steam reforming of bio-crude consists of a large and complicated reaction network. Thermal decomposition and steam reforming are probably the most important reactions [21]. Oxygenate steam reforming is generally expressed by [21] :

$$C_nH_mO_p + (2n - p)H_2O \rightarrow nCO_2 + (2n - p + \frac{m}{2})H_2 \qquad \text{(Eq. 2.10)}$$

Thermal decomposition is expressed by:

$$C_nH_mO_p \rightarrow C_xH_yO_z + gases + coke \qquad \text{(Eq. 2.11)}$$

Thermal decomposition of the bio-crude produces coke. Coking causes catalyst deactivation and lowers the hydrogen yield. Deactivation due to coking is one of the major problems and bio-crude has more deactivation problems than petroleum-derived feedstocks [33]. Many of the compounds in bio-crude are thermally unstable at temperatures of steam reforming and therefore reaction (2.10) competes with reaction (2.11), even at gas phase prior to entering the catalytic bed [118]. Deactivation mechanisms in the SR of bio-crude are similar to those in the conventional steam reforming such as sintering, carbon deposition, and sulfur poisoning [21]. Alkali and phosphor compounds can be present in the bio-crude, deposit on the catalyst, and may also cause deactivation [119, 120].

Bio-crude cannot be vaporized without leaving a significant amount of residue prior to reactor and rapid heating can cause thermal decomposition [21]. In order to minimize this carbon deposition, different experimental setups have been investigated. In the following subsection, one of this possibilities is introduced.

2.2.2.1 Pre-reforming technology

To avoid thermal decomposition reaction (equation 2.11) which leads to coke formation, a pre-reformer concept is useful. The initial coke formation from heating the bio-crude could be decreased as the reactor inlet temperature would be much lower (350–500°C) compared with a single step reformer, where temperatures between 600–800°C are needed for full conversion of bio-crude [21]. Carbon formation might still be a problem at pre-reforming temperatures as it is found that carbon formation in the steam reforming of oxygenates decreases with increasing temperature [118, 121]. However, carbon formation might be circumvented in the low temperatures of pre-reforming as shown in steam reforming of ethanol and acetic acid at low temperatures, resulting in low carbon laydown and reaching extended stable operation time [122-124]. Additionally, high steam-to-carbon ratio can be used as it is beneficial to the suppression of coking [95]. From the industrial point-of-view, high steam-to-carbon ratio is expensive and therefore an optimized catalyst and

reactor conditions are needed to achieve low carbon laydown at low steam-to carbon ratio [21, 75].

A two reactor plant consisting of a pre-reformer and reformer is an analogy to a conventional steam reforming plant. Figure 2.13 shows schematic and simplified naphtha reforming plant with a pre-reformer installed. The use of a pre-reformer in naphtha reforming eliminates the problems relating to carbon formation from higher hydrocarbons in the reformer [89]. A hydrodesulfurization (HDS) process here consists of a two-step process, hydrogenating the sulfur compounds and then absorbing the formed H_2S. In the case of bio-crude reforming, the pre-reformer requires a catalyst that could convert the bio-crude to C_1-species fully and be resistant to carbon formation and catalyst poisons. The desulfurization unit can be placed after the pre-reformer if the pre-reformer catalyst is sulfur resistant, but having a desulfurization unit between the reformers will impose heat penalty and is not economical. However, a desulfurization unit is necessary if a traditional steam reforming catalysts are used in the reformer reactor [21]. It is important to point out that depending on the end use of syngas, there may be a need for additional conditioning. For example, for high conversion to hydrogen, a separate shift reactor downstream operating at lower temperature is needed which is explained previously in section 2.1.

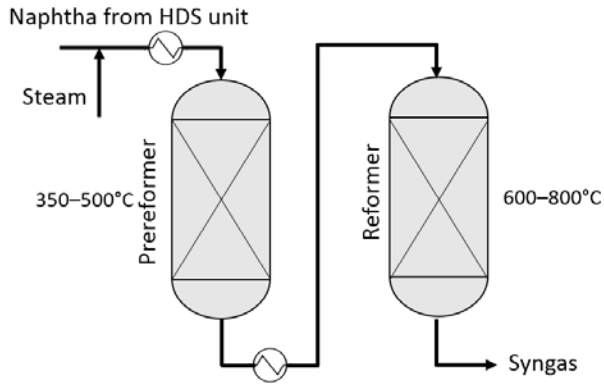

Fig. 2.12. Typical installation for a 2 stage pre-reformer and reformer in naphtha reforming plant; adapted from Ref. [89].

Once condensed, the re-evaporation of thermally labile bio-crude is difficult as bio-crude is very reactive and cause fouling of pipes [125] and condensation step after pyrolysis is disadvantageous for the heat recovery of the entire process [33]. Therefore, another advantage of a two reactor bio-crude steam reforming is that the pre-reformer temperatures are close to pyrolysis reactor exit temperatures and therefore bio-crude can be directly reformed without condensation of an unstable bio-crude. Additionally, a pre-conditioning step, similar to pre-reforming of the raw pyrolysis product prior to main reforming steps can have other benefits as a mild (or partial) deoxygenation of bio-crude lowering the pyrolysis gas dew point temperature, thus lowering the risk of undesired condensation in the process equipment, and also reducing the corrosive and polymerizing power of the condensate [126, 127].

PART B: EXPERIMENTAL

3 Experimental

3.1 Biomass-derived trace elements parametric study

3.1.1 Experimental setup and general procedures

During the experimental study of tar reforming, a bench-scale gasification system was used. This system was developed at KTH [128] and it is described in detail in paper I & II. The schematic sketch of the gasification system is displayed in figure 3.1 indicated by “A”. It consists of 5 kW atmospheric bubbling fluidized bed (ABFB) gasifier, a high temperature hot gas ceramic filter, a fixed bed catalytic reactor, a gas cleaning unit and an analytic section. All three reactor vessels are externally heated and all the piping connections are trace heated and insulated for isothermal conditions. Biomass is fed into the fluidized bed with a screw feeder. The raw producer gas is fed to the reformer after passing through the hot gas filter [64].

The inlet and outlet temperatures of the catalytic reactor were controlled by thermocouples in order to prevent a temperature gradient. The Haldor Topsoe A/S Ni-catalyst was crushed and sieved; the 3-6 mm sieved fraction were used in the tests mixed with inert filler. Sampling points for tar, indicated as “SPA” (solid phase adsorption), and permanent gas were located before and after the catalytic reactor. The system labeled as “B” in figure 3.1 was for precise dosing of alkali salts into the stream. Alkali salt compounds were produced by aerosol generator (Constant Output Atomizer model 3076, TSI Inc.), passed through a homemade diffusion dryer and get mixed with the dust-free raw produces gas. The produced droplets excess moisture was removed by diffusional capture in the dryer. The generated aerosol particles were then transported through tubes to the filter vessel where they evaporated into its molecular constituents as they enter the heated reactor. The section labeled as “C” in figure 3.1 is for the pre-treatment step, explained in chapter 4. It comprises of a steam

generator connected to the gasification system via an externally heated pipe and a feeding line of hydrogen sulfide mixture. It is important to note that both H_2S and alkali compounds were added after the filter to ensure fixed dosing rates are not affected by complex sorption effects on the filter cake as it gradually builds up. All cooling and heating of the catalytic reactor were carried out in a N_2 environment to minimize any oxidation or other changes of the catalyst surface properties.

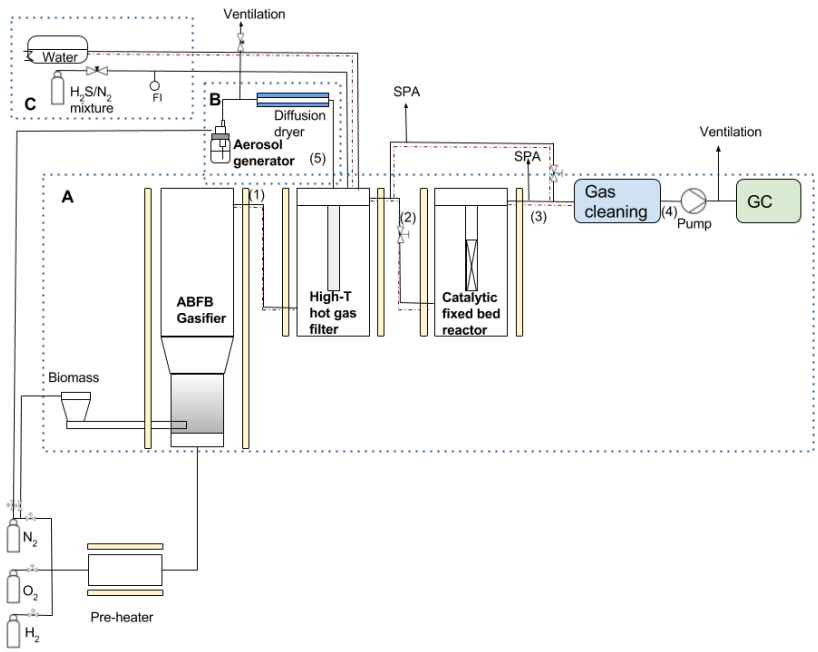

Fig. 3.1. Schematic figure of the biomass gasification setup at KTH. (1) Dusty raw producer gas, (2) dust-free raw producer gas, (3) conditioned producer gas (4) dry tar-free producer gas (5) dry KCl salt particles. (A) Section consisting of a atmospheric bubbling fluidized bed (ABFB) gasifier, high temperature hot gas filer, a fixed bed catalytic reactor, a gas cleaning unit, and an online gas chromatography. "SPA" indicates where the tar samples are taken. (B) Section consisting of an aerosol generator and a diffusion dryer. (C) Section consisting of a steam generator and a H_2S gas bottle.

3.1.2 Methodology

3.1.2.1 Activity tests

The methodology developed and implemented in activity tests is separately presented in section 4. Below is description of the methods used.

3.1.2.2 Aerosol characterization

To prove that alkali aerosol dosing was performed under realistic conditions and that the introduction of alkali was introduced in a well-controlled, repeatable environment, several characterization tests were performed. Particle number size distribution of the aerosol generator was verified before experiments with different alkali solution concentrations using scanning mobility particle sizer (SMPS), (TSI Inc., model 3936). This determines the size and number concentration of aerosol particles based on their electrical mobility in air. The calibration of alkali aerosol mass concentration was performed in a separate sets of experiments and described in paper I. The prepared alkali solution at each concentration corresponds to a specific gas phase concentration level, assuming all alkali evaporates into the gas phase which is a fair assumption as described in section 4.

3.1.2.3 Catalyst characterization

Various techniques were used to characterize the fresh and spent catalyst. The surface area measurements were performed and calculated by means of N_2 adsorption/desorption (Micromeritics, ASAP 2000) and Brunauer-Emmett-Teller (BET) method with data collected at relative pressures between 0.06 and 0.2. This method is described in detail in papers I and II. The total sulfur and carbon content on the catalyst surface was determined by IR quantification of sample high-temperature oxidation generated SO_2 using a LECO, CS230 series and ELTRA, CS-2000 series instruments**.** The K content of the catalyst was measured using atomic absorption spectrometry (AAS), (PerkinElmer, model 1100 B AAS

analyzer) and the description of the technique is described in detail in paper I.

3.1.2.4 Tar and gas analysis

The tar samples were collected and analyzed using the SPA method [36]. The composition of the dry, tar-free biomass gasification gas was determined using an online micro-GC (Thermo Scientific, C2V-200). The components measured is H_2, CO, CO_2, CH_4, N_2, and C_{2+}. For measurement of hydrogen sulfide in biomass gasification gas, two samples of dry tar-free gas were collected during the experiments in gas bags and sent to the SP Technical Research Institute of Sweden for analysis. The analysis was based on laser IR spectrometry.

3.1.2.5 Thermodynamic calculations

To determine the most abundant alkali species in the realistic producer gas composition with addition of different alkali concentrations, thermodynamic equilibrium calculations were performed using the NASA Chemical Equilibrium with Applications (CEA) Code program [129]. The program determines the minimum total free energy configuration by changing the relative amounts of given species among a broad set of candidates. Calculation of the water content in biomass gasification gas was based on the water-gas shift equilibrium (WGS), as shown in equations (3.1) and (3.2):

$$CO + H_2O \leftrightarrow CO_2 + H_2 \,, \qquad \text{(Eq. 3.1)}$$

$$K_{eq} = \frac{[CO_2][H_2]}{[CO][H_2O]} \,. \qquad \text{(Eq. 3.2)}$$

3.1.3 Materials

Pine pellets in the size range of 1.5-2 mm were used for gasification. The results of ultimate and proximate analyses for the feedstock are reported in papers I and II. The bed material used in the fluidized bed was dense alpha-alumina (350 g) with a particle size of 63-125 µm and density of 3960 kg/m^3. In the experimental campaigns, inert silica free filler

(Vereinigte Füllkörper-Fabriken, DURANIT® Inert Balls D99 with the size of 1/8") was used with the studied catalyst. It is important to choose fillers with a low silica content because silica is volatile at high temperatures and steam pressures and may deposit on the catalyst surfaces [2]. It is also important that the inert fillers have low surface area and small pore volume. The steam reforming catalyst was a $Ni/MgAl_2O_4$ catalyst (HT-25934, Haldor Topsoe A/S).

3.1.4 Data treatment and analysis

3.1.4.1 Sulfur coverage

The actual sulfur coverage, θ_S, on the Ni-based catalyst was determined by the equilibrium reaction in equation (3.3) and is therefore given by the H_2S/H_2 ratio and temperature. It can be calculated using isobars for the chemisorption of H_2S on Ni catalysts using equation (3.4) [93].

$$H_2S\ (g) \leftrightarrows H_2\ (g) + S_{surface} \quad \text{(Eq. 3.3)}$$

$$\theta_s = 1.45 - 9.53 \times 10^{-5} T + 4.17 \times 10^{-5} T ln\left(\frac{P_{H_2S}}{P_{H_2}}\right) \quad \text{(Eq. 3.4)}$$

For values of θ_s very close to 1 and at very low coverages, the model is less accurate (see figure 2.9).

3.1.4.2 Conversion

The catalyst activity was determined by evaluating the conversion (X_i) of hydrocarbon samples collected before and after the reformer. The conversion was calculated according to equation (3.5):

$$X_i = 1 - \frac{N_{i,out}}{N_{i,in}} \quad \text{(Eq. 3.5)}$$

, where N_i is the number of moles of species *i*.

3.1.4.3 Activation energy

The activation energy of desorption for potassium was calculated from the desorption rates determined by SR-TAD, assuming a first-order reaction, Arrhenius temperature dependence, and the amount of potassium on the sample surface not changing noticeably. The flux of desorbing potassium is therefore expressed by equation 3.6:

$$s = vexp(\frac{-E_{des}}{K_b T}) \qquad \text{(Eq. 3.6)}$$

Where, s is the desorption rate (signal measured using SR-TAD), $E_{des}$is the activation energy of desorption (eV), v is pre-exponential factor (s^{-1}), K_b is the Boltzman constant (eV/K), and T is temperature (K). The Arrhenius plots was then constructed from potassium thermal desorption data (ln(s) versus 1/T) and the desorption energies of potassium atoms were calculated from the linear part of the plot as shown in figure 3.2.

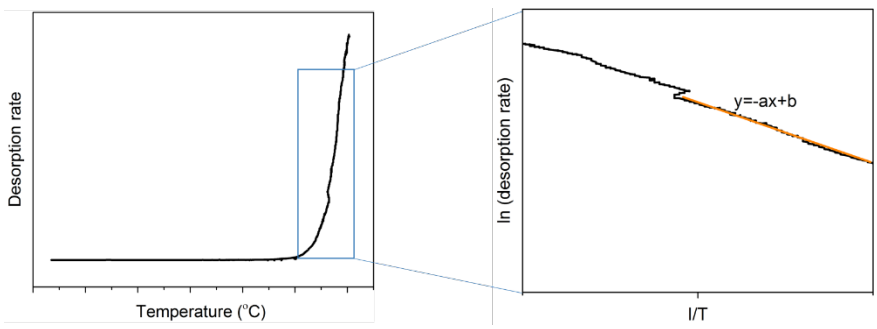

Fig. 3.2. Desorption activation energy calculated using TPD data.

3.1.4.4 Mass transfer calculation

External and intra-particle mass transfer limitation were evaluated for methane and tar, in this case, naphthalene. The estimation was performed using 2 criteria, Mears and Weisz-Prater.

Weisz-Prater (M_w) criterion: The M_w criterion is used to determine the limits for negligible and strong pore diffusion resistance. It is useful for interpreting the catalyst activity toward methane and tar reforming because it includes only observables. Narváez et al.[41] used a model of overall tar elimination that is the first-order reaction. Furthermore, Depner et al. [130], experimentally observed that the reaction order for naphthalene and methane reforming is one. It is therefore possible to use the M_w equation (3.7) [131]:

$$M_W = \frac{L^2(-r'''_{A,obs})}{C_{A,obs}D_e} \qquad \text{(Eq. 3.7)}$$

where, L is the characteristic size of a porous catalyst particle (m), $r'''_{A,obs}$is the rate of reaction (moles formed)/(volume)(time), $C_{A,obs}$is the concentration (mol/m3), and $D_e$is the effective diffusion coefficient in a porous catalyst (m3/m solid.S).

For values of M_W lower than 0.15, the diffusion limitation is negligible and no concentration gradient exists within the pellet, whereas for values greater than 4, there is a strong diffusion limitation.

Mears' criterion: The Mears' criterion uses the measured reaction rate to determine whether the mass transfer from the bulk gas phase to the catalyst surface can be neglected. This criterion is presented as equation (3.8) [132]:

$$\frac{(-r'_{A,obs})\rho_b Rn}{k_C C_{Ab}} \qquad \text{(Eq. 3.8)}$$

where, $r'_{A,obs}$is the rate of reaction: (moles formed)/(mass of solid)(time), R is the catalyst particle radius, n is the order of reaction, ρ_b is the density, $k_C$is the mass transfer coefficient, and $C_{Ab}$is the bulk concentration. If the

calculated criterion is less than 0.15, the external mass transfer can be neglected.

3.1.5 Species-resolved thermal alkali desorption (SR-TAD)

Preferential potassium adsorption sites were investigated using SR-TAD. This method is described in full detail somewhere else [133] and it has proven to be useful in examining different catalytic systems [133, 134]. In summary, the prepared samples in the form of wafers were heated from room temperature to 700°C in a stepwise mode at the rate of 5°C/min. The flux of desorbing atoms were ionized by a platinum filament. The filament had an applied voltage of +150 V, which pushes the ions away towards a collector. The desorption flux of the potassium atoms was then determined using a surface ionization detector. This experiment was carried out in vacuum apparatus with a background pressure of 10^{-8} kPa.

3.1.5.1 Catalyst preparation

The rationale for undertaking SR-TAD was to compare the desorption energies of potassium from spent catalyst and fresh catalyst and support impregnated with potassium. To prepare the impregnated samples, wet impregnation technique was used, in which bare $MgAl_2O_4$ support and fresh $Ni/MgAl_2O_4$ samples were impregnated with $KHCO_3$. The objective is to ensure that the K content of the impregnated samples was in the range of the spent catalyst K content measured after activity tests. The potassium content of each sample was determined using AAS before the SR-TAD experiments.

3.2 Tar reforming surface chemistry

Figure 3.3 summarizes the methods used for tar reforming surface chemistry study. Each method is described and discussed in section 5. Details of the DFT modelling procedure can be found in paper III.

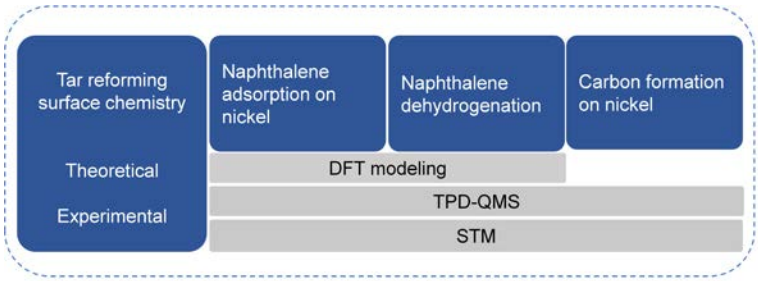

Fig. 3.3. Methodology of the tar reforming surface chemistry study.

3.2.1 Temperature programmed desorption (TPD)

The system used in this study was an ultra-high vacuum (UHV) chamber developed at Stockholm University and during the course of this work modifications were done making it possible to perform TPD study in this chamber as well. The schematic of the setup is shown in figure 3.4, including a chamber equipped with standard surface science tools; low-energy electron diffraction (LEED), a quadrupole mass-spectrometer (QMS), an ion gun, and a gas dosing system, including naphthalene dosing system. The sample was a polished Ni(111) crystal and was mounted on a holder at the end of the manipulator connected to a liquid nitrogen cooled cryostat with both resistive and electron beam heating for sample heating. The temperature was then measured with a thermocouple connected to the side of the sample. The entire system was vacuum pumped using turbo and ion pumps giving a base pressure in the low 10^{-10} Torr range. TPD process was performed in the UHV chamber with base pressure of 1×10^{-10} Torr. The heating ramp for desorption measurement was set to 0.83 K/sec. During the measurements, the desorption fluxes of both naphthalene and hydrogen were continuously monitored with the QMS.

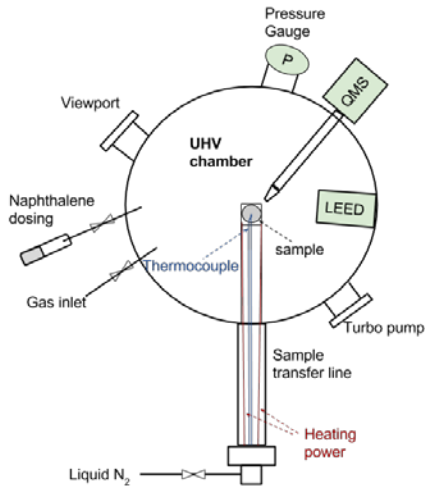

Fig. 3.4. Experimental setup for the TPD study. UHV chamber (chamber pressure: 10^{-10} Torr), equipped with QMS, LEED, and gas dosing system.

Prior to TPD experiments, sample cleaning must be performed. The sample cleaning procedure, which is dependent on the type of metal, can be extremely difficult due to different types of impurities that may diffuse to the surface at certain temperatures. The general procedure for sample preparation starts with sample cleaning and it is to bombard the surface of the crystal sample with ionized atoms and knock out the impurities. This procedure is called sputtering and is accompanied by annealing which is to re-distribute and smoothen out the surface that became rough after sputtering. The Ni(111) crystal used here underwent one cycle of 5-min sputtering and annealing at 1100 K in vacuum before experiments. More details of the sample cleaning procedure can be found in paper III.

Naphthalene was deposited through a precision leak valve at room temperature in the vacuum chamber at a base pressure of 1×10^{-10} Torr. The procedure here was to reach a monolayer of naphthalene deposited on the surface of Ni(111) sample. Afterwards, the sample was heated with a fixed heating ramp for desorption measurement. The desorption rate, total

amount of released gases, and the kinetics of desorption were measured. Three types of study was performed. One examined the adsorption and structure of naphthalene on Ni(111), the second probed the dehydrogenation occurred for various coverages of naphthalene on Ni(111). Third investigated the deactivation of the surface. Scanning tunnel microscopy (STM) was used to investigate the chemical pathway from naphthalene to possibly graphene; this was done in a separate vacuum chamber and is described in the subsequent section.

All experimental TPD data presented were treated in the same manner using 6-fold binning and a background subtraction based on a linear fit of the background. For STM image processing and surface analysis, Gwyddion free software was used.

The activation energy for C–H breakup is based on the TPD data and is calculated as explained in section 3.1.4.3, assuming weak pre-factor and Arrhenius temperature dependence. The activation energies are calculated from the linear parts of Arrhenius plots for ln (desorption rate/coverage) versus I/T as shown in figure 3.5.

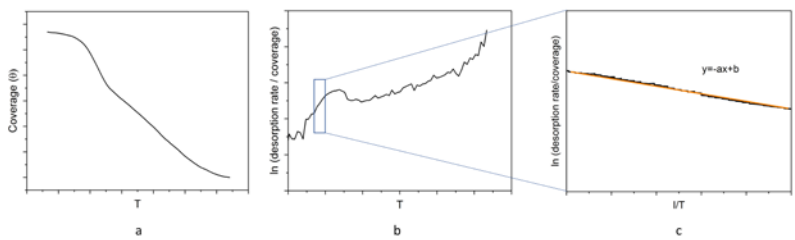

Fig. 3.5. Activation energy for C-H break up calculation. a) coverage versus temperature b) (ln (desorption/coverage)) versus T c) linear parts of Arrhenius plot (ln (desorption/coverage)) versus I/T.

3.2.2 Scanning tunnel microscopy (STM)

STM experiments were conducted in a RHK UHV 3500 SPM system; with a base pressure of 3×10^{-11} Torr. The sample was prepared by repeated

cycles of Ar-sputtering (1 kV) and annealing at 1073 K, until a sharp (1×1) LEED pattern was observed with low background and STM revealed a smooth surface with large flat terraces. Sample heating was done by electron bombardment, and the temperature was measured with a pyrometer from 300°C and higher. STM was conducted using etched W and Au tips. The bias was applied to the tip; negative bias thus corresponds to imaging empty states and positive bias images the filled states on the surface. Naphthalene was deposited through a precision leak valve at 5×10^{-8} Torr. Exposures are given in Langmuir (L), where $1\ L = 1 \times 10^{-6}$ Torr·sec.

3.2.3 Density functional theory (DFT)

The naphthalene adsorption energies, geometric distortion, and redistribution of electron density has been investigated using DFT molecular modeling. The description of the DFT method used can be found in paper III.

3.2.4 Materials

Pure naphthalene was purchased from Sigma Aldrich and dosed to the sample surface through a precision leak valve at 5×10^{-8} Torr. The Ni monocrystal with the exposed (111) surface was purchased from Surface Preparation Laboratory (SPL) in the Netherlands. The sample was polished and aligned to less than 0.1° from the (111) plane.

3.3 Pyrolysis gas conditioning

3.3.1 Experimental setup

The setup used in this study was developed and built at KTH Royal Institute of Technology during the course of this work and the activity tests were performed both at the KTH Royal Institute of Technology pyrolysis reactor facility and Cortus Energy's biomass gasification test facility in Sweden [135]. The schematic of the setup is displayed in figure 3.7. It consists of part A, a high-emperature filter, a fixed bed catalytic reactor,

piping trace heated and insulated and part B, and a sampling system. Both filter and reactor was heated externally. The filter was used to remove particulates from pyrolysis gas before entering to the reactor and was purged periodically with nitrogen to remove the build-up of the filter cake and a consequential pressure drop. The reactor's volume was 2.3 dm^3 and its inner diameter was 55mm. the catalyst used was provided by Haldor Topsoe A/S with a cylindrical pellet shape form of 6 × 6 mm size. Three thermocouples monitored the temperature inside the reactor the temperature of the reactor was controlled by the wall temperature that was measured by another set of thermocouples installed.

The sampling system comprised a series of impinger bottles. The sampling was conducted with a known sampling flow and was used to condense out bio-crude, including water. The first three impinger bottles with glass frit were placed in a cooling water bath, preventing evaporation of the iso-propanol. The use of a low sampling rate helped minimize losses due to evaporation [136]. Impinger bottles with glass frit were used because of the breakdown of aerosols possibly formed during the cooling of the pyrolysis gas [136], and alcohol was used in the cooled impinger bottles to minimize aerosol formation during the condensation [137]. The bio-crude- and moisture- free flow was then sent to the online gas chromatograph. The condensed samples were all collected and mixed for analysis off-site.

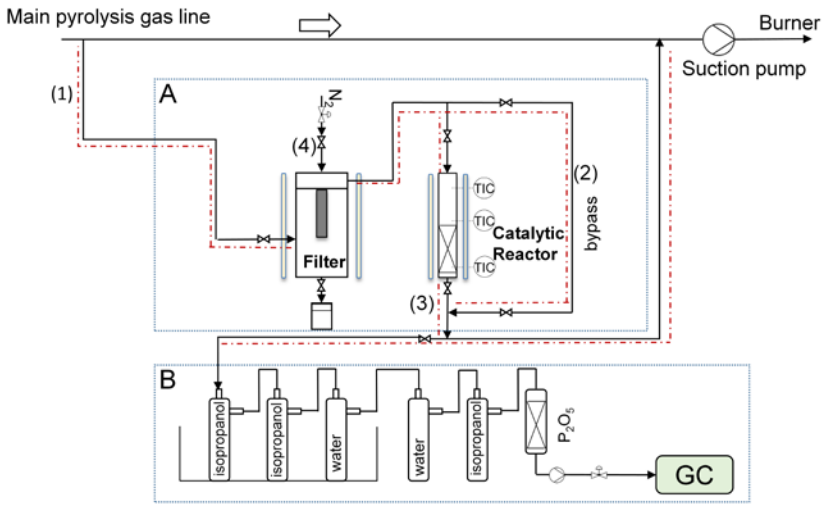

Fig. 3.6. Schematic of the experimental setup for the catalytic conditioning of pyrolysis gas: (1) raw pyrolysis gas before filter (2) raw pyrolysis gas (dust-free) (3) treated pyrolysis gas (4) purging nitrogen. (A) Section consisting of a high T filter and a fixed bed catalytic reactor. (B) Section consisting of a sampling system for condensates, a P_2O_5 filter for moisture absorption, and an online gas chromatograph.

3.3.2 Methodology

Figure 3.7 summarizes the experimental methodology for pyrolysis gas conditioning. It is divided into initial catalyst activation, catalytic testing, and characterization of raw and treated bio-crude as well as fresh and spent catalyst.

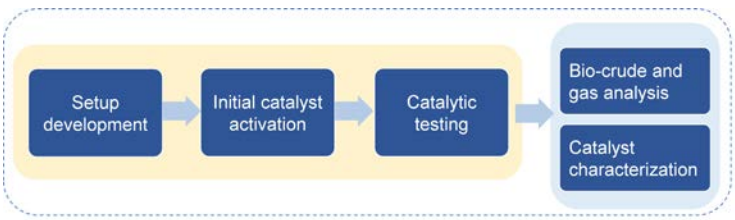

Fig. 3.7. Experimental procedure applied for catalytic conditioning of biomass pyrolysis gas.

3.3.2.1 Initial stabilization and activity tests

Before each experiment, a stabilization period of the catalyst was observed and the resulting catalyst bulk phase after use was determined by X-ray diffraction. The raw pyrolysis gas was produced in a pyrolysis reactor consisting of a rotary kiln, where dried biomass was fed and pyrolyzed at a temperature of 380°C and at slow heating rates (approx. 15°C/min) and the produced pyrolysis gas was fed into the experimental setup at 380°C. All experimental units and parts were kept at 450°C except during the stabilization period of the catalyst when the temperature was kept at 400°C. To minimize catalyst sintering and thermal cracking of oxygenates, temperatures during the initial period of catalyst stabilization were monitored inside the bed and kept as low as possible. After the initial stabilization in the pyrolysis gas, the reactor temperature was raised to 450 °C. The total stable operation and time on stream was 8 hours. The hot gas filter was purged periodically, using nitrogen. The online micro-GC monitored the permanent gas composition, including C_{2+} compounds, and the stability of the test. The condensate samples were collected from the raw and treated pyrolysis gas for further analysis. Spent catalyst samples were taken from top, middle, and bottom of the bed for characterization.

3.3.2.2 Catalyst characterization

The surface area was measured using the technique described in section 3.1.2.3. Total carbon and sulfur contents were measured using the same technique describe in section 3.1.2.3 (LECO). The state of the spent catalyst was also analyzed at Haldor Topsoe by means of XRD using a PANalytical Empyrian instrument, and an in-house WGS activity test procedure. Temperature programmed oxidation of the fresh and used Fe-based catalyst catalyst was performed at a heating rate of 6 °C /min up to 800°C in a 30 ml/min flow of 5% O_2 in He. This characterization test was performed as a fingerprinting technique to compare the fresh and spent Fe-based catalyst.

3.3.2.3 Bio-crude and gas analysis

For analyzing the content of the bio-crude, condensate samples were analyzed using an Agilent 7890 gas chromatograph coupled to an Agilent 5975C mass selective detector (MSD). The GC was equipped with a 30 m × 250 µm × 0.25 µm HP-5ms column using He as carrier gas. Chemstation software was used for peak integration and NIST11 library for peak identification. Furthermore, gravimetric determination of condensate before and after the catalytic treatment of the pyrolysis gas was carried out. The increase in weight of the sampling bottles was a measure of the bio-crude and water content. The C/H/O/N/S analyses, as well as the water content analysis of condensate samples, were performed at Karlhamnsverkets Laboratory, UNIPER. Carbon and hydrogen content were determined by the ASTM D5291 analysis method. Oxygen and water content were determined by difference and Karl Fischer titration (ASTM E 203), respectively. Condensate samples were also analyzed using ^{1}H-NMR to determine the change of the functional groups, such as aromatics, phenols, and aldehydes, of different components in raw and treated bio-crude. The ^{1}H-NMR spectra were recorded at 400 MHz on a Bruker DMX-400 spectrometer at room temperature. The composition of the permanent gases in the pyrolysis gas, after condensing out water and bio-crude, was analyzed using an online micro-GC (Thermo Scientific, C2V-200).

3.3.2.4 Mass balance calculation

For evaluation of results, a mass balance calculation was performed for carbon, hydrogen, and oxygen based on equation (3.9). The flow of the raw pyrolysis gas is denoted with the index “in” and the treated flow by “out”.

$$N_{i,IN} = \int_0^t \dot{f}_{OUT}\, y_i M_{wi} \alpha_i dt + \int_0^t x_i \dot{G}_{OUT} dt + \Delta C \qquad \text{(Eq. 3.9)}$$

where, i= C, H, or O, $N_{i,IN}$ is the inlet mass, y_i is the molar fraction of a compound in the gas, $\dot{f}_{out}$is the total outlet molar flow of gas, α_i is the

number of atoms of element *i* in a compound, x_i is the mass fraction of *i* element in the condensate, M_{wi} is the atomic weight of *i* element (C, H, and O), $\dot{G}_{OUT}$ is the outlet mass flow rate of the condensate, ΔC is the carbon deposit on the catalyst wherein the accumulation of carbon on the catalyst surface is determined by the total mass of the accumulated carbon, and *t* is the total experimental time.

3.3.3 Materials

The tests were carried out using chips of tree-tops and branches. The catalyst used for experiments was a Fe-based catalyst (Haldor Topsoe A/S, HT-25409) with a cylindrical pellet shape form of 6 × 6 mm size. Inert filler used was the same as described in section 3.1.3. It was used in the volume of the reactor above and below the catalytic bed to increase the thermal conductivity, as well as improving radial mixing, reducing the axial dispersion and minimizing channeling over the catalytic bed.

3.3.4 Data treatment and analysis

3.3.4.1 Conversion

It is important to note that though all bio-crude analyses were performed with isopropanol as a solvent, the results reported are on isopropanol-free basis. With respect to conversion of compounds and compound classes in bio-crude, they are reported on a water- and isopropanol- free basis. The conversion of main compounds in the bio-crude over the reactor was calculated using equation (3.10):

$$X_i = 1 - \frac{yield_{i,treated\ bio-crude}}{yield_{i,raw\ bio-crude}} \qquad \text{(Eq. 3.10)}$$

where, *i* denotes different compounds in the condensate. The *yield* is proportional to the yields of bio-crude components and is normalized on solvent- and water-free basis. The yield is calculated based on equation 3.11:

$$yield \propto \frac{area * \dot{M}}{(1 - x_{H_2O})} \quad \text{(Eq. 3.11)}$$

where, *area* is the integrated area of GC-MS results, normalized on solvent-free basis, $\dot{M}$ is the total mass flow of bio-crude (dry-basis), and x_{H_2O} is the mass fraction of water in the condensate.

PART C:

RESULTS AND DISCUSSION

4 Biomass-derived trace elements parametric study (papers I and II)

This chapter provides a three-step procedure implemented to study effect of biomass-derived trace elements, in this case alkali and sulfur, on tar reforming catalysts downstream of gasifiers:

a. Methodology development
b. Validation of the methodology
c. Application of the methodology to activity tests

The summary of the methodology, its validation and application is shown in figure 4.1. First, the system is initially characterized. The methodology was then validated and activity tests were performed for K influence under exposure to real producer gas from biomass based on the observations from the first step. Based on the validation results, the methodology was implemented and the combined effect of sulfur and potassium on tar reforming activity is investigated under realistic conditions approaching steady-state over time. This methodology is described in detail and its results are presented in subsequent sections.

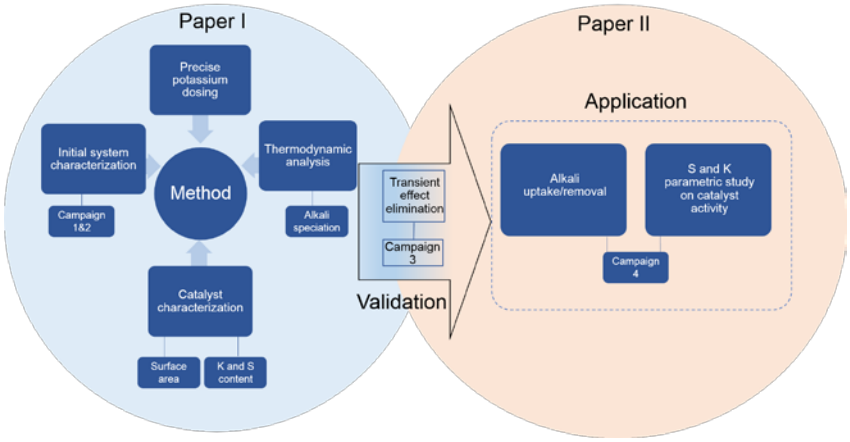

Fig. 4.1. Schematic of the methodology developed for parametric studies of the effect of biomass-derived trace elements on tar reforming catalyst.

4.1 General information

Four activity test campaigns were performed in this study to determine the potassium-equilibrated surface content, dynamics of sulfur and potassium through the bed and the pellet, and effect of gas-phase alkali on tar and methane reforming. In all four campaigns:

1. Catalyst samples were collected from the bed inlet in small amounts for characterization after cooling down in nitrogen flow to ambient temperature every first, second or third runs. Samples were also collected through the bed in Campaign 4. The sampled amount was small compared with the loaded catalyst so that the performance of the reactor was not affected significantly.

2. Before the experiments, the catalyst was reduced for 4 hours in H_2 at 700°C for phase transition of NiO to Ni.

3. The loaded catalyst volume and total gas flow rates were selected to obtain partial hydrocarbon conversion. This was done to obtain an effective conversion range, meaning not too high conversion,

so that it enables us to compare conversion degrees at different conditions.

4. Tar reformer operating temperature for Campaign 1, 2, 3, and 4 were 850°C and 800°C, respectively.

5. Mass balance calculations were performed over the reactor for C, H and O based on approximately all measured gas components, excluding only tar components other than benzene and naphthalene. The output-to-input ratio were calculated to be in the range of 0.91−1.07, proving an acceptable mass balance.

4.2 Methodology development

4.2.1 Alkali dosing and speciation

In the few studies of the effect of alkali on tar reforming catalyst, the limitation is the method used to investigate influence of gas-phase potassium compounds on catalyst [56, 57, 91, 103]. Common limitation are mechanisms of potassium transport, deposition and equilibration on the catalyst which are not similar to the realistic mechanism. Alkali dosing should be well-controlled, continuous, and repeatable for variable content of alkali in the biomass gasification gas. Application of an aerosol dosing system, guarantees a precise control of the dosing since the particles are kept in the gas stream without deposition or impaction on the walls during the transport to the reactor. Furthermore, the system allows for precise control of the amount of water fed to the gas stream whereas other methods such as direct pumping of aerosol solution into the reactor, spraying through a nozzle and alkali vaporization [57], cannot control over the amount of water fed. In an aerosol alkali dosing system, extra moisture is removed by the diffusion dryer, as shown in figure 3.1. Furthermore, complete evaporation is important as at steam reforming temperature, most of the alkali species are in vapor phase. Consequently, a proper particle

size distribution of the generated aerosol particles is vital for complete evaporation of the dosed alkali salts and methods such as pumping or spraying system does not guarantee that. SMPS measurements indicate that the sizes of the generated particles are in agreement with the specifications of aerosol generator manufacturer and are suitable for the highly efficient transmission of particles through a tube [138]. The alkali salt particles rapidly evaporated in the high-temperature reactors based on separate sets of experiments concluding 100 nm KCl particles evaporate fully at temperatures above 700°C with the residence time of 0.5 s [139]. The experimental setup used in this study had a higher residence time for alkali salt particles and operates at 850°C, ensuring full evaporation.

Thermodynamic calculations do not provide the complete picture due to the non-equilibrium state of the investigated system. However, they do provide information on the state of alkali compounds present in the producer gas after dosing with alkali. The average wet gas composition at the catalytic reactor inlet was used for chemical equilibrium composition calculations at different KCl dosing concentrations. The amount of biomass-derived K in the gas is estimated to less than 0.2 ppmv [43], and based on the N and Cl content in the biomass, the levels of NH_3 and HCl are calculated to be about 400 and 30 ppmv, respectively, assuming complete conversion to gas-phase species and no hot gas filter effects. This assumption is reasonable, since the H_2S concentration was calculated to be 14 ppmv, based on assumption used in paper I, which is very close to the measured H_2S content in gas (15±3 ppmv) presented in paper II. Thermodynamic calculations performed revealed that the most abundant K species in the operating conditions of this study are KCl, KOH, and elemental K. Addition of KCl to the gas stream increases the content of K species, which may decompose when adsorbed on the catalyst surface. The domination of KCl over the other two main components is more pronounced at larger amounts of initially added KCl concentrations in the gas. Changes in the gas composition will affect the K distribution. For example, accounting for an estimated 30 ppmv HCl content from the biomass itself increase the relative KCl content ($KCl + H_2O \leftrightarrow KOH + HCl$). These results are described in greater detail in paper I.

The efficient transmission of produced aerosol particles to the producer gas must be guaranteed. In the previous studies on effect of gas-phase alkali on tar reforming [56, 57, 91, 103], all the catalyst samples were deposited with alkali prior to exposure tests which is different from realistic alkali deposition on the catalyst surface. Albertazzi et al. [103] and Einvall et al. [56] observed a minor loss or a complete recovered reforming activity of the K pre-deposited Ni catalysts under real producer gas. The reason for both phenomena was related to cleaning, volitilizaiton-induced effect of steam during activity tests. The amount of deposited alkali salt in Albertazzi et al. [103] study , decreased after couple of hours of reaction in all samples, thus stressing the importance of alkali volatilization under reaction conditions. In the present study, this limitation was excluded by developing an alkali dosing system for continuous, precise dosing during the activity tests.

4.2.2 Initial catalytic system characterization

Next step was to apply the alkali dosing technique and perform activity tests. Two experimental campaigns were performed. A series of test campaigns was designed and performed with each campaign consisting of several experimental runs with 3–4 hours of continuous operation. The initial catalytic system characterization was performed during Campaigns 1and 2. In Campaign 1, 11 ppmv KCl was added to the dust-free raw producer gas. H_2S is biomass-derived and the concentration was estimated to be 14 ppmv. In Campaign 2, 11 ppmv KCl was added to the dust-free raw producer gas. Additional H_2S is added together with KCl during the activity test. The H_2S concentration was estimated to be 84 ppmv. In both campaigns, catalytic reactor operating temperature was 850°C. Figure 4.2 presents the catalyst BET surface area and normalized K content and S content/S capacity versus time on stream. Decelerating reduction of BET surface area is mainly related to carrier sintering caused by elevated temperature and steam exposure being significant in sintering rates the first 200 hours of run [53, 88] . The catalyst sulfur content in Campaign 2 has reached an equilibrium between the adsorbed and gas phase S in the reactor

inlet after approximately 6 hours under the operating conditions of Campaign 2.

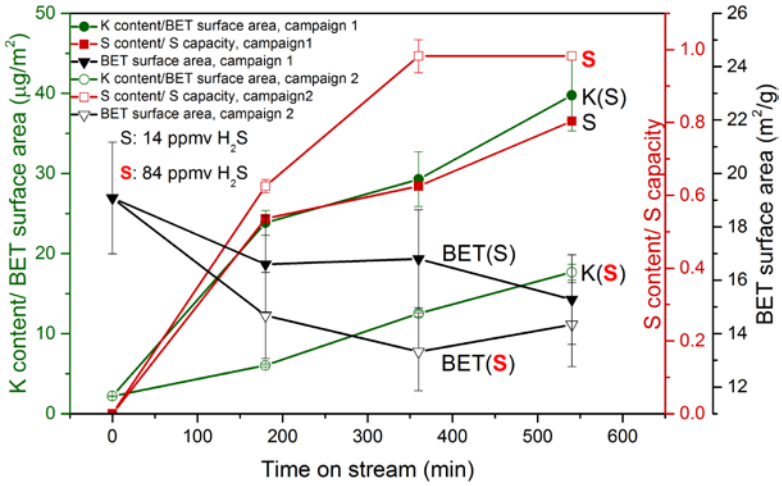

Fig. 4.2. BET surface, normalized K and S content samples from reactor inlet versus time on stream. Campaign 1: 14 ppmv H_2S, 11 ppmv added KCl. Campaign 2: 84 ppmv added H_2S, 11 ppmv added KCl.

The trend for the normalized catalyst K content in Campaign 1 and 2 is similar, but with a slower uptake of K in Campaign 2 compared to Campaign 1. This appears to be the primary effect of higher sulfur chemical potential in Campaign 2. The details of S and K interaction is discussed more in detail in section 4.3.1. Results of potassium uptake obtained from Campaign 1 and 2 as well as additional results obtained from dosing 6 ppmv of KCl are presented in figure 4.3. Adsorbed potassium in Campaign 1 and 2 with identical KCl addition and different sulfur chemical potential shows a clear suppression of K adsorption as the sulfur chemical potential increases in the producer gas. The combination of the results suggest that different KCl concentrations in the gas phase result in different initial uptakes of K on the catalyst surface, linearly proportional to time on stream for low K coverage (θ_K). Based on this initial characterization, there were indications that the start of a slow approach to K equilibration at the catalyst bed inlet was observed.

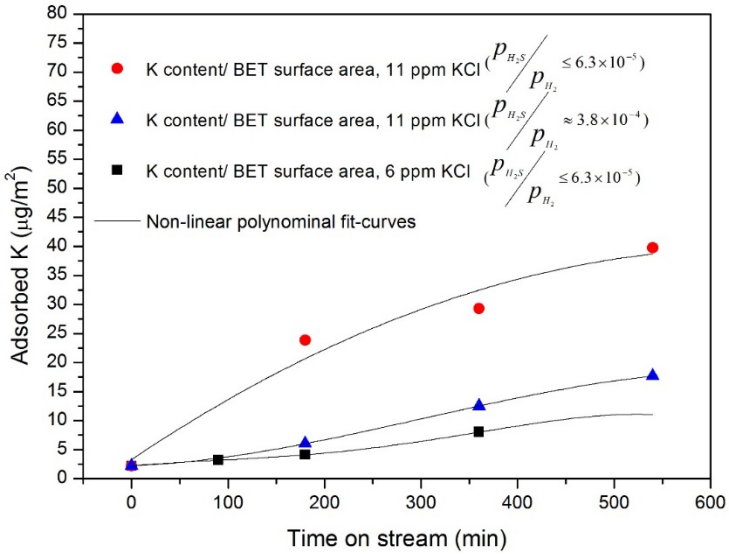

Fig. 4.3. Potassium (K) uptake curves as the function of time on stream (TOS) for different gas-phase K concentrations and sulfur chemical potential. The fits only serve as a guide to the eye.

Figure 4.4 presents activity of the catalyst toward methane and naphthalene reforming as 2 hour average for Campaign 1 and 2. The catalyst activity drop rate is significantly faster in Campaign 2 compared to Campaign 1. This explicit decrease in activity toward methane reforming is due to a passivation of the catalytic surface [97, 98] caused by adsorption of sulfur on active surface sites. The reduction in activity toward naphthalene reforming is also due to sulfur poisoning. Reduced steam reforming, especially for methane, results in less H_2 and CO formation. That leads to less water consumption, shifting the WGS reaction toward more CO_2 formation.

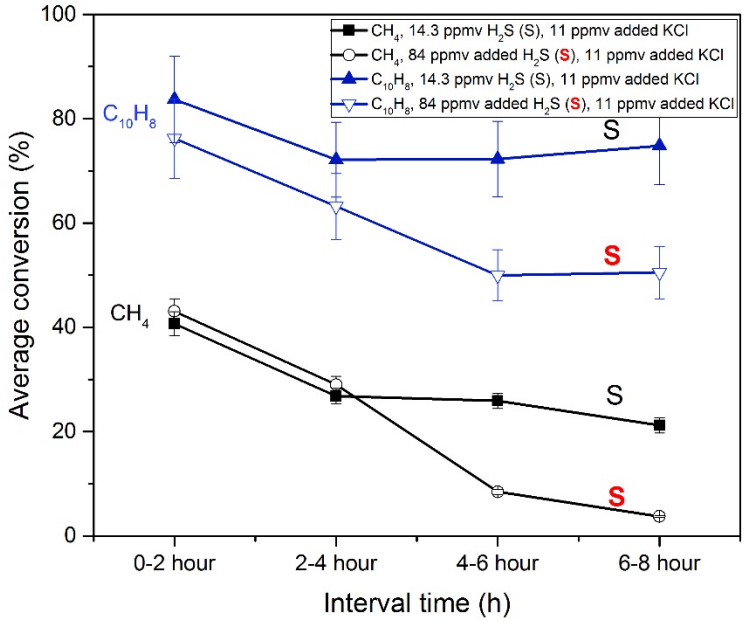

Fig. 4.4. Activity transients: average methane and naphthalene conversion versus time on stream in the catalytic reactor for campaigns 1 and 2. Campaign 1: 14 ppmv H_2S, 11 ppmv added KCl. Campaign 2: 84 ppmv added H_2S, 11 ppmv added KCl.

In Campaign 2, the reduction of CH_4 reforming continues beyond 2–4 hours, whereas CH_4 reforming activity in Campaign 1 and naphthalene reforming in both campaigns reach a stable conversion after 6 hours of run. Progressive sulfur uptake and equilibration in bed during Campaign 2 being more rapid in presence of higher H_2S concentrations may partly explain the transients in activity. Therefore, for elimination of this transient effect, the catalyst bed should reach S-equilibrium before actual experiments. Changes in mass transfer limitation for methane and naphthalene may also clarifies difference in the transients in activity.

Under operating conditions of the reactor, the lower methane reforming activity due to sulfur passivation may change the transport limitation from external, which usually is the case for conventional steam reforming, to internal. Weisz-Prater and Mears criteria is calculated and presented in table 4.1 for start and end of Campaigns 1 and 2 for naphthalene and

methane. Based on calculations for Mears [132] criterion defined in section 3.1.4.4, there may be limited external diffusion for naphthalene and no external diffusion for methane at the operating conditions of Campaign 1 and 2. Mass transfer coefficient (K_c) is calculated from diffusion coefficient, average particle number and Sherwood number (total mass transfer/diffusive mass transfer) for naphthalene and methane respectively.

Table 4.1. Weisz-Prater and Mears criteria for methane and naphthalene in Campaign 1 and 2

	Criteria	**Mears**		**Weisz-Prater**	
	Component	Naphthalene	Methane	Naphthalene	Methane
Campaign 1	Beginning of the activity tests	0.36	0.06	6.23	2.88
	End of the activity tests	0.34	0.02	5.87	1.07
Campaign 2	Beginning of the activity tests	0.38	0.06	6.46	3.05
	End of the activity tests	0.3	0.01	5.15	0.33

Due to larger size of naphthalene, the intra-particle diffusion limitations are more severe for this molecule compared to methane. This was established by Weisz-Prater [131] criterion (M_w bigger than 4), defined

earlier in section 3.1.4.4. Effective diffusion coefficient (D_{eff}) is calculated for naphthalene and methane from the catalyst porosity, the tortuosity factor and the diffusion coefficient in the bulk and the Knudsen diffusion coefficient [2]. In figure 4.5a, highlighted A and B area represents the Weisz-Prater criterion range calculated for methane and naphthalene, respectively, at the end of campaigns 1 and 2. It is evident that as the sulfur coverage increases in the catalyst, methane appears to be more sensitive to internal diffusion limitation than naphthalene (highlighted A versus B area). Schematic of shell/core poisoning by sulfur [95] in Campaigns 1 and 2 as well as the utilized shell volume for methane and naphthalene reforming reactions as shown in figure 4.5b, demonstrate that steady-state activity is reached faster for naphthalene than methane, since equilibrated S coverage is reached earlier in a shell volume utilized for naphthalene reforming than for methane. Sulfur-equilibrated shell volumes that are shown in figure 4.5b represent a snap shot at similar time (before full S-equilibration throughout the pellet) for two different initial sulfur levels and at similar location in the catalytic bed before S-equilibration in all of the pellets throughout the bed. Both pellet and bed equilibration will be faster in the case of higher sulfur concentration.

This preliminary observation reveals methane and tar (naphthalene) mass transfer limitations under tar reforming conditions and the importance of pre-sulfidation in establishing fixed θ_S .

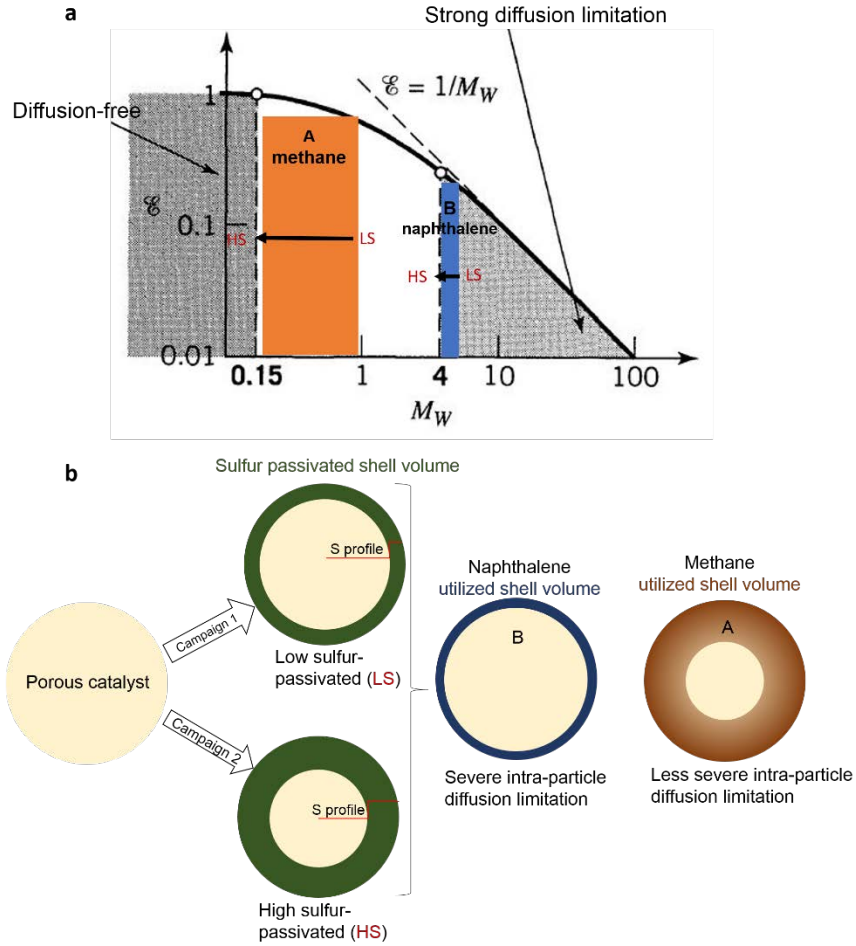

Fig. 4.5. a) Weisz modulus criterion, figure adapted from Ref. [131]: spent $Ni/MgAl_2O_4$ catalyst under the operating conditions of Campaign 1 and 2 catalytic reactor for A: methane B: naphthalene. LS: low sulfur coverage HS: high sulfur coverage. b) Schematic of sulfur passivated shell volume and of utilized shell volume for naphthalene and methane reforming in Campaigns 1 and 2.

4.2.3 Validation of the methodology

To be able to measure potassium uptake behavior at varying gas-phase concentration and its influence on reforming activity when alkali is equilibrated and co-adsorbed with sulfur, transient effects due to sintering and sulfur poisoning, as observed in characterization and activity results above, must be eliminated. None of the previous investigations on effect of gas-phase alkali on the catalyst was conducted under realistic steady-state conditions [56, 57, 91, 103] and only few of these studies were under exposure to real biomass gasification gas [103]. Albertazzi et al. [103] observed decrease in active Ni surface area during the activity tests which may be connected to sintering of Ni particles. Li et al. [57], exposed a monolithic Ni-based catalyst to alkali salt vapors (KCl, K_2SO_4, and K_2CO_3) and observed the most poisonous effect for K_2SO_4 which is related to extra sulfur dosing and sulfur poisoning effect. Einvall et al. [56], exposed reforming catalysts to species in fly ash, as well as aerosol particles containing K_2SO_4 and observed decrease in surface area and available metal area but the corresponding loss in activity was not severe, probably due to volatilization-induced effect of steam during activity tests. In this work, pre-sulfidation was implemented to reach S-equilibrated surface and accelerated-aging was performed to reach a rather constant surface area with minimal changes during activity test. Validation of the methodology was confirmed under Campaign 3, in which the catalyst was going through pre-treatment steps, prior to exposure tests with a tailored H_2S/H_2 ratio and a KCl addition similar to Campaign 1 and 2. An aging time of 5-hour was selected, based on Sehested et al. [140] study. It was estimated that a 5-hour aging procedure would result in minimal (<5%) changes in catalyst support and Ni surface areas even after a large number of operating hours [140]. 6-hour sulfidation was selected based on observation from Campaign 2, in which the catalyst reached its sulfur capacity. The desired sulfur coverage is θ_S=0.9–0.95, so that the nickel particles were not completely covered with sulfur and there was still considerable reforming activity. The pretreatment step is explained more in detail in paper I. After the final pre-treatment step, two subsequent experimental tests were carried out with the total operational time of 9 hours, exposing the same

catalyst batch to the dust-free raw producer gas to investigate the K uptake and activity of the catalyst. Figure 4.6 shows BET surface area, normalized K content, S concentration for fresh, pre-treated and spent catalyst samples after test 1 (5 hour) and 2 (4 hour) as well as the average naphthalene and methane conversions in tests 1 and 2.

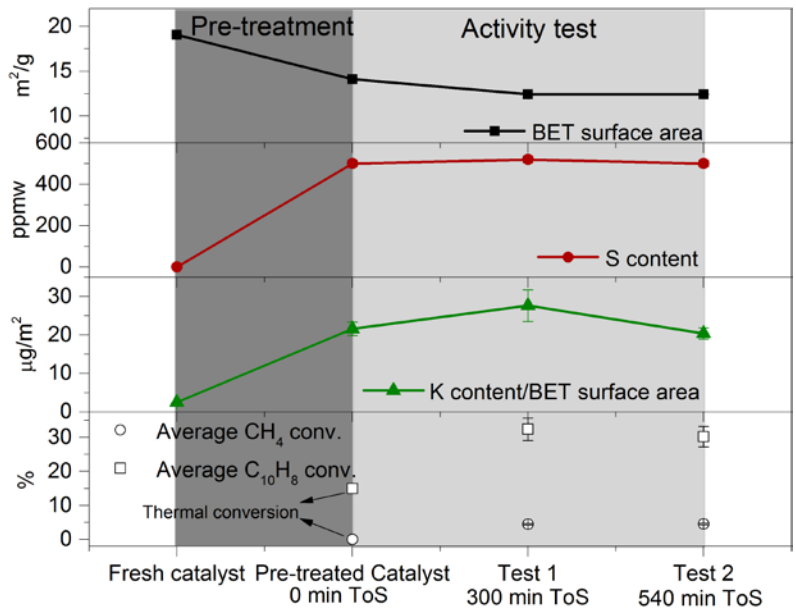

Fig. 4.6. BET surface area, potassium content divided by BET surface area, sulfur concentration obtained for fresh, pre-treated, and spent catalyst at the bed inlet, and average conversion of methane and naphthalene versus exposure time in Campaign 3, tests 1 and 2.

Sulfur content of the catalyst was constant during the activity test after pre-sulfidation, indicating that the catalyst equilibrated sulfur coverage was reached in the catalyst bed inlet. This means that the pre-treatment of the catalyst via sulfidation was successful and that the active surface area was constant from the beginning of the activity tests. The BET surface area was near constant after 5 m^2/g drop in accelerated aging procedure during pretreatment indicating a successful accelerated aging procedure. Although earlier studies have indicated a clear K-effect on sintering [140],

the operating conditions of this work is different (significantly more reducing gas). A substantial uptake of K is observed after the pre-treatment step which was related to vaporization of residual K in the system due to high temperature and high partial pressures of water. To avoid the memory effect of potassium in system, a thorough steam-cleaning is required prior to pretreatment and this is described in section 4.3. As shown in figure 4.6, the normalized K content is stable throughout the activity tests. As judged by the sulfur content, no active Ni surface area changes were observed. This explains the stable activity of the catalyst toward methane and tar reforming when comparing 300 min and 540 min time on stream average conversions. This is also reflected in the constant gas composition during tests 1 and 2, discussed in more detail in paper I. The pre-treatment methodologies used, including pre-sulfidation and accelerated aging, effectively stabilized the catalyst activity (activity transient elimination), allowing for further investigations of the effects of gas phase alkali on the catalytic activity. An expanded parametric study was designed to establish the K uptake curves and study the K influence on the catalyst performance (paper II).

4.3 Biomass-derived trace elements effect on catalyst performance

As stated in section 2.1 , negative (catalytic steam reforming activity suppression) and positive (carbon whisker coking resistance) sulfur and potassium influence on steam reforming activity have been studied separately [2, 53, 94, 96, 101, 102]. However, none of these studies presented a clear picture of the combined effect of sulfur and potassium on the Ni-based catalyst under steady state conditions. The extended activity tests in Campaign 4 were performed to determine the K uptake and its effect on catalyst activity under steady-state tar reforming conditions.

Before the tests and pretreatment, steam-cleaning was performed. Steam cleaning of the system was introduced to remove the K residuals effectively on the surfaces in the gasification setup upstream of the

catalytic bed. It also enabled the study of K uptake in a more precise manner. More details of steam-cleaning are discussed in paper II. In Campaign 4, catalyst was gone through pre-treatment steps of accelerated aging and sulfidation after steam-cleaning the system. Thirty hour ToS with KCl dosing was followed by 6 hours ToS with no KCl dosing. The first 30 hour is named Period 1 and the last 6 hours is named Period 2. Because of the lower temperature in Campaign 4 compared to Campaign 2 and 3 (800°C versus 850°C), no additional H_2S was added during the activity tests to the producer gas since the desired sulfur coverage was achieved without the need to tailor the sulfur chemical potential in the gas. In Campaign 4, samples were taken from different depths through the bed after Period 2, to investigate the concentration profiles of K and S through the bed.

4.3.1 Potassium (K) uptake and interaction with sulfur (S)

Figure 4.7 presents the normalized catalyst K and S content at the bed inlet, where exposure time is defined as the time for pretreatment plus the time on stream. The catalyst sulfur content was equilibrated and BET surface area is constant after pretreatment. Normalized K content increases up to 28 hours and varies around the same value up to 40 hours, reaching a plateau. This is a confirmation of early stages of K uptake and its approach to equilibrium as implied in section 4.2.2. Potassium equilibrium coverages on the $Ni/MgAl_2O_4$ catalyst is established to 10–40 µg K/m^2 under realistic steady-state tar reforming conditions with approximately 1 ppmv KCl concentration in gas phase. Continuing 6 hours without KCl dosing, the potassium content of the bed decreases as displayed in figure 4.7. This reduction was clearly due to the altered KCl partial pressure in the gas phase, resulting in changes in potassium equilibrium coverage. Normalized S content after pre-sulfidation gradually decreased in Period 1 but increased in Period 2 which appears to be the primary effect of K uptake and removal.

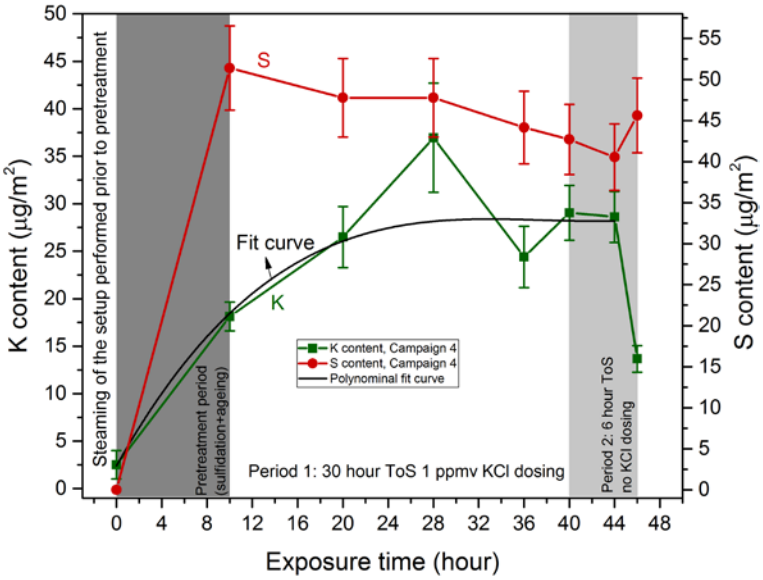

Fig. 4.7. Normalized sulfur and potassium content at the bed inlet vs exposure time, Campaign 4. The fit curve only serves as a guide to the eye. The average BET surface area for samples taken during time on stream is 14.3 ± 1.6 m^2/g

Figure 4.8 shows the K and S concentration profiles in the catalyst bed versus the axial bed distance after the end of Period 2. The K profile and the results shown in figure 4.7, K reaches a stable value at the inlet of the catalytic bed, indicating that the bed nearly reached its saturation of K most probably at the end of Period 1. The dashed line for K concentration after 30 hour also indicates that the bed nearly reached its K saturation. In the subsequent Period 2, adsorbed potassium was removed up to 1/3 of the bed, related to K migration from the inlet with desorption front moving through the bed. This indicates significant K mobility. For the remaining part of the bed, K was in a pseudo-equilibrium state. The K desorption is also displayed when comparing to the dashed horizontal lines representative of approximate inlet K concentration at 0 hour (beginning of activity test) and 36 hour time on stream. A clear trend for S profile is difficult to distinguish. A change through the bed is more evident for K, as the partial pressure of dosing K changes in Period 2, possibly due to faster

diffusivity and higher mobility of K in catalyst pellets, as well as in the bed compared to S.

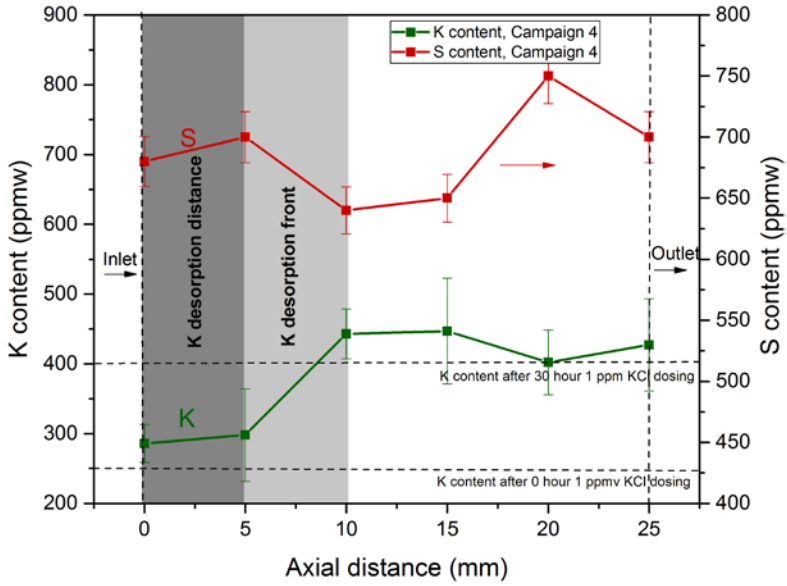

Fig. 4.8. Sulfur and potassium content profile in the catalytic bed at the end of Period 2, Campaign 4. The average BET surface area for samples taken at different axial bed distances is 13.7 ± 1.6 m^2/g.

Apparently, there is a correlation between the uptake of sulfur and potassium based on findings of paper I and II. A summary of the discussion and interpretations is presented here:

1. *K uptake suppression with increasing sulfur chemical potential:* It is known that alkalis adsorb with initial preferential titration of oxide carrier sites [90, 141-143], in particular defect/OH-group surface sites [90, 142, 144, 145], whereas sulfur is more nickel specific relative to $MgAl_2O_4$ support [146]. As reported by Bengaard et al. [100] from the density functional theory calculation point of view, although both S and K bind preferentially to the nickel step sites, sulfur adsorption is somewhat favored over potassium adsorption [100]. Therefore, the suppression of K uptake by S may be related to an S site blocking

effect on nickel and/or the spillover of sulfur to the support, blocking the K adsorption sites.

2. *Decrease in S content on a K-equilibrated surface:*
    - **a.** Increased Ni sulfur resistivity could be related to K-induced Ni-S bond softening. This was observed in previous studies by Chen et al. [147] and Politano et al. [148] similarly in the K-O/Ni system, confirming prior DFT results regarding the same system [149]; a donation of electron density by K to anti-bonding states of S-Ni. Another idea regarding the observed changes in S content is bond-order conservation model, where a strong K-S attractive interaction is expected to weaken the S-Ni bond. Similarly, Papageorgopoulos et al. [150] and Blaszczyszyn et al.[151, 152] observed strong interaction between K and S. All the suggested scenarios indicate S-Ni bond weakening with K co-adsoprtion, pushing S speciation equilibrium toward the gas phase and most likely increase in reactivity of surface S possibility toward hydrogenation or oxidation. The site-blocking effect of alkali in hindering H_2S adsorption was also suggested by Ferrandon et al. [153] for benzene hydrogenation on Rh-based catalyst.

    - **b.** The presence of K on nickel may increase the oxygen surface coverage on Ni, thus reduces S coverage. Surface NiO is reduced by hydrogen at temperatures starting around 200–250°C [2], whereas surface Ni-S is reduced by dry hydrogen (no steam) at temperatures around 650°C [154], meaning that the adsorption energy of S is higher than that of O on pure Ni. However, a K-modified Ni surface may shift the balance toward higher O coverage at the expense of S coverage.

K uptake suppression by higher sulfur passivation in early stages of K uptake (paper I) does not contradict the co-adsorption of K and S on Ni. It may reflect the reduction in the ability of K to titrate the hydroxyl sites on the support [155, 156], possibly due to sulfur spillover to the support as mentioned earlier. Section 4.4 presents a preliminary study of the preferential adsorption site for potassium.

Based on the K-equilibrated surface results obtained, relevant K surface coverages under the tar reforming conditions for a typical Ni on high-T alumina-based catalyst is calculated to below 100 μg/m^2. Assuming support hydroxyl sites being the main fraction of K adsorption sites on the catalyst and estimating the concentration of these sites to be in the range of 0.1–2.0 OH/nm^2 based on prior studies [157-159] and under the tar reforming conditions, quantitative K-titration calculation corresponds to 8–163 μg K/m^2. This can be compared with the observed K uptake of 10–40 μg /m^2, in the range of the calculated K content.

4.3.2 Potassium influence on catalyst activity

Figure 4.9a displays the methane, naphthalene, and C_{10+} conversions over time. The C_{10+} components include 2-methylnaphthalene, 1-methylnaphthalene, biphenyl, acenaphthylene, acenaphthene, fluorene, phenanthrene, anthracene, fluoranthene and pyrene. There is a significant initial increase in conversion for methane and higher hydrocarbons during first 10–15 hour ToS with the stabilized activities toward the end of Period 1 as K is reaching equilibrium on the surface and the bed. S-Ni bond weakening and subsequently lower coverage of S at active sites may explain the improved activity toward methane and tar. Since S adsorbs stronger than K on Ni [150], it is a worse inhibitor and reducing its coverage improves the reforming activity of the catalyst. It is of importance to point out that all the studies conducted here involced essentially carbon-free operation. The average C content was stable over time during activity tests meaning the promoting effect of K on the catalyst performance was not related to changes in carbon deposition.

Increased activity with K has been observed for methane and tar reforming in other studies [91, 160, 161]. K promoted activation of methane on a K doped NiO/Ni(100) surface was observed by Chen et al. [160], relating the activity promotion to improved selectivity of NiO toward C–H cleavage. Wangen et al. [91] investigated a reforming catalyst doped with KCl and KNO_3 and detected minor enhancement of the CH_4 reforming rates, although a severe deactivation was observed at higher concentrations. Similarly for tar reforming, Kuchonthara et al. [56] reported on improved steam reforming of tar in the presence of potassium. K-doped support(alumina) displayed reactivity toward tar molecules [162] meaning a K-modified support may also contribute to the observed improved activity. Moreover, there is a less retarding effect of tar components on the steam reforming of benzene and methane. This has been revealed in other studies by Jess [163] and Wangen et al.[91] in the presence of higher hydrocarbons in gas mixture. These studies attributed the loss of activity to retarding site blocking effect (strong adsorption) and competitive adsorption, proving that the loss in activity was due to the influence of increased concentration of tar (naphthalene). In summary, the findings of this work under steady-state tar reforming conditions indicate that potassium promotes methane and tar reforming activity of Ni-based catalyst, even though in traditional steam reforming, K is known to block active nickel sites and decrease the catalyst activity above a certain threshold concentration [2, 53, 96]. In the recent studies by Marinkovic et al. [164] and Alamia et al. [47], positive effect of potassium in total tar destruction was observed in biomass gasification process. The observation was that addition of sulfur increases further the catalytic effect of already added potassium, decreasing the tar yield significantly [164]. Feeding sulfur enhances the activation effect by making a bond with potassium in the combustion side of the dual-fluidized bed system, keeping K in the system, and transporting it from combusting to gasification side which possibly become catalytically active as KOH or K_2CO_3 [164]. Although this observation is made for primary mitigation techniques and not in hot gas conditioning applications, it still describes an important influence of sulfur on potassium adsorption energy and their interaction in tar abatement applications.

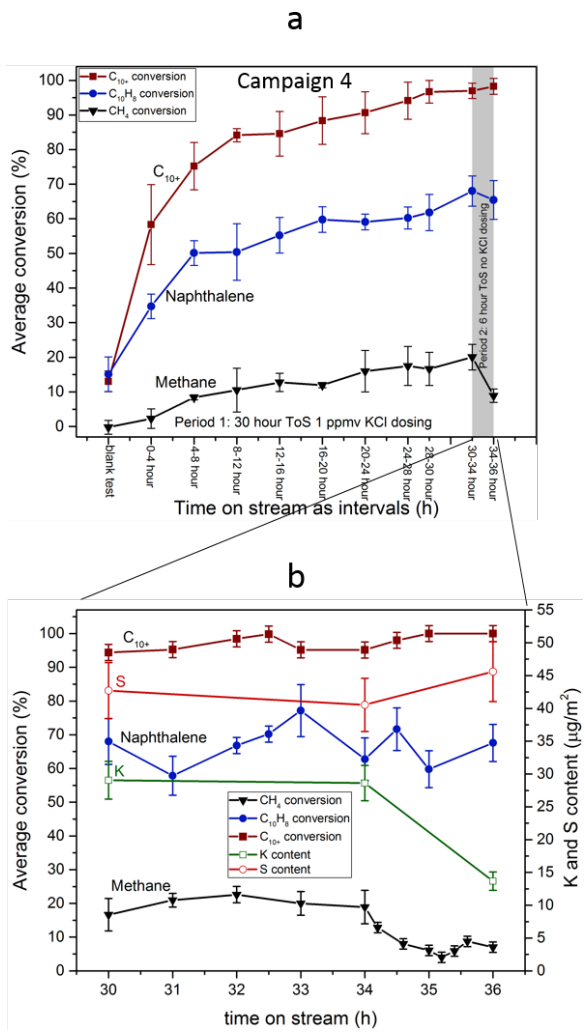

Fig. 4.9. a) Average methane, naphthalene and C_{10+} conversion versus time on stream as intervals for Periods 1and 2, Campaign 4. b) Average methane and tar conversion as well as bed inlet S and K contents versus time on stream for Period 2 (no KCl dosing) with higher time resolution, Campaign 4.

Figure 4.9b presents the Period 2 with higher time resolution and it also displays the bed inlet K and S concentrations during no KCl dosing. As the K content decreases and S content increases with a 3–4 hour delay,

methane conversion decreases significantly. The reverse phenomena explained for Period 1 due to K adsorption could explain the behavior of methane conversion in Period 2. Taking into account the standard deviation in tar measurement, its conversion appears to have no significant changes during Period 2. This may be because methane is more intra-particle sensitive than is naphthalene (see section 4.2.2) as well as dynamics of the bed changing due to K desorption front moving over time. Other studies observed selective deactivation toward methane and no or less hindering of tar reforming in presence of H_2S [163] [165]. Similarly, the core/shell behavior of K and the inter-particle diffusion limitations for naphthalene may be the reasons why methane conversion is more affected by K desorption than are the higher hydrocarbons.

4.4 Preferential adsorption site for potassium

To deepen the understanding of alkali adsorption and its influence on tar reforming activity, experiments were performed to clarify the preferential adsorption sites by measuring the activation energy of potassium desorption. Table 4.2 presents the prepared samples for SR-TAD study, the K and S content of each sample and desorption energies of potassium determined from the linear parts of Arrhenius plot. Due to experimental limitations, the highest temperature for SR-TAD experiments was 600°C, therefore there may be higher desorption energy states that were not probed in this study. The spent samples were taken from different campaigns, as explained earlier.

Table 4.2. Sample characterization and the potassium desorption energies

Samples	K content, ppm	S content, ppm	Desorption activation energy (eV)
1. $MgAl_2O_4$ impregnated with K	540	0	1.09
2. Fresh Ni/$MgAl_2O_4$ impregnated with K	270	0	2.35
3. Spent Ni/$MgAl_2O_4$	425	700	1.7
4. Spent Ni/$MgAl_2O_4$	300	500	1.7
5. Spent Ni/$MgAl_2O_4$	232	1100	1.9
6. $MgAl_2O_4$ impregnated with K and calcined to 420 °C	540	0	2.3
7. $MgAl_2O_4$ impregnated with K and calcined to 800 °C	540	0	1.8
8. Fresh Ni/$MgAl_2O_4$ impregnated with K and calcined to 420 °C	270	0	2.2

The interpretation of the results are done by classifying the desorption energies as type of sites available for K adsorption in different samples:

1. (2.2–2.35 eV): Fresh Ni-based and low-temperature (420°C) calcined support ($MgAl_2O_4$) has the highest desorption energy, meaning highest binding energy sites. This may be related to the availability of more active defective and OH sites on support that are eventually removed by high-T treatment of the samples.

2. (1.7–1.9 eV): High-temperature calcination and tar reforming at 800°C appears to remove high energy binding sites, resulting in the 1.7–1.9 eV desorption energy range for potassium. The desorption energy of K for spent catalysts are quite similar to each other and in the same range as high-T calcined support.

3. 1.1 eV: This was observed for K-impregnated support with no calcination. The 1.1 eV sites are just loosely bound K which if mildly calcined (420°C) will be better distributed over the 2.2–2.35 eV sites.

Bengaard et al. [100] studies on DFT calculated binding energy for potassium on nickel terrace sites pre-covered or without oxygen resulted in 1.3 eV and 1.35 eV respectively. Comparing the DFT calculated data by Bengaard et al. [100] and the experimental results in this work, K adsorption on the support appears to be the preferential adsorption site at the operating temperatures of tar reforming. This is in line with discussions in section 4.3.1, stating that alkali adsorbs with the initial preferential titration of oxide carrier OH- group /defects sites [90, 142, 144, 145]. It is important to state that these results are not solely conclusive and the observation for preferential adsorption site does not necessarily mean there is no adsorption of K on the active Ni surface, especially since sulfur significantly enhances the K adsorption strength at Ni surfaces compared to clean Ni [151, 152].

4.5 Summary: equilibrium K coverage and its effect on tar reforming

Figure 4.10 is a simplified schematic of S-K/Ni/support system with the main findings summarized.

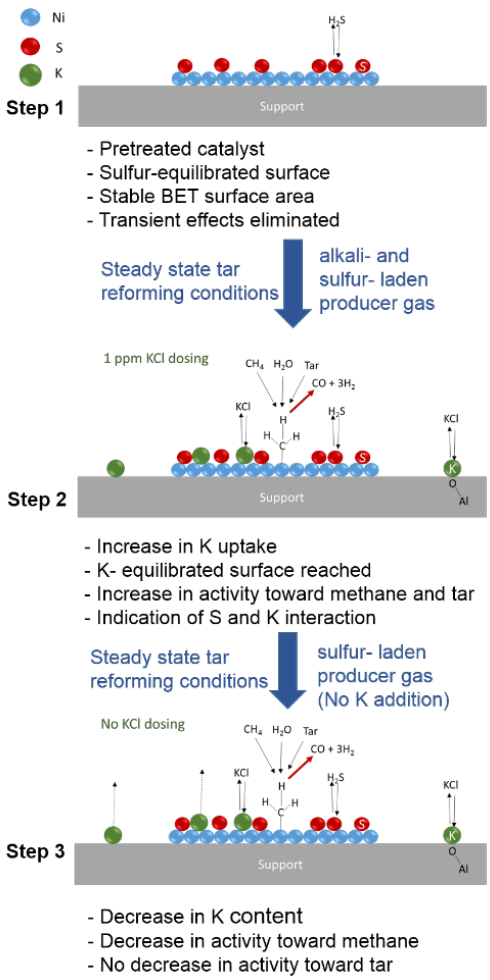

Fig. 4.10. S-K/Ni/support schematic and the observed parametric study of S and K under steady-state tar reforming conditions.

A methodology was successfully developed and implemented to enable controlled investigation of gas-phase alkali influence on tar reforming catalyst activity under realistic steady state conditions (paper I). In summary, after elimination of transient effects caused by sulfur poisoning and sintering, the pre-treated catalyst (Step 1) was exposed to alkali and sulfur laden biomass gasification gas. K uptake was correlated with the gas-phase KCl concentration. A K-equilibrated surface under steady state tar reforming conditions was reached (Step 2). K-equilibrated coverage on the studies Ni/$MgAl_2O_4$ steam reforming catalyst under real tar reforming conditions was measured to be in the range of 10 to 40 μg / m^2 BET and was calculated to be below 100 μg/m^2 for a typical Ni-based steam reforming catalyst under tar reforming conditions (paper II). Although in traditional steam reforming, K is known to block active nickel sites and decrease the catalyst activity, findings of this study showed that it increases methane as well as tar reforming (paper II). This may be related to K interaction with S on nickel and/or support and the subsequent decrease in sulfur content of the catalyst. Retarding the site blocking effect of higher hydrocarbons and K-modified support surface may also contribute to the observed increase in activity (paper II). Furthermore, there was reduced methane reforming activity and no changes in activity toward tar, after decreasing the gas-phase KCl partial pressure (no KCl addition period) and the observed K desorption from the K-equilibrated catalyst surface (Step 3). The preliminary study of the preferential adsorption site for K revealed that the support appears to be the preferential adsorption site on the Ni-based tar reforming catalyst. However, these findings do not exclude the possibility of K and S co-adsorption and interaction on nickel.

5 Tar (naphthalene) reforming surface chemistry (paper III)

Naphthalene, a tar molecule commonly present in raw producer gas from biomass gasification and one of the most difficult ones to decompose [20], was chosen as a model compound for tar reforming surface chemistry study. Temperature dependent naphthalene adsorption, dehydrogenation and carbon formation on a model system, Ni(111), was studied using TPD and STM in an ultra-high vacuum environment from 110 K up to 780 K. Naphthalene adsorption energies, geometric distortion and redistribution of electronic density has been investigated using DFT molecular modeling. The most important results and discussion points are presented in this section.

5.1 Naphthalene adsorption and structure

Adsorption of naphthalene in room temperature on Ni(111) is shown in STM images in figure 5.1a. Results suggest a monolayer adsorption of naphthalene with a somewhat ordered structure on Ni(111) terraces. The order is not in the long range. The orientation of naphthalene molecules are following the substrate. Figure 5.1b was acquired after annealing the sample to 373K and shows that the ordered patches have grown to 10–15 nm and the molecule exhibits same orientations. DFT studies in this work suggests the planar configuration to be the energetically favorable structure for naphthalene. It also depicts three different preferred adsorption sites with quite similar adsorption energies (Figure 5.2), which confirms the less ordered structure of naphthalene on Ni in formats of small ordered domains. Compared with the Santarossa et al. [166] study, adsorption of naphthalene on Ni(111) found here is stronger than that of Pt(111) and Rh(111) in all three preferred geometries.

Conclusively, the naphthalene adsorbs flat on the smooth terraces with the aromatic rings centered over Ni-bridge sites. The naphthalene on nickel is

strongly activated, reflected not only by the high adsorption energy, but also by the aromatic ring distortion. This has important practical implications since a bent molecule is much more prone to the catalytic modification, in particular, to dehydrogenation.

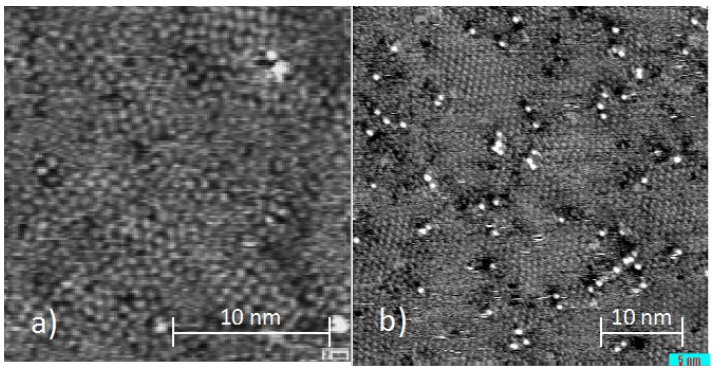

Fig. 5.1. STM images from naphthalene adsorbed on Ni(111). a) 20x20 nm (-2.8 V, 80 pA), b) 40x40 nm^2 high resolution image after deposition at 373 K.

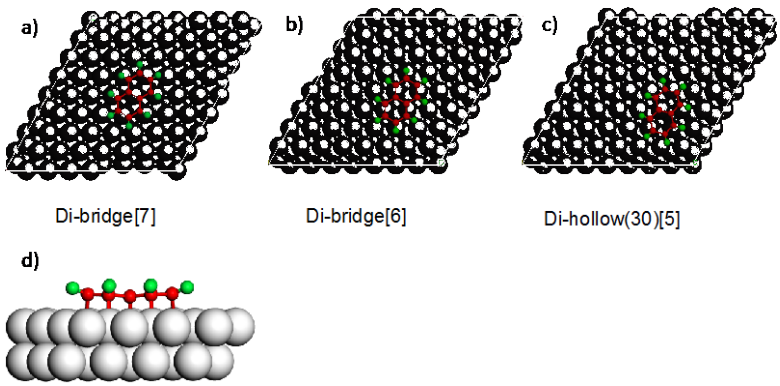

Fig. 5.2. Three adsorption geometries for naphthalene on Ni(111), obtained from DFT simulations,. a) Di-bridge[7], b) Di-bridge[6] and Di-hollow(30)[5]. Side view of an adsorbed naphthalene molecule is shown in d).

5.2 Naphthalene dehydrogenation and carbon passivation

Figure 5.3a presents the TPD results for desorption rate of naphthalene. There is peak at temperatures below room T, related to naphthalene multilayers loosely bound and coming off below room temperature. No desorbed carbon species were detected QMS at above room temperatures, meaning all the C species were intact and no carbon is lost to the gas. Figure 5.3b presents TPD results for desorption of hydrogen at different naphthalene dosed coverage. The TPD temperature range of molecular hydrogen desorption (red-dashed spectra in Figure 5.3b) compared to temperature range of hydrogen desorption from naphthalene-dosed Ni surface is a proof that naphthalene only undergoes dehydrogenation at temperature above 380 K. There are two distinctive peaks for naphthalene dosed TPD, a low temperature peak and a high temperature peak. Previous TPD studies of naphthalene on Pt(111) and Rh(111) also revealed TPDs with two main features [167, 168]. The first dehydrogenation peak temperature happens at much lower temperature on Ni compared to Pt and Rh. The first peak is related to first two hydrogen desorption since the integrated area underneath the first peak accounts for 25% of the total area, and the second peak with the wider temperature range accounts for the rest of the dehydrogenation of the hydrocarbon fragments.

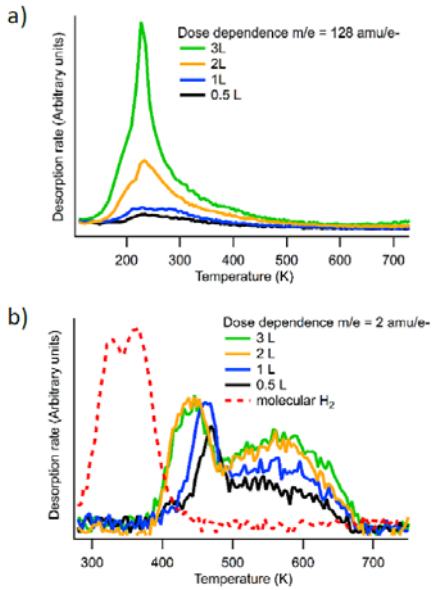

Fig. 5.3. TPD spectra after 0.5 L, 1 L, 2 L, and 3 L naphthalene dosing on Ni(111) at T=110 K a) m/z=128 b) m/z=2.

The onset temperature of the TPD signal can be used as a fingerprint for C–H breakup. Based on calculations explained in Section 3.2, activation energy for H_2 desorption from naphthalene-dosed Ni was calculated to be 1.3 eV for 1 L dosing (low coverage). Pre-factor for linear parts of Arrhenius plots was calculated to be approximately 1 order of magnitude lower than expected (10^{-13}). This is not surprising as it has been recently reported that pre-factors for dissociations are 1 to 3 orders of magnitude lower than pre-factors for desorption of the same molecule [169]. H_2 activation energy for desorption from clean Ni(111) surface was calculated to be 0.99 eV for low coverage and lower for high coverage[170]. The calculated activation energy for C–H break-up agrees with the calculated energy barrier for the first dehydrogenation coronene on Ir(111) [80].

To gain further insight into the dehydrogenation mechanism of naphthalene, several consecutive TPD experiments were performed with no cleaning step (see Section 3.2) in between. The results are displayed in figure 5.4. The intensity of the molecular hydrogen dosed surface also

decreased after each cycle of dosing, meaning the available surface on nickel is decreasing. The intensities of low-T peaks (around 450 K) and high-T peak (around 600 K) were lower due to passivation of the surface with C-containing molecules occupying the available surface sites for reactions. The formation of carbon fragments on the surface passivated the surface for both hydrogen adsorption and naphthalene dissociation.

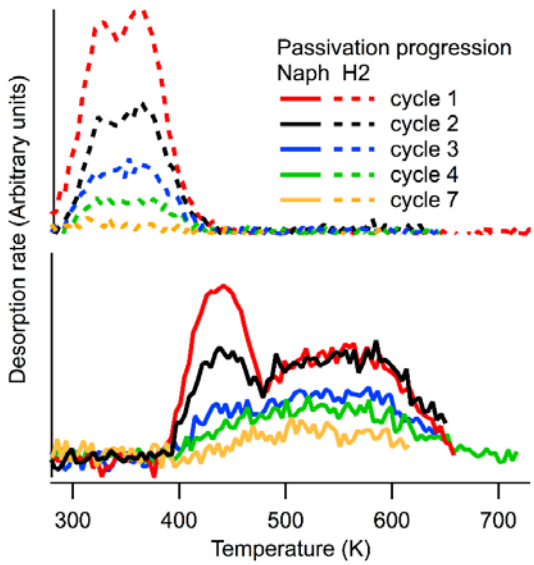

Fig. 5.4. TPD spectra for a hydrogen and naphthalene covered sample at 278 K and 3 L with seven passivation cycle

Figure 5.5 presents STM image acquired after annealing a naphthalene monolayer at different temperatures. After annealing at a temperature of <470 K, the image shows ordered patches of naphthalene molecules and small height variations over larger distances, which could be due to work function variations over the surface, perhaps due to hydrogen atoms within the naphthalene layer. When annealing at temperatures up to 520 K, the ordered naphthalene patches vanished and approximately 1.5 Å higher areas appeared. 520 K is above the first hydrogen peak observed in TPD, and apparently the molecular order was broken. After annealing at 570 K, bright chain grew with an apparent height of 1.5 Å and ca 20 Å width. At

650 K, the chains have merged into a network like structure. The height of the bright pattern is 1.5 Å. Finally, after annealing at 780 K the height variation disappeared, leaving behind a smooth surface.

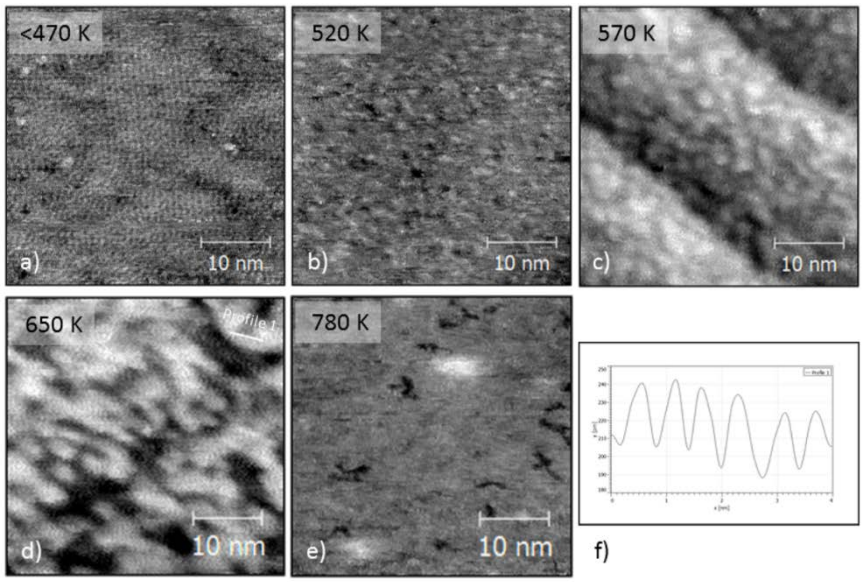

Fig. 5.5. STM images of Ni(111) exposed to naphthalene (monolayer coverage) at room temperature and annealed to a) T<470 K, b) T=520 K, c) T= 573 K, d) T=650 K and d) T =780 K. The temperature was measured with a pyrometer. All images are recorded at 2 V positive tip bias. The longitudinal periodicity f) extracted from the STM image along the Profile 1 line is approximately 8–10 Å.

The STM and TPD observations are in line with Wang et al.'s [81] STM and Lu et al.'s [82] molecular simulation studies. The chains observed in this study exhibit a longitudinal corrugation periodicity of 8–10 Å, as illustrated by the profile 1 line in figure 5.8f, close to the expected distance between carbon rings. Lu et al. [82] showed the formation of 5-m and 6-m rings and Wang et al. [81] observed formation of chains from C4 to C6 species at 470 K on Rh(111), attributing this formation to one-dimensional linear polyaromatic hydrocarbons. Furthermore, at high temperatures, network formation was also observed by Wang et al. [81], who suggested that it was due to coalescence of carbon clusters into chains, and further to

broader chains and finally to graphene. This observation is in line with Lu et al. [82] findings. On contrary, Patera et al. [171] and Lahiri et al. [172] suggested that surface carbides formed adsorbed hydrocarbons transforming into graphene at temperatures below 780 K. Although the obtained data were not directly able to distinguish between these two observations, they agree with the reaction pathway described by Wang et al. [81] and Lu et al. [82].

5.3 Naphthalene reaction pathway on nickel

The obtained model system results, provide insight into the chemical reaction pathway leading from tar, in this case naphthalene, to carbon formation on nickel. Figure 5.6 is a schematic of elementary steps involved in catalytic reaction pathway for naphthalene on Ni(111).

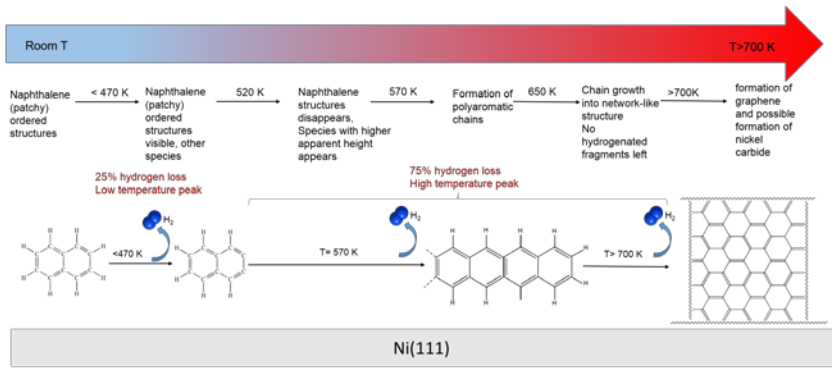

Fig. 5.6. Schematic of the chemical reaction pathway from naphthalene to graphene on Ni(111).

Naphthalene undergoes dehydrogenation on Ni(111) at 380 K. The second dehydrogenation step is accompanied by transformation of the adsorbate layer to graphene. This pathway starts with transformation from a surface of naphthalene ordered domains via a surface with patches, chains and a network like structures. From the catalysis point of view, the identity of molecule is important when it comes to degree of deactivation and carbon formation. For example, ethylene and aromatics are some of the worst and this has also been shown to be the case for PAHs of increasing size [89]. Within a surface carbide route to graphene, one would not expect such a drastic dependence on the molecular identity of the hydrocarbon. Therefore, the coalescence of reactive (hydro)-carbon structures seems much more likely on the basis of the catalysis literature.

6 Catalytic conditioning of pyrolysis gas (paper IV)

The industrial use of Fe-based catalyst for pyrolysis gas conditioning was successfully explored, including an investigation and elaboration of the chemistry taking place over the Fe-based catalyst. After the catalyst's initial stabilization and fluctuations in temperature and during the stable run, the real pyrolysis gas was treated for 8 hours in a small industrial scale facility. The conditions of the operation were deemed stable, based on the stable temperature profile and permanent gas compositions during the run. An endotherm developed at the inlet of the catalytic bed and a lift in temperature along the bed was observed which was partly related to oxygenate deoxygenation and cracking/steam reforming of the pyrolysis gas and forward WGS reaction, respectively. Section 6.1 and 6.2 presents the most important results gained from characterization of bio-crude, permanent gas and spent catalyst.

6.1 In-depth bio-crude and gas analyses

Figure 6.1 presents the yield changes for some of the components in bio-crude as observed in the GC-MS results. Significant oxygenate cracking/steam reforming activity of pyrolysis gas was observed with high reduction of acetic acid, methoxy phenols, ketones, catechol, and heterocyclic compounds indicating a slightly stabilized resultant bio-crude. A significant conversion was observed even for stable BTX compounds. Arab et al. [173] observed hydroxylation of benzene to phenol over an Fe-based catalyst that may describe the changes in the stable BTX compounds in the bio-crude. Based on phenolic and alkylated compounds yield changes, it appears that the catalyst is less active toward reduction of phenol compounds. The increased conversion of p-cresol and 3-ethyl phenol is in line with other studies, displaying increased yields of alkyl phenols in gas-phase HDO [174-176] and alkylation [177, 178] processes using Fe-based catalyst.

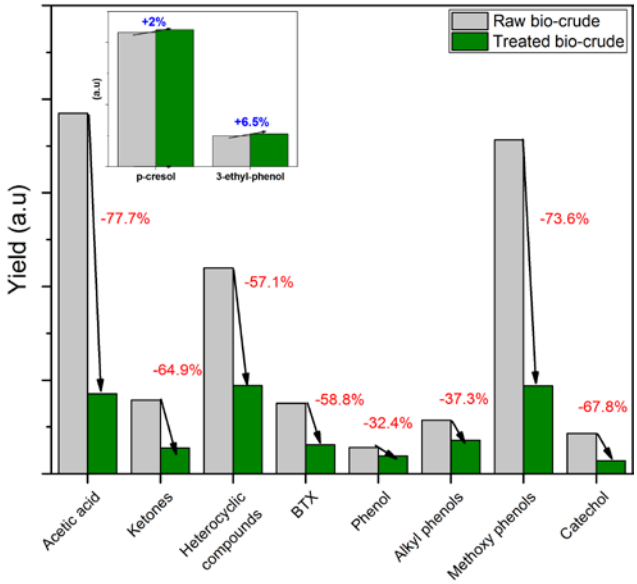

Fig. 6.1. Yield changes of compounds in raw and treated bio-crude determined using GC-MS.

As displayed in table 6.1 for bio-crude C/H/O/S ,ash analysis, and KF titration, and mass distribution in raw and treated bio-crude as shown in figure 6.2, increase in water content of bio-crude and decrease in oxygen content and bio-crude flow rates was observed. The increase in water content originated primarily from the very facile and fast oxygenate dehydration reactions.

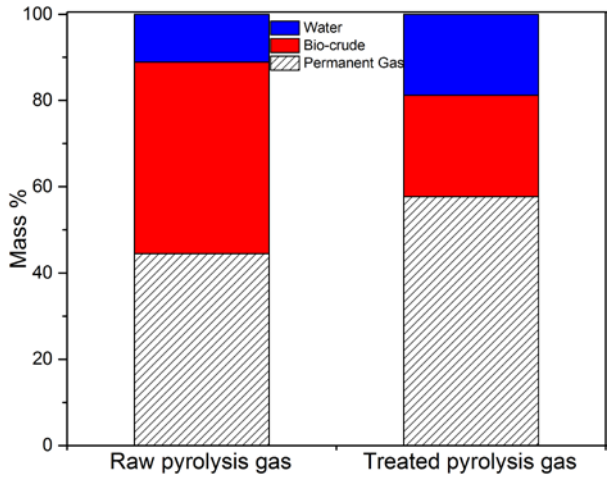

Fig. 6.2. Mass distribution of bio-crude, permanent gas and water in raw and treated N_2-free pyrolysis gas.

Table 6.1. C/H/O/S and ash analysis on dry basis (db), water content, Steam/C, O/C, and H/C of the raw and treated solvent-free condensate

		Raw condensate	**Treated condensate**
C	wt% db	50.3	59.3
H		4.9	5
O		44.8	35.7
S		<0.05	<0.05
N		<0.1	<0.1
Ash		0.007	<0.001
Water content		20	44.3
Steam/C of condensate	mol/mol	0.33	0.9
O/C of condensate		0.99	1.34
H/C of condensate		1.84	2.81

Permanent gas flow rates are shown in figure 6.3. Increase of hydrogen and CO_2 flow rates in permanent gas and decrease in CO and a negligible changes in methane and lighter hydrocarbons demonstrated significant WGS activity and minimal, if any, CO hydrogenation.

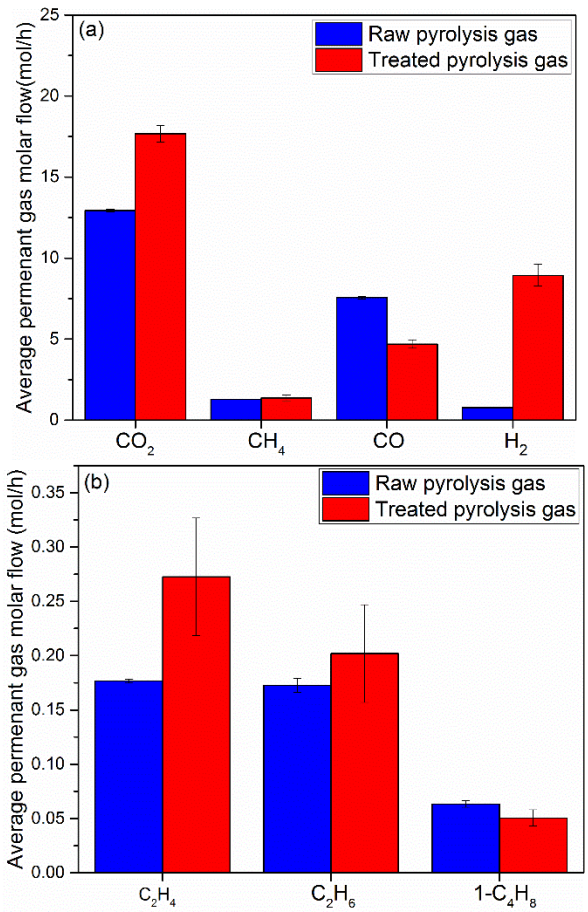

Fig. 6.3. Average molar flows of permanent gas components in the raw and treated pyrolysis gas: a) CO_2, CH_4, CO, and H_2, b) C_{2+} compounds.

Based on Van Krevelen diagram shown in figure 6.4, and the changes in CO_2 and H_2 content, one would expect other reactions beside oxygenate dehydration and forward WGS reaction to take place to a lesser extent (decarbonylation, decarboxylation) that contributes to syngas production, such as the observed acetic acid decomposition shown in GC-MS results. A high acetic acid decomposition activity is in accordance with Brijaldo et al. [179], who observed a high selectivity toward hydrogen production via catalytic decomposition of acetic acid by supporting palladium on an iron oxide carrier.

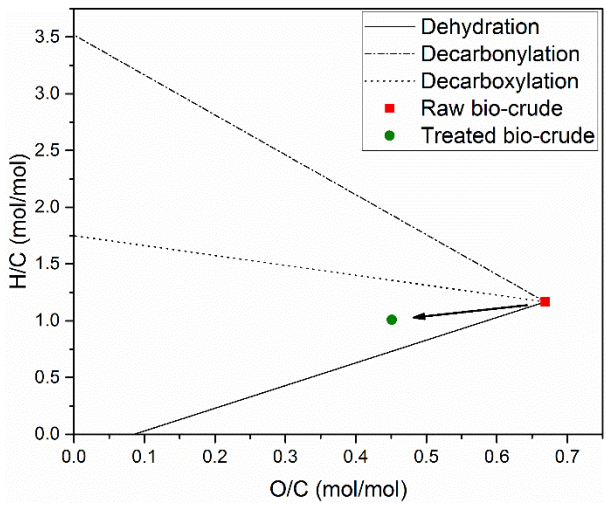

Fig. 6.4. Van Krevelen diagram of the elemental compositions of raw and treated solvent-free bio-crude (water-free).

6.2 Catalyst activity

Table 6.2 shows XRD, carbon content and BET surface area of samples taken from inlet, middle and bottom of the bed. A drastic difference in surface chemistry of the gas components is anticipated depending on whether the active surfaces of the catalyst are of Fe-oxide or Fe-carbide character under the process conditions. In the case of Fe-carbide, a significant activity for CO and CO_2 hydrogenation into methane and lighter hydrocarbon FT-products is expected [180-182]. The XRD analysis confirmed Fe_3O_4 as the bulk phase of the catalyst after the test and in line with the observed permanent gas changes, showing surface of the Fe-based catalyst under the process conditions was of Fe-oxide type rather than Fe-carbide.

Despite observed catalyst carbon laydown and sintering, there was no noticeable catalyst deactivation during the stable 8-hour of operation as the catalyst permanent gas composition was stable. The decrease in BET surface area is directly related to sintering as the decrease directly correlates with the relative increase in average crystallize sizes. Based on the carbon yield results, the carbon laydown is significant, however it is a small fraction of the total carbon in pyrolysis gas passed through the bed the entire test when compared with coke deposition on zeolite catalysts because of the strong adsorption of compounds on zeolites strong acid sites as well as steric hindrances [183-186].

Table 6.2. Catalyst characterization results for fresh and spent samples.

	Fresh catalyst	**Spent catalyst**		
		Top	Middle	Bottom
BET surface area (m^2/g)	72	39.7	35.1	34.41
ΔC (wt%)	0	10.8	10.2	9.7
Relative Crystallite size (spent/fresh ratio)	1	1.7	2.1	2.0

6.3 Proposed reaction pathways

A simplified mechanism for the conversion of the pyrolysis gas, using the iron-based catalyst is proposed and illustrated in figure 6.5. Besides establishing the expectedly facile bio-crude dehydration, also other deoxygenation routes (decarbonylation and/or decarboxylation) and oxygenate cracking/steam reforming reactions (e.g., for acetic acid, methoxy phenols, BTX and heterocyclic compounds) were confirmed to take place as indicated by the results. Dehydrogenation is not favoured at low operating temperatures and hydrodeoxygenaiton is unlikely due to low partial pressures of H_2 in this work and it is consistent with the fact that the hydrogen content does not increase in the bio-crude after catalytic treatment. On basis of the insignificant amounts of methane and minor amounts of higher hydrocarbons formed over the catalyst, CO/CO_2 methanation and higher hydrocarbon formation via FT chemistry is very limited, if taking place at all. The non-catalytic thermochemical conversions were negligible because the changes in the gas composition over the bed filled with inert material was insignificant [187].

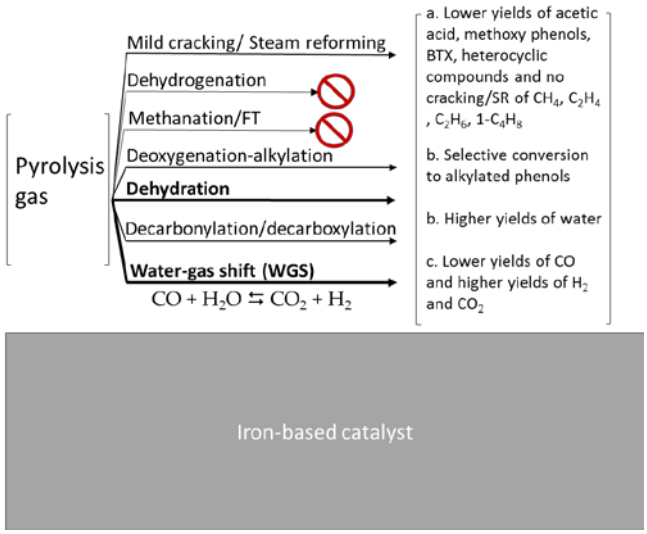

Fig. 6.5. A simplified reaction network for conversion of the pyrolysis gas.

6.4 Implications of the technology

Most of the techniques discussed in the literature on bio-crude steam reforming have drawbacks and are far from being applicable in industrial conditions. In conventional steam reforming, a pre-reformer is often used for converting higher hydrocarbons to syngas and CH_4 prior to reformer. This allows flexibility in the choice of feedstock and higher inlet temperatures into the reformer. Trane et al. [21] suggested that a pre-reformer concept, in which bio-crude is first converted into C_1- species at low temperature, before steam reforming at higher temperatures, has a potential to overcome the weaknesses in bio-crude steam reforming [21]. However, this possibility must be further investigated before the commercialization of bio-crude stream reforming. Some beneficial aspects of the pre-reforming concept are pointed out previously in section 2.2, such as low carbon laydown and extended stable operation times.

The previously reported bio-crude conditioning concepts are for condensed bio-crude as well as high hydrogen pressures being used [188]. There are previous lab-scale studies on catalytic upgrading (HDO) of catalytic flash

pyrolysis [176, 189], uncondensed pyrolysis vapors [175, 190, 191] and model compounds [125, 192] studies, pointing out the advantage of direct pyrolysis gas condition process and indicating that Fe-based catalysts are interesting as low cost materials for oxygenate deoxygenation/conversion at intermediate temperatures. The results of the pyrolysis gas conditioning in this work, indicate that iron-based materials are potential candidates for application in a pyrolysis gas as a pre-conditioning step as illustrated in figure 6.6, prior to further treatment or use. The catalytic treatment is conducted without the need to condense out bio-crude and the operating temperature of the catalyst corresponds well to the conventional pre-reformer conditions (350–500°C). Since the active phase of the catalyst under the process conditions was of Fe-oxide type (Fe_3O_4 observed for the bulk phase of the catalyst), a certain sulfur tolerance of the catalyst used can thus be expected [3, 193]. This is a very important feature for catalysts in biomass applications because of the non-negligible sulfur content in biomass. Therefore, a desulfurizaiton unit may be used after the pre-conditioner to prevent coke formation in the unit in line with the suggestion of Trane et al. [21].

Additionally, based on the results, a direct way to reduce the carbon laydown on the catalyst would be to recycle part of the exit gas, which is significantly richer in H_2, H_2O, and CO_2, and significantly leaner in bio-crude, than the inlet gas. Recycling reformate in the pre-reforming of heavy feedstocks was demonstrated to effectively decrease coke deposition [2].

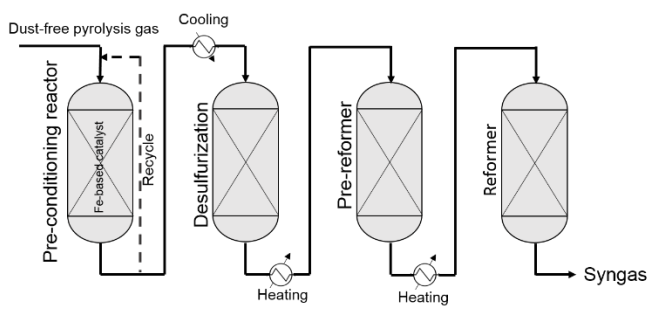

Fig. 6.6. Implication of the pyrolysis gas conditioning technology over an Fe-based catalyst: two-reactor concept (pre-reformer and reformer) for pyrolysis gas conditioning to syngas

7 Conclusions and future outlook

This work was performed in the field of thermochemical conversion of biomass to synthesis gas via gasification and pyrolysis, ranging from atomic to small industrial scale. The aim of this work was to investigate the effect of potassium, a biomass-derived impurity, on tar reforming catalyst under realistic conditions and deeper understanding of tar reforming mechanism as well as exploring the industrial use of Fe-based catalyst for pyrolysis gas conditioning. The main conclusions and suggestions for future work are presented in the following sections.

7.1 Catalytic (steam) tar reforming

7.1.1 Complexity of the S-K/Ni/$MgAl_2O_4$ system

Nickel-based catalysts are commonly used in industry for the catalytic steam reforming of non-renewable feedstocks and are also expected to be technically and economically feasible in applications such as biomass gasification. The complexity of biomass tar and the presence of impurities such as sulfur and alkali compounds remains a challenge for understanding the catalytic processes such as the effect of gas-phase alkali on tar reforming catalyst performance. Experimental studies were carried out on a Ni/$MgAl_2O_4$ steam reforming catalyst to evaluate the possibilities of investigating the interactions between gas-phase potassium species and the catalyst surface under fully realistic conditions. A methodology was successfully developed to facilitate a controlled investigation of combined potassium and sulfur influence on the catalyst performance. The crucial elements of this methodology were the accurate dosing of gas-phase alkali and the elimination of activity transients due to sintering and sulfur poisoning. After evaluating and implementing the methodology, it was concluded that the relevant K equilibrium coverages on the Ni/$MgAl_2O_4$ steam reforming catalyst used under real tar reforming conditions, which were previously unknown, were in the range of 10–40 µg/m^2 BET. Based on this, relevant K equilibrium coverages for a typical Ni-based steam

reforming catalyst under tar reforming conditions at temperatures exceeding 800°C were extrapolated to be below 100 µg/m^2 BET. This is an important finding in terms of the gas-phase alkali uptake and equilibration on the catalyst surface.

The most striking result found in this study was that as K coverage (θ_k) increases and reaches its equilibrium, it appears to lower the surface sulfur coverage (θ_s) at active Ni sites and increase methane as well as tar reforming. Although K can retard the activity of the catalyst in conventional steam reforming by blocking the active Ni (step) sites, the results observed here indicates an improving effect of potassium on both tar and methane reforming. It was suggested that K-induced softening of S-Ni bonds appears to explain the observed reduction in θ_s. The mechanism underlying sulfur and potassium interaction was discussed. However, this mechanism is not immediately clear and the results are not solely conclusive. Preliminary results indicate that the preferential adsorption site for potassium is on the support, possibly defect/O(H) sites, of a sulfur-passivated Ni-based catalyst. Therefore, a K-modified support surface may also contribute to the increase in reactivity toward tar components. This finding does not rule out the possible interaction of sulfur and potassium on the active Ni sites. During no KCl dosing period, K desorbed and methane reforming activity considerably decreased while higher hydrocarbon conversion did not change significantly. This observations was discussed to be the outcome of intra-particle diffusion limitations being less severe for methane as well as the dynamics of the bed changing over time as the K desorption front moves through the bed.

In terms of industrial relevance, the positive effect of K on the methane and tar reforming catalyst in presence of the sulfur could be to change potassium or sulfur coverage on the catalyst surface by having a potassium (or sulfur) source upstream of the dusty/clean tar reformer, possibly after filtration, and adding the potassium (or sulfur) to tailor θ_k, so that the activity toward tar molecules improves. Another alternative for tailoring θ_k could be to modify the filtration process to achieve the desired θ_k, since the level of impurities depend on the filtration temperature as well as chemical

and physical properties of the dust collected in the filter cake. A better understanding of sulfur and potassium interactions with the Ni-based catalyst and the tar reforming mechanism is therefore required to optimize tar reforming processes.

Future work could focus on extended methane and tar reforming activity studies during the K desorption period. More experimental and theoretical work is needed to further elucidate the complexity of S-K/Ni/$MgAl_2O_4$ system. This could establish decay curves for potassium desorption and also address the importance of K-modified support in tar reforming for Ni-based catalysts. To deepen the understanding of alkali adsorption and its influence on tar reforming activity, experiments must be designed to elucidate the influence of K on S adsorption energetics on Ni and determine K adsorption energy on sulfur-passivated nickel. Furthermore, design-enabling surface science and computer technologies (DFT modeling) may establish the thermodynamics of the speciation and distribution of K on support and S/Ni and clarify the interaction of potassium and sulfur on Ni, which will eventually leads to the development of a thermodynamic model of K-relevant species on steam reforming catalyst. In terms of alkali and tar measurement, use of more novel methods for accurate on-line characterization of alkali and heavy tar compounds in hot producer gas is suggested for future work. Another suggestion for future study is to investigate the possible effect of potassium uptake on Ni-based catalyst sintering in reducing environment of tar reforming.

7.1.2 Tar reforming surface chemistry

This part of the study focused on better understanding the mechanism of tar reforming using a model system. Experimental and theoretical studies of naphthalene, a tar molecule commonly found in raw producer gas from the low-temperature biomass gasification route, adsorption and dehydrogenation on Ni(111) are scarcely reported in the literature. A combined experimental and theoretical approach to understand the catalytic reaction pathways revealed that the naphthalene on nickel is strongly activated, meaning that it is prone to catalytic modification. The STM and TPD studies demonstrated that naphthalene dehydrogenation

occurs in two steps. The first step is accompanied by the dehydrogenation of 25% of the hydrogen. The second dehydrogenation step goes along with dehydrogenation of rest of the hydrocarbon fragments and transformation of the adsorbed naphthalene to graphene. The mechanism for this reaction pathway starts with surface of ordered domains of naphthalene molecules transforming into surface with patches, polyaromatic-like chains merging into network-like structure, and finally the coalescence of reactive (hydro)-carbon structures into graphene. In conclusion, the obtained model system results provide insight into tar reforming surface chemistry and may serve as a good starting point to advance the design of new catalysts and processes for aromatic hydrocarbons reforming. One should, however, keep in mind the pressure and material gaps in the model system study and their influence on the observed results.

Future work with this model system could focus on investigating dehydrogenation in different environments, such as added steam, potassium, and sulfur as well as for different aromatic molecules, such as toluene and pyrene. Other model systems such as Ni(110), Ni(100), and Ni(211) must be investigated and compared with Ni(111) results. Performing the experiments in near-ambient pressure could help bridge the pressure gap to a certain extent.

7.2 Biomass pyrolysis gas conditioning

The main focus here was to investigate the industrial use of an Fe-based catalyst for pyrolysis gas conditioning and its potential as a pre-conditioning step before further treatment or use of the gas. The study included the elaboration of the chemistry of pyrolysis gas conditioning resulting in bio-crude deoxygenation and a hydrogen-rich gas, using an Fe-based catalyst, without addition of hydrogen or steam. After the in-situ initial stabilization of the catalyst, an increase in permanent gas and reduction in the bio-crude and its oxygen content were observed in the treated pyrolysis gas. A major dehydration of oxygenate occurred over the catalyst. Significant oxygenate cracking/ steam reforming activity of

pyrolysis gas was displayed with high reduction in the yields of for instance, acetic acid and methoxy phenols. Despite the carbon laydown and sintering, there was no clear catalyst deactivation during the run and catalyst displayed strong WGS activity. No CO/CO_2 hydrogenation activity into lighter hydrocarbons was observed, pointing out the active surface of the catalyst being of Fe-oxide type rather than Fe-carbide type. This is in line with the observed Fe_3O_4 as the bulk phase of the catalyst. The results indicate that iron-based catalysts are a potential candidate for direct pyrolysis gas conditioning and also for application in a pre-conditioning step, for example in a two-stage reformer concept for synthesis gas production.

Longer exposure times are necessary to evaluate the lifetime of the catalyst and the viability of the proposed technology. Even though the iron-based catalyst is sulfur-tolerant to a certain degree, research efforts must also focus on the influence of sulfur in pyrolysis gas conditioning. Experiments at different operating conditions, improved catalyst stabilization method, and recycling part of the treated pyrolysis gas to reduce carbon laydown are some possible measures to investigate in the future.

8 Acknowledgments

A very special gratitude goes out to the Swedish Energy Agency financed program Swedish Gasification Center (SFC) and all the external partners (E.ON, ANDRITZ, Haldor Topsoe A/S, Cortus Energy, and Energiforsk) for funding my research and people whom I worked with during my industrial collaborations.

My deep and special thanks goes out to my family for their continuous love, help, and support. I am forever grateful to my parents. They encouraged me to take new directions in life and find my own destiny. If not for them, this could not have been possible. I dedicate this milestone to them.

I would like to express my special gratitude and thanks to my supervisors Professor Dr. Klas Engvall and Dr. Klas J. Andersson, who have been wonderful mentors to me in many aspects. Your advice on my research has been priceless. Your words were encouraging every step of the way. My PhD was an enjoyable experience thanks to you. I hope this will be just the beginning of our collaboration.

I would also like to thank my supervisors Dr. Roberto Lanza and Professor Dr. Mats Ahmadi Götelid for their tremendous tutorship, contribution, and guidance throughout this journey.

I would like to express my gratefulness to the head of the chemical engineering division, Professor Dr. Lars J. Pettersson, for his support, motivation, and contribution to my education. I would also like to thank Professor Dr. Jens Rostrup-Nielsen for sharing his knowledge on catalyst deactivation and for the kind permission to use some of his research materials in this work.

I want to thank Professor Dr. Andrzej Kotarba and his research group for hosting me during my stay at Faculty of Chemistry, Jagiellonian University (JU) in Kraków, Poland.

I am thankful to my colleagues and all the staff at KTH Royal Institute of Technology, Department of Chemical Engineering for their support in research and friendship throughout these years. My special thanks goes out to Monika Gołda-Cępa (JU), Moa Ziethén Granlund, Javier Barrientos,

and Efthymios Kantarelis for critically reading this thesis and giving me feedback.

I would also like to thank all my co-authors and the master students who contributed to this work. My special thanks goes out to Milad G.Yazdi, Professor Dr. Jan B. C. Pettersson, Dr. Henrik Öström, Professor Dr. Tony Hansson, and Kess Marks for the productive discussions and making the external research collaborations possible during this work.

Outside the university, I have received the continuous support of my lovely friends. Thank you for the pleasant company. My special thanks goes out to Payam Pourmand, who has been a wonderful friend since the very first day, inside and outside the university.

Last but not least, I would like to thank all my teachers, instructors, and coordinators for their contribution.

9 References

[1] Rostrup-Nielsen JR. New aspects of syngas production and use. 2000;63:159-164.

[2] Rostrup-Nielsen JR, Christiansen LJ. Concepts in syngas manufacture. London: Imperial College Press; 2011.

[3] Bartholomew CH, Farrauto R. Fundamentals of industrial catalytic processes. Hoboken, New Jersey: John Wiley & Sons, Inc.; 2006.

[4] U.S Energy Information Administration, https://www.eia.gov/outlooks/aeo/; 2017.

[5] United Nations Department of Economy and Social Affairs, https://www.esa.un.org/unpd/wpp/; 2015.

[6] Cavattoni T, Garbarino G. Catalytic abatement of biomass tar: a technological perspective of Ni-based catalysts. Rendiconti Lincei 2017;28:1-17.

[7] International Energy Agency key world energy statistics, https://www.iea.org/publications/freepublications/publication/key-world-energy-statistics.html; 2016.

[8] Demirbas A. Progress and recent trends in biofuels. Prog Energy Combust Sci 2007;33:1-18.

[9] Coll R, Salvado J, Farriol X, Montane D. Steam reforming model compounds of biomass gasification tars : conversion at different operating conditions and tendency towards coke formation. Fuel Process Technol 2001;74:19-31.

[10] Devi L, Ptasinski KJ, Janssen FJJG. A review of the primary measures for tar elimination in biomass gasification processes. Biomass Bioenergy 2003;24:125-140.

[11] McKendry P. Energy production from biomass (Part 1): Overview of biomass. Bioresour Technol 2002;83:37-46.

[12] Chan FL, Tanksale A. Review of recent developments in Ni-based catalysts for biomass gasification. Renewable Sustainable Energy Rev 2014;38:428-438.

[13] Berndes G, Hoogwijk M, Broek VDR. The contribution of biomass in the future global energy supply: a review of 17 studies. Biomass Bioenergy 2003;25:1-28.

[14] Kurkela E, Kurkela M, Hiltunen I. Steam–oxygen gasification of forest residues and bark followed by hot gas filtration and catalytic reforming of tars: Results of an extended time test. Fuel Process Technol 2015;141:148-158.

[15] Kumar A, Jones DD, Hanna Ma. Thermochemical Biomass Gasification: A Review of the Current Status of the Technology. Energies 2009;2:556-581.

[16] Higman C, Burgt MVD. Chapter 5 - Gasification Processes. Gasification (Second Edition). Burlington: Gulf Professional Publishing; 2008, pp. 85-170.

[17] Andersson KJ, Skov-Skjøth Rasmussen M, Højlund Nielsen PE. Industrial-scale gas conditioning including Topsoe tar reforming and purification downstream biomass gasifiers: An overview and recent examples. Fuel 2017;203:1026-1030.

[18] http://blog.topsoe.com/2015/01/first-ever-large-scale-demonstration-biogas-plant-goes-stream-sweden-technology-topsoe.

[19] Dayton D. A review of the literature on catalytic biomass tar destruction National Renewable Energy Laboratory (NREL); 2002.

[20] Engvall K, Kusar H, Sjöström K, Pettersson LJ. Upgrading of raw gas from biomass and waste gasification: Challenges and opportunities. Top Catal 2011;54:949-959.
[21] Trane R, Dahl S, Skjøth-rasmussen MS, Jensen AD. Catalytic steam reforming of bio-oil. Int J Hydrogen Energy 2012;37:6447-6472.
[22] Basu P. Biomass gasification and pyrolysis: practical design and theory. Burlington, USA: Academic Press; 2010.
[23] Bridgwater AV, Toft AJ, Brammer JG. A techno-economic comparison of power production by biomass fast pyrolysis with gasification and combustion. 2002.
[24] Milne TA, Abatzoglou N, Evans RJ. Biomass gasifier" tars": their nature, formation, and conversion. Colorado: 1998.
[25] Torres W, Pansare SS, Goodwin Jr. JG. Hot gas removal of tars, ammonia, and hydrogen sulfide from biomass gasification gas. Catal Rev 2007;49:407-456.
[26] Salo K, Mojtahedi W. Fate of alkali and trace metals in biomass gasification. Biomass Bioenergy 1998;15:263-267.
[27] Turn SQ, Kinoshita CM, Ishimura DM, Zhou J. The fate of inorganic constituents of biomass in fluidized bed gasification. Fuel 1998;77:135-146.
[28] https://www.ecn.nl/phyllis2. Phyllis2, database for biomass and waste; Accessed: August 2017.
[29] Bridgwater AV. The technical and economic feasibility of biomass gasification for power generation. Fuel 1995;74:631-653.
[30] Engvall K, Liliedahl T, Dahlquist E. Chapter 6- Biomass and black liquor gasification Dahlquist E. (Ed.) Technologies for converting biomass to useful energy. London: Taylor & Francis Group; 2013.
[31] Wang L, Weller CL, Jones DD, Hanna MA. Contemporary issues in thermal gasification of biomass and its application to electricity and fuel production. Biomass Bioenergy 2008;32:573-581.
[32] Yung MM, Jablonski WS, Magrini-Bair KA. Review of catalytic conditioning of biomass-derived syngas. Energy Fuels 2009;23:1874-1887.
[33] Huber GW, Sara I, Corma A. Synthesis of Transportation Fuels from Biomass. Chem Rev 2006;2:4044-4098.
[34] Devi L. Catalytic removal of biomass tars; Olivine as prospective in-bed catalyst for fluidized-bed biomass gasifiers. Technische Universiteit Eindhoven 2005.
[35] Maniatis K, Beenackers AACM. Tar Protocols. IEA Bioenergy Gasification Task: Introduction. Biomass Bioenergy 2000;18:1-4.
[36] Brage C, Yu Q, Chen G, Sjöström K. Use of amino phase adsorbent for biomass tar sampling and separation. Fuel 1997;76:137-142.
[37] Ahmadi M, Knoef H, Van De Beld B, Liliedahl T, Engvall K. Development of a PID based on-line tar measurement method - Proof of concept. Fuel 2013;113:113-121.
[38] Baumhakl C, Karellas S. Tar analysis from biomass gasification by means of online fluorescence spectroscopy. Optics and Lasers in Engineering 2011;49:885-891.
[39] Gall D, Pushp M, Davidsson KO, Pettersson JBC. On-line measurements of alkali and heavy tar components in biomass gasification. Energy Fuels 2017;31:8152−8161.
[40] Elliott DC. Relation of Reaction Time and Temperature to Chemical Composition of Pyrolysis Oils. ACS Symposium 1988;Series 376-Series 376.

[41] Narváez I, Corella J, Orío A. Fresh tar (from a biomass gasifier) elimination over a commercial steam-reforming catalyst. Kinetics and effect of different variables of operation. Ind Eng Chem Res 1997;3:317-327.
[42] Mojtahedi W, Ylitalo M, Maunula T, Abbasian J. Catalytic decomposition of ammonia in fuel gas produced in pilot-scale pressurized fluidized-bed gasifier. Fuel Process Technol 1995;45:221-236.
[43] Erbel C, Mayerhofer M, Monkhouse P, Gaderer M, Spliethoff H. Continuous in situ measurements of alkali species in the gasification of biomass. Proc Combust Inst 2013;34:2331-2338.
[44] Fatehi H, He Y, Wang Z, Li ZS, Bai XS, Aldén M, et al. LIBS measurements and numerical studies of potassium release during biomass gasification. Proc Combust Inst 2014;35:2389 – 2396.
[45] Wellinger M, Biollaz S, Wochele J, Ludwig C. Sampling and online analysis of alkalis in thermal process gases with a novel surface ionization detector. Energy Fuels 2011;25:4163-4171.
[46] Higman C, van der Burgt M. Chapter 5 - Gasification Processes. Gasification (Second Edition). Burlington: Gulf Professional Publishing; 2008, pp. 91-191.
[47] Alamia A, Larsson A, Breitholtz C, Thunman H. Performance of large-scale biomass gasifiers in a biorefinery, a state-of-the-art reference. International Journal of Energy Research 2017.
[48] Van der Drift A, Boerrigter H. Synthesis gas from biomass for fuels and chemicals. ECN-C–06-001; 2006.
[49] Nemanova V, Nordgreen T, Engvall K, Sjöström K. Biomass gasification in an atmospheric fluidised bed: Tar reduction with experimental iron-based granules from Höganäs AB, Sweden. Catal Today 2011;176:253-257.
[50] Anis S, Zainal ZA. Tar reduction in biomass producer gas via mechanical, catalytic and thermal methods: A review. Renewable Sustainable Energy Rev 2011;15:2355-2377.
[51] Boerrigter H, van Paasen SVB, Bergman PCA, Könemann JW, Emmen R, Wijnands A. “Olga” Tar Removal Technology. ECN; 2005.
[52] Srinakruang J, Sato K, Vitidsant T, Fujimoto K. Highly efficient sulfur and coking resistance catalysts for tar gasification with steam. Fuel 2006;85:2419-2426.
[53] Sehested J. Four challenges for nickel steam-reforming catalysts. Catal Today 2006;111:103-110.
[54] Rostrup-Nielsen JR. Coking on nickel catalysts for steam reforming of hydrocarbons. J Catal 1974;33:184-201.
[55] Zhang R, Brown RC, Suby A, Cummer K. Catalytic destruction of tar in biomass derived producer gas. Energy Convers Manage 2004;45:995-1014.
[56] Einvall J, Albertazzi S, Hulteberg C, Malik A, Basile F, Larsson A-C, et al. Investigation of reforming catalyst deactivation by exposure to fly ash from biomass gasification in laboratory scale. Energy Fuels 2007;21:2481-2488.
[57] Li YP, Wang TJ, Wu CZ, Gao Y, Zhang XH, Wang CG, et al. Effect of alkali vapor exposure on Ni-MgO / γ-Al_2O_3 / cordierite monolithic catalyst for biomass fuel gas reforming. Ind Eng Chem Res 2010;49:3176-3183.
[58] Sutton D, Kelleher B, Ross JRH. Review of literature on catalysts for biomass gasification. Fuel Process Technol 2001;73:155-173.
[59] Simell P, Hannula I, Tuomi S, Nieminen M, Kurkela E, Hiltunen I, et al. Clean syngas from biomass-process development and concept assessment. Biomass Conversion and Biorefinery 2014;4:357-370.

[60] Kurkela E, Ståhlberg P, Laatikainen J, Simell P. Development of simplified IGCC-processes for biofuels: Supporting gasification research at VTT. Bioresour Technol 1993;46:37-47.

[61] Simeone E, Siedlecki M, Nacken M, Heidenreich S, de Jong W. High temperature gas filtration with ceramic candles and ashes characterisation during steam–oxygen blown gasification of biomass. Fuel 2013;108:99-111.

[62] Tuomi S, Kurkela E, Simell P, Reinikainen M. Behaviour of tars on the filter in high temperature filtration of biomass-based gasification gas. Fuel 2015;139:220-231.

[63] Nemanova V, Abedini A, Liliedahl T, Engvall K. Co-gasification of petroleum coke and biomass. Fuel 2014;117:870-875.

[64] Nemanova V, Engvall K. Tar variability in the producer gas in a bubbling fluidized bed gasification system. Energy Fuels 2014;28:7494–7500.

[65] Nacken M, Ma L, Heidenreich S, Baron GV. Catalytic activity in naphthalene reforming of two types of catalytic filters for hot gas cleaning of biomass-derived syngas. Ind Eng Chem Res 2010;49:5536-5542.

[66] Eriksen WL, Nielsen RM, Madsen J, Voss B, Andersson KJ, Højlund Nielsen PE. “dusty” vs. “clean” tar reforming of biomass, gasification gas – An operational point of view; 2014.

[67] Hannula I, Lappi K, Simell P, al. e. High efficiency biomass to power operation experiences and economical aspects of the novel gasification process. 15th European Biomass Conference and Exhibition, from Research to Market Deployment 2007.

[68] Rhyner U. Gas Cleaning. Synthetic Natural Gas from Coal, Dry Biomass, and Power-to-Gas Applications. John Wiley & Sons, Inc.; 2016, pp. 41-76.

[69] Turn SQ. Chemical Equilibrium Prediction of Potassium, Sodium, and Chlorine Concentrations in the Product Gas from Biomass Gasification. Ind Eng Chem Res 2007;46:8928-8937.

[70] Bell DA, Towler BF, Fan M. Coal gasification and its applications. Boston: William andew publishing; 2011.

[71] Cheah S, Carpenter DL, Magrini-Bair KA. Review of mid- to high-temperature sulfur sorbents for desulfurization of biomass- and coal-derived syngas. Energy Fuels 2009;23:5291-5307.

[72] Skrzypski J, Bezverkhyy I, Heintz O, Bellat JP. Low temperature H2S removal with metal-doped nanostructure ZnO sorbents: Study of the origin of enhanced reactivity in Cu-containing materials. Ind Eng Chem Res 2011;50:5714-5722.

[73] Coll R, Salvadó J, Farriol X, Montané D. Steam reforming model compounds of biomass gasification tars: Conversion at different operating conditions and tendency towards coke formation. Fuel Process Technol 2001;74:19-31.

[74] Rostrup-Nielsen JR. Activity of nickel catalysts for steam of hydrocarbons reforming. J Catal 1973;31:173-199.

[75] Rostrup-Nielsen JR, Sehested J, Nørskov JK. Hydrogen and synthesis gas by steam- and CO_2 reforming. Advances in Catalysis 2002;47:65-139.

[76] Kaewpanha M. Catalytic steam reforming of biomass tar at low temperatures (Ph.D. dissertation). 2015.

[77] Corella J, Toledo JM, Aznar MP. Improving the modeling of the kinetics of the catalytic tar elimination in biomass gasification. Ind Eng Chem Res 2002;41:3351-3356.

[78] Corella J, Caballero MaMa, Aznar MPPM-P, Brage C. Two advanced models for the kinetics of the variation of the tar composition in its catalytic elimination in biomass gasification. Ind Eng Chem Res 2003;42:3001-3011.
[79] Li C, Suzuki K. Tar property, analysis, reforming mechanism and model for biomass gasification—An overview. Renewable Sustainable Energy Rev 2009;13:594-604.
[80] Curcio D, Omiciuolo L, Pozzo M, Lacovig P, Lizzit S, Jabeen N, et al. Molecular Lifting, Twisting, and Curling during Metal-Assisted Polycyclic Hydrocarbon Dehydrogenation. J Am Chem Soc 2016;138:3395-3402.
[81] Wang B, König M, Bromley CJ, Yoon B, Treanor M-J, Garrido Torres JA, et al. Ethene to Graphene: Surface Catalyzed Chemical Pathways, Intermediates, and Assembly. The Journal of Physical Chemistry C 2017;121:9413–9423.
[82] Lu Y, Yang X. Molecular simulation of graphene growth by chemical deposition on nickel using polycyclic aromatic hydrocarbons. Carbon 2015;81:564-573.
[83] Shen Y, Yoshikawa K. Recent progresses in catalytic tar elimination during biomass gasification or pyrolysis—A review. Renewable Sustainable Energy Rev 2013;21:371-392.
[84] He L, Berntsen H, Ochoa-Fernandez E, Walmsley JC, Blekkan EA, Chen D. Co-Ni catalysts derived from hydrotalcite-like materials for hydrogen production by ethanol steam reforming. Top Catal 2009;52:206-217.
[85] Hu X, Lu G. Investigation of steam reforming of acetic acid to hydrogen over Ni-Co metal catalyst. J Mol Catal A: Chem 2007;261:43-48.
[86] Urasaki K, Tokunaga K, Sekine Y, Matsukata M, Kikuchi E. Production of hydrogen by steam reforming of ethanol over cobalt and nickel catalysts supported on perovskite-type oxides. Catal Commun 2008;9:600-604.
[87] Cui H, Turn SQ, Keffer V, Evans D, Tran T, Foley M. Study on the fate of metal elements from biomass in a bench-scale fluidized bed gasifier. Fuel 2013;108:1-12.
[88] Sehested J, Carlsson A, Janssens TVW, Hansen PL, Datye AK. Sintering of nickel steam-reforming catalysts on $MgAl_2O_4$ spinel supports. J Catal 2001;197:200-209.
[89] Rostrup-Nielsen JR, Christensen T, Dybkjaer I. Steam Reforming of Liquid Hydrocarbons. Recent Advances in Basic and Applied Aspects of Industrial Catalysis 1998;113:81-95.
[90] Rostrup-Nielsen JR, Nielsen PEH. Catalyst deactivation in synthetic gas production, and important syntheses. Wise H., Oudar J. (Eds.) Catalyst Poisoning and Deactivation. New York: Marcel Dekker; 1985, pp. 259-323.
[91] Wangen ES, Osatiashtiani A, Blekkan Ea. Reforming of Syngas from Biomass Gasification: Deactivation by Tar and Potassium Species. Top Catal 2011;54:960-966.
[92] Wise H, MacCarty J, Oudar J. Deactivation and poisoning of catalysts. New York: Marcel Dekker; 1985.
[93] Alstrup I, Rostrup-Nielsen JR, Røen S. High temperature hydrogen sulfide chemisorption on nickel catalysts. Appl Catal 1981;1:303-314.
[94] Rostrup-Nielsen J. Sulfur-passivated nickel catalysts for carbon-free steam reforming of methane. J Catal 1984;85:31-43.
[95] Rostrup-Nielsen JR. Catalytic steam reforming. Anderson J.R., Boudart M. (Eds.) Catalysis - science and technology. Berlin: Springer-Verlag; 1984, pp. 1-117.

[96] Bartholomew CH. Mechanisms of catalyst deactivation. Appl Catal A: Gen 2001;212:17-60.
[97] Rostrup-Nielsen JR. Sulfur-passivated nickel catalysts for carbon-free steam reforming of methane. J Catal 1984;85:31-43.
[98] Koningen J, Sjöström K. Sulfur-deactivated steam reforming of gasified biomass. Ind Eng Chem Res 1998;37:341-346.
[99] Rostrup-Nielsen JR. Promotion by poisoning. Stud Surf Sci Catal 1991;68:85-101.
[100] Bengaard HS, Nørskov JK, Sehested J, Clausen BS, Nielsen LP, Molenbroek AM, et al. Steam reforming and graphite formation on Ni catalysts. J Catal 2002;209:365-384.
[101] Alstrup I, Clausen BS, Olsen C, Smits RHH, Rostrup-Nielsen JR. Promotion of steam seforming catalysts. Stud Surf Sci Catal 1998;119:5-14.
[102] Shigehara Y, Ozaki A. The effect of metallic potassium addition on catalytic properties of nickel for hydrogenation of ethylene. J Catal 1973;31:309-312.
[103] Albertazzi S, Basile F, Brandin J, Einvall J, Fornasari G, Hulteberg C, et al. Effect of fly ash and H_2S on a Ni-based catalyst for the upgrading of a biomass-generated gas. Biomass Bioenergy 2008;32:345-353.
[104] Collard FX, Blin J. A review on pyrolysis of biomass constituents: Mechanisms and composition of the products obtained from the conversion of cellulose, hemicelluloses and lignin. Renewable Sustainable Energy Rev 2014;38:594-608.
[105] Bridgwater AV, Meier D, Radlein D. An overview of fast pyrolysis of biomass. Org Geochem 1999;30:1479-1493.
[106] Tripathi M, Sahu JN, Ganesan P. Effect of process parameters on production of biochar from biomass waste through pyrolysis: A review. Renewable Sustainable Energy Rev 2016;55:467-481.
[107] Mohan D, Pittman CU, Steele PH. Pyrolysis of wood / biomass for bio-oil : A critical review. Energy Fuels 2006;20:848-889.
[108] Mortensen PM, Grunwaldt JD, Jensen Pa, Knudsen KG, Jensen AD. A review of catalytic upgrading of bio-oil to engine fuels. Appl Catal A: Gen 2011;407:1-19.
[109] Venderbosch RH, Prins W. Fast pyrolysis technology development. Biofuels, Bioproducts and Biorefining 2010;4:178-208.
[110] Kantarelis E, Yang W, Blasiak W. Chapter 8- Biomass pyrolysis for energy and fuels production Daulquist E. (Ed.) Technologies for converting biomass to useful energy. London: Taylor & Francis Group; 2013.
[111] Demirbas A, Arin G. An Overview of Biomass Pyrolysis. Energy Sources 2002;24:471-482.
[112] Le Brech Y, Jia L, Cissé S, Mauviel G, Brosse N, Dufour A. Mechanisms of biomass pyrolysis studied by combining a fixed bed reactor with advanced gas analysis. J Anal Appl Pyrolysis 2016;117:334-346.
[113] Lin Y-c, Cho J, Tompsett Ga, Westmoreland PR, Huber GW. Kinetics and Mechanism of Cellulose Pyrolysis Kinetics and Mechanism of Cellulose Pyrolysis. Journal of physical chemistry C 2009;20097-20107.
[114] Raffelt K, Henrich E, Koegel A, Stahl R, Steinhardt J, Weirich F. The BTL2 Process of Biomass Utilization Entrained-Flow Gasification of Pyrolyzed Biomass Slurries. Appl Biochem Biotechnol 2006;129:153-164.

[115] Higman C, van der Burgt M. Chapter 4 - Feedstocks and Feedstock Characteristics. Gasification (Second Edition). Burlington: Gulf Professional Publishing; 2008, pp. 47-90.
[116] Wang D, Czernik S, Montane D, Mann M, Chornet E. Biomass to Hydrogen via Fast Pyrolysis and Catalytic Steam Reforming of the Pyrolysis Oil or Its Fractions. Abstracts of Papers of the American Chemical Society 1997;36:1507-1518.
[117] Czernik S, French R, Feik C, Chornet E. Biomass Thermoconversion Processes. Ind Eng Chem Res 2002;41:4209-4215.
[118] Kechagiopoulos PN, Voutetakis SS, Lemonidou AA, Vasalos IA. Hydrogen production via steam reforming of the aqueous phase of bio-oil in a fixed bed reactor. Energy Fuels 2006;20:2155-2163.
[119] Oasmaa A, Czernik S. Fuel oil quality of biomass pyrolysis oil - State of the art for the end users. Energy Fuels 1999;13:914-921.
[120] Zhang Q, Chang J, Wang T, Xu Y. Review of biomass pyrolysis oil properties and upgrading research. Energy Convers Manage 2007;48:87-92.
[121] Basagiannis AC, Verykios XE. Reforming reactions of acetic acid on nickel catalysts over a wide temperature range. Appl Catal A: Gen 2006;308:182-193.
[122] Basagiannis AC, Panagiotopoulou P, Verykios XE. Low temperature steam reforming of ethanol over supported noble metal catalysts. Top Catal 2008;51:2-12.
[123] Li Z, Hu X, Zhang L, Lu G. Renewable hydrogen production by a mild-temperature steam reforming of the model compound acetic acid derived from bio-oil. J Mol Catal A: Chem 2012;355:123-133.
[124] Sun J, Qiu XP, Wu F, Zhu WT. H2 from steam reforming of ethanol at low temperature over Ni/Y2O3 and Ni/La2O3 catalysts for fuel-cell application. Int J Hydrogen Energy 2005;30:437-445.
[125] Olcese RN, Bettahar M, Petitjean D, Malaman B, Giovanella F, Dufour a. Gas-phase hydrodeoxygenation of guaiacol over Fe/SiO2 catalyst. Appl Catal B: Environ 2012;115-116:63-73.
[126] Dielbold J. A review of the chemical and physical mechanisms of the storage stability of fast pyrolysis bio-oils. National Renewable Energy Laboratory (NREL); 1999.
[127] Gayubo AG, Aguayo AT, Atutxa A, Aguado R, Olazar M, Bilbao J. Transformation of oxygenate components of biomass pyrolysis oil on a HZSM-5 zeolite. II. aldehydes, ketones, and acids. Ind Eng Chem Res 2004;43:2619-2626.
[128] Heginuz E, Gregertsen B, Sorvari V, Vriesman P, Sjöström K. Studies on solid fuel pyrolysis and fluidisation in a laboratory-scale, atmospheric, fluidised bed reactor,. Finnish-Swedish Flame Days 1996.
[129] Gordon S, McBride BJ. Computer program for calculation of complex chemical equilibrium compositions and applications I. analysis 1994.
[130] Depner H, Jess A. Kinetics of nickel-catalyzed purification of tarry fuel gases from gasification and pyrolysis of solid fuels. Fuel 1999;78:1369-1377.
[131] Levenspiel O. Chemical reaction engineering. New York : Wiley 1999.
[132] Fogler HS. Elements of chemical reaction engineering. New Jersey: Prentice-Hall: 1986.
[133] Engvall K, Holmlid L, Kotarba A, Pettersson JBC, Menon PG, Skaugset P. Potassium promoter in industrial ammonia synthesis catalyst: Studies by surface ionization. Appl Catal A: Gen 1996;134:239-246.

[134] Borowiecki T, Denis A, Rawski M, Gołębiowski A, Stołecki K, Dmytrzyk J, et al. Studies of potassium-promoted nickel catalysts for methane steam reforming: Effect of surface potassium location. Appl Surf Sci 2014;300:191-200.
[135] Amovic M, Donaj P, Moner B, Alzuheri R, Ljunggren R. Fuel testing procedure for pyrolysis and gasification of biomass using TGA and WoodRoll test plant. Cortus Energy; 2014.
[136] Dufour A, Girods P, Masson E, Normand S, Rogaume Y, Zoulalian A. Comparison of two methods of measuring wood pyrolysis tar. J Chromatogr A 2007;1164:240-247.
[137] Ringer M, Putsche V, Scahill J. Large-scale pyrolysis oil production: A technology assessment and economic analysis. NREL/TP-510-37779. National Renewable Energy Laboratory; 2006.
[138] Hinds WC. Aerosol technology - properties, behaviour and measurement of airborne particles. New York: Wiley; 1999.
[139] Gall D, Pushp M, Davidsson KO, Pettersson JBC. On-line measurements of alkali and heavy tar components in biomass gasification. Energy Fuels 2017.
[140] Sehested J, Gelten JaP, Helveg S. Sintering of nickel catalysts: effects of time, atmosphere, temperature, nickel-carrier interactions, and dopants. Appl Catal A: Gen 2006;309:237-246.
[141] Bailey KM, Campbell TK, Falconer JL. Potassium promotion of Ni /Al_2O_3 catalysts. Appl Catal 1989;54:159-175.
[142] Pedrero C, Waku T, Iglesia E. Oxidation of CO in H_2–CO mixtures catalyzed by platinum: alkali effects on rates and selectivity. J Catal 2005;233:242-255.
[143] Huang CP, Richardson JT. Alkali promotion of nickel catalysts for carbon monoxide methanation. J Catal 1978;51:1-8.
[144] Shao Y, Paul J. TPD studies of the interaction of D_2O and Na with clean and oxidized Al (100) surfaces. 1993;72:113-124.
[145] Onishi H, Egawa C, Aruga T, Iwasawa Y. Adsorption of Na atoms and oxygen-containing molecules on MgO(100) and (111) surfaces. Surf Sci 1987;191:479-491.
[146] Rostrup-Nielsen JR. Some principles relating to the regeneration of sulfur-poisoned nickel catalysts. J Catal 1971;21:171-178.
[147] Chen I, Shiue D. Resistivity to Sulfur Poisoning of Nickel-Alumina Catalysts. Ind Eng Chem Res 1988;27:1391-1396.
[148] Politano A, Formoso V, Agostino RG, Colavita E, Chiarello G. Evidences of alkali-induced softening of the oxygen-substrate bond. J Chem Phys 2008;128:1-5.
[149] Liu ZP, Hu P. An insight into alkali promotion: A density functional theory study of CO dissociation on K/Rh(111). J Am Chem Soc 2001;123:12596-12604.
[150] Papageorgopoulos AC, Kamaratos M. K and S coadsorption on Ni(100) surfaces. J Phys: Condens Matter 2000;12:9281–9291.
[151] Błaszczyszyn M. Influence of adsorbed sulfur on surface diffusion of potassium on nickel Surf Sci 1985;151:351-360.
[152] Błaszczyszyn M, Błaszczyszynowa M, Gubernator W. Thermal desorption of potassium from clean and sulfur covered nickel Acta Phys Pol, A 1995;88:1151-1160.
[153] Ferrandon M, Mawdsley J, Krause T. Effect of temperature, steam-to-carbon ratio, and alkali metal additives on improving the sulfur tolerance of a

Rh/La–Al2O3 catalyst reforming gasoline for fuel cell applications. Appl Catal A: Gen 2008;342:69-77.
[154] Rostrup-Nielsen JR. Some principles relating to the regeneration of sulfur-poisoned nickel catalyst. J Catal 1971;21:171-178.
[155] Iordan A, Zaki M, Kappenstein C. Interfacial Chemistry in the Preparation of Catalytic Potassium-modifier Aluminas. J Chem Soc Faraday Trans 1993;89:2527-2536.
[156] Zhang Z, Zhang Y, Wang Z, Gao X. Catalytic performance and mechanism of potassium-promoted Mg-Al hydrotalcite mixed oxides for soot combustion with O_2. J Catal 2010;271:12-21.
[157] Digne M, Sautet P, Raybaud P, Euzen P, Toulhoat H. Hydroxyl Groups on γ-Alumina Surfaces: A DFT Study. J Catal 2002;211:1-5.
[158] Knözinger H, Ratnasamy P. Catalysis Reviews : Science and Engineering Catalytic Aluminas : Surface Models and Characterization of. Catal Rev 1978;17:31-70.
[159] Di Cosimo JI, Díez VK, Xu M, Iglesia E, Apesteguía CR. Structure and Surface and Catalytic Properties of Mg-Al Basic Oxides. J Catal 1998;178:499-510.
[160] Chen JG, Weisel MD, Hardenbergh JH, Hoffmann FM, Mims Ca, Hall RB. Evidence for the potassium-promoted activation of methane on a K-doped NiO/Ni(100) surface. J Vac Sci Technol A 1991;9:1684-1687.
[161] Kuchonthara P, Puttasawat B, Piumsomboon P, Mekasut L, Vitidsant T. Catalytic steam reforming of biomass-derived tar for hydrogen production with K2CO3/NiO/γ-Al2O3 catalyst. Korean J Chem Eng 2012;29:1525-1530.
[162] Mudge LK, Baker EG, Mitchell DH, Brown MD. Catalytic Steam Gasification of Biomass for Methanol and Methane Production. Journal of Solar Energy Engineering 1985;107:88-88.
[163] Jess A. Catalytic upgrading of tarry fuel gases: a kinetic study with model components. Chem Eng Process 1996;35:487-494.
[164] Marinkovic J, Thunman H, Knutsson P, Seemann M. Characteristics of olivine as a bed material in an indirect biomass gasifier. Chem Eng J 2015;279:555-566.
[165] Aznar MP, Caballero MA, Gil J. Commercial steam reforming catalysts to improve biomass gasification with steam-oxygen mixtures. 2. Catalytic tar removal. Ind Eng Chem Res 1998;5885:2668-2680.
[166] Santarossa G, Iannuzzi M, Vargas A, Baiker A. Adsorption of naphthalene and quinoline on Pt, Pd and Rh: A DFT study. ChemPhysChem 2008;9:401-413.
[167] Lin RF, Koestner RJ, Van Hove MA, Somorjai GA. The adsorption of benzene and naphthalene on the Rh(111) surface: A LEED, AES and TDS study. Surf Sci 1983;134:161-183.
[168] Dahlgren D, Hemminger JC. Chemisorption and thermal chemistry of azulene and naphthalene adsorbed on Pt(111). Surf Sci 1982;114:459-470.
[169] Campbell CT, Árnadóttir L, Sellers JRV. Kinetic prefactors of reactions on solid surfaces. Z Phys Chem 2013;227:1435-1454.
[170] Christmann K, Schober O, Ertl G, Neumann M. Adsorption of hydrogen on nickel single crystal surfaces. The Journal of Chemical Physics 1974;60:4528-4540.
[171] Patera LL, Africh C, Weatherup RS, Blume R, Bhardwaj S, Castellarin-Cudia C, et al. In Situ Observations of the Atomistic Mechanisms of Ni Catalyzed Low Temperature Graphene Growth. ACS Nano 2013;7:7901-7912.

[172] Lahiri J, Miller T, Adamska L, Oleynik II, Batzill M. Graphene Growth on Ni (111) by Transformation of a Surface Carbide. Nano Lett 2010;1-5.
[173] Arab P, Badiei A, Koolivand A, Ziarani GM. Direct hydroxylation of benzene to phenol over Fe_3O_4 supported on nanoporous carbon. Chinese Journal of Catalysis 2011;32:258-263.
[174] Aho A, Kumar N, Lashkul aV, Eränen K, Ziolek M, Decyk P, et al. Catalytic upgrading of woody biomass derived pyrolysis vapours over iron modified zeolites in a dual-fluidized bed reactor. Fuel 2010;89:1992-2000.
[175] Olcese RN, Lardier G, Bettahar M, Ghanbaja J, Fontana S, Carré V, et al. Aromatic chemicals by iron-catalyzed hydrotreatment of lignin pyrolysis vapor. ChemSusChem 2013;6:1490-1499.
[176] Dayton DC, Gupta RP, S. TB, Kataria A, Shen J-P. Catalytic biomass pyrolysis process. International patent WO/2013/134391 (PCT/US2013/029379)

[177] Łysik P, Górska A, Szarlik S. Gas-Phase Methylation of Phenol over Iron − Chromium Catalyst. Industrial & Engineering Chemistry Research 2014;53:17558−17562.
[178] Żukowski W, Berkowicz G, Baron J, Kandefer S, Jamanek D, Szarlik S, et al. Selective phenol methylation to 2,6-dimethylphenol in a fluidized bed of iron-chromium mixed oxide catalyst with o-cresol circulation. Chemistry Central Journal 2014;8:51-51.
[179] Brijaldo MH, Rojas HA, Martínez JJ, Passos FB. Effect of support on acetic acid decomposition over palladium catalysts. J Catal 2015;331:63-75.
[180] Abelló S, Montané D. Exploring iron-based multifunctional catalysts for fischer-tropsch synthesis: A review. ChemSusChem 2011;4:1538-1556.
[181] Dry ME. The Fischer-Tropsch process: 1950-2000. Catal Today 2002;71:227-241.
[182] Govender NS, Botes FG, de Croon MHJM, Schouten JC. Mechanistic pathway for methane formation over an iron-based catalyst. J Catal 2008;260:254-261.
[183] Bridgwater AV. Catalysis in thermal biomass conversion. Appl Catal A: Gen 1994;116:5-47.
[184] Foster AJ, Jae J, Cheng YT, Huber GW, Lobo RF. Optimizing the aromatic yield and distribution from catalytic fast pyrolysis of biomass over ZSM-5. Appl Catal A: Gen 2012;423-424:154-161.
[185] Huber GW, Corma A. Synergies between bio- and oil refineries for the production of fuels from biomass. Angew Chem Int Ed 2007;46:7184-7201.
[186] Ramasamy KK, Gerber MA, Flake M, Zhang H, Wang Y. Conversion of biomass-derived small oxygenates over HZSM-5 and its deactivation mechanism. Green Chem 2014;16:748-760.
[187] Halvarsson A. Catalytic conversion of pyrolysis gas in the WoodRoll process for enhancing process reliability. KTH Royal Institute of Technology; 2015.
[188] Elliott DC. Historical developments in hydroprocessing bio-oils. Energy Fuels 2007;21:1792-1815.
[189] Agblevor FA, Elliott DC, Santosa DM, Olarte MV, Burton SD, Swita M, et al. Red mud catalytic pyrolysis of pinyon juniper and single-stage hydrotreatment of oils. Energy Fuels 2016;30:7947-7958.
[190] Olcese RN, Francois J, Bettahar MM, Petitjean D, Dufour A. Hydrodeoxygenation of guaiacol, a surrogate of lignin pyrolysis vapors, over iron

based catalysts: Kinetics and modeling of the lignin to aromatics integrated process. Energy Fuels 2013;27:975-984.
[191] Sonoyama N, Nobuta K, Kimura T, Hosokai S, Hayashi JI, Tago T, et al. Production of chemicals by cracking pyrolytic tar from Loy Yang coal over iron oxide catalysts in a steam atmosphere. Fuel Process Technol 2011;92:771-775.
[192] Olcese R, Bettahar MM, Malaman B, Ghanbaja J, Tibavizco L, Petitjean D, et al. Gas-phase hydrodeoxygenation of guaiacol over iron-based catalysts. Effect of gases composition, iron load and supports (silica and activated carbon). Appl Catal B: Environ 2013;129:528-538.
[193] Ratnasamy C, Wagner JP. Water Gas Shift Catalysis. Catal Rev 2009;51:325-440.